NASA CONTRACTOR REPORT

EVALUATION OF THE EFFECTS OF SPACE ENVIRONMENT EXPOSURE ON INDEX OF REFRACTION AND EXTINCTION COEFFICIENTS OF APOLLO WINDOW MATERIALS

by J. T. Neu, E. J. Philbin, P. Mahadevan, and J. Compton

Prepared by
GENERAL DYNAMICS CORPORATION
San Diego, Calif.
for Manned Spacecraft Center

NATIONAL AERONAUTICS AND SPACE ADMINISTRATION • WASHINGTON, D. C. • APRIL 1968

EVALUATION OF THE EFFECTS OF SPACE ENVIRONMENT EXPOSURE ON INDEX OF REFRACTION AND EXTINCTION COEFFICIENTS OF APOLLO WINDOW MATERIALS

By J. T. Neu, E. J. Philbin, P. Mahadevan,
and J. Compton

Issued by Originator as Report No. GDC-DBE 67-001

Prepared under Contract No. NAS 9-4948 by
GENERAL DYNAMICS CORPORATION
San Diego, Calif.

for Manned Spacecraft Center

NATIONAL AERONAUTICS AND SPACE ADMINISTRATION

For sale by the Clearinghouse for Federal Scientific and Technical Information
Springfield, Virginia 22151 – CFSTI price $3.00

INDEX

INDEX (Cont'd)

LIST OF TABLES

LIST OF TABLES (Cont'd)

LIST OF FIGURES

LIST OF FIGURES (Cont'd)

I. INTRODUCTION

Under NASA Contract NAS9-4948 an experimental program has been completed to determine the effects of elevated temperature and space environmental radiation on Apollo window materials. The materials examined were fused silica, Corning Code 7940, Ultraviolet Grade; Vycor, Corning Code 7913, Optical Grade; aluminosilicate glass, Corning Code 1723. Measurements were made of the transmittance and index of refraction of these materials as a function of wavelength at room and elevated temperatures prior to irradiation. After irradiation at a dosage chosen to simulate a 30 day Apollo mission, the transmittance measurements were repeated. Index of refraction measurements were made on the irradiated samples only at room temperature as no change in refractive index was observed, within experimental error, as a result of irradiation. Because significant changes in transmittance were observed after the 30 day equivalent irradiation, a second set of samples was subjected to a 3 day equivalent dose and a third set to a 0.3 day equivalent dose. Within experimental error, no change in transmittance was observed after the 0.3 day equivalent dose.

Graphs of transmittance vs wavelength are presented for the sample materials at room temperature showing the effects of the various anti-reflection coatings employed and the effects of the 30 day and 3 day space equivalent irradiation doses. The effect of elevated temperatures on transmittance for both irradiated and non-irradiated samples is presented in tabular form.

The results of index of refraction measurements for irradiated and non-irradiated samples are given as a function of wavelength and temperature in tabular form.

The extinction coefficient for the uncoated, Apollo window materials was calculated from the measured values of transmittance and index of refraction for both non-irradiated and irradiated samples. The extinction coefficients as a function of wavelength are given in tabular form.

II. LITERATURE SURVEY

1. Introduction

A search was made of the literature (both journals and reports) for radiation coloration information of use in the present study. Particular attention was directed toward electron, proton and ultraviolet effects on various fused silicas and glasses. The chief object of this survey was to identify those phenomena which are likely to be important in the experimental program, to determine which interactions of those phenomena are likely to be significant, and to prepare a theoretical structure on which the experimental results can be systematically assembled and understood.

The coloration of glasses by ionizing radiation is well known. Many studies have been made of the fundamental processes occurring and have also been directed towards such engineering needs as radiation resistant glasses for hot-cell windows and solar-cell covers, and permanently radiation-colored glasses for radiation dosimetry. Recent surveys of this field include an annotated bibliography[1] issued by the Radiation Effects Information Center; a similar compilation[2] for infrared materials including fused silica glasses; a bibliography on quartz,[3] and a bibliography

on glasses.[4] Measurement programs of particular interest to the present application include an Apollo window material radiation testing program at Atomics International (unfortunately the report on this program[5] is not distributed outside Atomics International); and a NASA study[6] of the effect of 1.2 and 0.3 MeV electrons on the transmission of a variety of optical materials. Another bibliography[6a] is concerned with expected radiation effects on the optics of an orbiting solar observatory. Experiments on radiation effects on materials for aerospace enclosures were reported[6b] by Chinn et al, and on solar cell covers by Campbell.[6c]

2. Mechanisms by Which High Energy Radiation Produces Optical Effects

Exposure to ionizing radiation can affect optical properties in a number of ways. These include optical absorption produced by the introduction of color centers; additional light scattering; changes of refractive index; fluorescence which may be introduced into previously non-fluorescent materials; and thermoluminescence which may occur after irradiation. It is useful to divide the mechanisms of introduction of these effects into two classes; ionization radiation effects and displacement radiation effects. The first class is associated with excitation and de-excitation of electrons due to ionization and can be produced by low-energy radiation such as soft X-rays, low-energy electrons, or even energetic ultraviolet photons. Typical mechanisms by which ionization effects cause changes in optical properties are:

a. Trapping of electrons or holes, produced by the radiation, in defect centers, which may already be present or produced by irradiation. The classic examples are the F centers in the alkali halides. Because of their disordered structure, glasses

are very subject to this mode of coloration, which can often be produced by ultraviolet light.

b. Change of valency of an impurity ion by capture of a hole or electron. Examples include substitutional aluminum in quartz which is responsible for much of the coloration.[7]

Changes in optical properties, resulting from irradiation, are attributed to ionization effects, even when their detailed mechanism is unknown, if they can be produced by low-energy radiation and if they can be reversibly removed by optical bleaching or mild thermal treatment (see below). A typical case of this kind is provided by changes in absorption in quartz.[8] The magnitude of ionization radiation effects is determined by the ionization energy deposited in the sample, and for equivalent doses and dose rates is essentially independent of the nature and energy of the radiation. The equivalence of electrons, fast protons, and γ rays (interacting via electrons produced) when compared in this manner is well established, and ionization energy deposition rates by various types and energies of radiation are known reasonably well.[9]

Chemical radiation effects are a special case of ionization effects and are associated with the breaking and rearrangement of chemical bonds. Typical examples are cross-linking and bond breaking of polymers. Effects of this type are important in materials such as silica glasses because the bonds are partly covalent and not completely ionic.

Displacement radiation effects are associated with the displacement of atoms from their lattice sites. They result from a close collision of a fast particle with the nucleus of an atom, giving the atom enough energy to displace it from its lattice site. Typical mechanisms by which displacement effects produce optical changes include:

a. Introduction of defect levels in the forbidden gap of an insulator. Optical absorption can then take place by excitation of an electron from the center to the conduction band or to a higher excited state of the center, or of an electron from the valence band to the center. Since electronic excitation is involved, the observation of optical absorption will depend upon whether the levels involved are full or empty of electrons. Cases of this kind include vacancies in MgO,[10] and many centers in semiconductors;

b. Broadening of the band edge, extending the optical absorption to longer wavelengths. This effect is well known in many semiconductors;

c. Introduction of light scattering from disordered regions produced by energetic interactions ("stars" from high-energy protons);

d. Perturbation of the selection rules in a crystal near a defect, thus shifting the wavelength of a transition. An example is the α center in alkali halide crystals.

Displacement radiation effects are very sensitive to both the type and the energy of the radiation concerned. The displacement properties of atoms in a solid can be characterized reasonably well for a given material by the threshold energy below which an atom will not be displaced. Hence, for a fast nuclear particle to cause a displacement, it must have a minimum threshold energy, which will depend upon the mass of the particle and the mass of the struck nucleus. Following the intial displacement, the displaced atom may move through the material and collide with

other atoms, displacing some of them until all of the displaced atoms come to rest; this mechanism causes defects in the material. These defects, including vacant sites and interstitial atoms, may then migrate, either at the irradiation temperature or upon annealing at a higher temperature. This process may result in the annihilation of the defect, or in the formation of a complex defect with an impurity atom already present in the material.

For the case where the fast nuclear particle is an electron, displacements are produced by the Coulombic (Rutherford) interaction between the electron and the atomic nucleus, with a cross section independent of electron energy for relativistic electrons (> 1 MeV). The distribution function of the energy E of the primary recoil atom in a Coulombic collision is proportional to E^{-2}, so that most of the recoil atoms produced have low energies. The total number of displaced atoms can be roughly estimated by dividing the energy of the primary displaced atom by twice the atomic displacement threshold energy. Electrons with energy of approximately 1 to 2 MeV thus tend to displace only one atom and form simple defects, while collisions of higher energy electrons (5 to 50 MeV) result in an average displacement of several atoms and may give different, more complicated, aggregate defects.

For protons, Coulombic (Rutherford) scattering is also the chief mechanism for producing defects at low energies (< about 20 MeV). Since protons in this energy range are nonrelativistic, the cross section for Rutherford scattering decreases with increasing proton energy as 1/E, a result which is confirmed experimentally. Low-energy protons are thus responsible for most of the displacement-effects damage in the unshielded space environment, but effective shielding is possible.

At higher proton energies (but beginning at ~10 MeV), it is necessary to allow for the effects of nuclear elastic scattering; i.e., scattering involving the short-range nuclear forces, rather than the Coulombic interactions. This additional contribution can be estimated fairly accurately using the optical model of the nucleus and the numerous experiments on various elements; the cross sections vary only slowly with atomic number. At higher proton energies, nuclear inelastic processes (nuclear reactions) are also important. These add to the cross sections and change the momentum of recoil atoms. Protons with energies greater than ~100 MeV may produce another mode of interaction: nuclear "star" production. This spallation reaction is violent enough to produce a marked effect on the number of displacements produced, in spite of a rather low interaction cross section (~1 b for 500-MeV protons). This extra effect can be considered as two mechanisms: (1) The production of lower energy "star secondary" nucleons. These produce additional displacements and are relatively more effective than the primary protons because the protons of the star secondary nucleon have higher scattering cross sections and its neutrons have a more effective interaction mechanism. (2) Displacement of atoms by the recoiling residual nucleus; this may displace a very large number of atoms before coming to rest.

Calculations made at General Atomic indicate that (1) in comparison with the primary beam, the star secondaries can be neglected, (2) because the recoiling nucleus produces several thousand displacements, this process has a considerably higher over-all efficiency of displacement production than all other processes involved in star reactions combined.

Complete simulation of the displacement effects of space radiation thus needs careful consideration of electron and proton energies and flux, since

exact duplication is not possible. Establishment of correlation among proton, electron, and neutron damage rates at various energies has been under theoretical and experimental study at General Atomic for Ge and Si.[11] For Ge, the calculations predict, for 30-MeV proton, a defect-introduction rate of 20 times that for 30-MeV electrons. For carrier-removal and lifetime changes on samples with a variety of dopings, the measured values range from 13 to 40.

A third mechanism for formation of defects is, in a sense, intermediate to the two aforementioned mechanisms. Ionization effects in some materials can result in the displacement of atoms. This is well known in the formation of color centers in alkali halides. Continued formation of F centers involves the displacement of negative ions to leave vacancies, but displacements can be achieved with radiation that cannot cause them directly, e.g., 50-kV x-rays. The detailed mechanism is still uncertain, but may involve an Auger effect or the energy of electron-hole combination.[12] The process is of a typically ionization type, e.g., work at General Atomic has shown that equal F-center generation is produced by soft x-rays or by 30-MeV electrons depositing the same ionization energy.

These mechanisms differ greatly in their relative efficiencies for producing optical effects. For example, if expressed in terms of the number of electron volts needed on the average to form a defect (although this is not really a fair method of presentation), optical absorption introduced by ionizing processes will require only a few electron volts. An example is the initial range of coloration of KCl, where approximately 80 eV are required per F center formed. Ionization-type processes leading to displacement of atoms, such as the later stages of coloration of KCl, require of the order of 1000 eV per F center. Displacement effects of a fairly

simple nature, as, for example, those produced by 4.5 MeV electrons in Si, require, when expressed in these terms, approximately 1.5 MeV per defect. Fortunately, for irradiation by protons and electrons at the doses to be experienced in the Apollo mission, the effects expected to be produced are all of ionization type, as will be discussed further below. This makes simulation much simpler since it is only necessary to reproduce the ionization energy deposition.

3. Annealing of Radiation Effects

The radiation effects, once introduced, are apt to disappear in several ways. One is by thermal annealing. Annealing of this kind occurs for virtually all types of radiation damage, and often in a series of discrete steps as the temperature is raised.

Many optically absorbing centers introduced by irradiation can be bleached by optical illumination, a process known as optical bleaching.

It should be mentioned that optical bleaching, and certain types of thermal bleaching, may remove the coloration from a crystal, but may not leave it in the state it was in before irradiation. To give a specific example, irradiation may produce vacancies in a material via displacement effects. These may be filled with electrons and absorb light. Optical bleaching may remove these electrons, but leave the vacancies. The vacancies can then be filled by any type of ionizing radiation, not necessarily one capable of producing displacement effects, so that the material is now much more readily colorizable.

4. Combined Effects of High Energy and Ultraviolet Radiation

Optical radiation, especially in the ultraviolet, can also produce color in transparent materials. For glasses this is known as solarization[13]:

this process is discussed fully in another section of this report.

Combined exposure to irradiation by high energy charged particles and by ultraviolet light may thus give both effects, the light bleaching coloration that would be produced by the high energy particles, and also possibly producing solarization. In addition, synergistic effects are possible, for example, where a center is formed by the displacement effects of high energy particle irradiation, and filled with electrons or holes produced by the ultraviolet irradiation. For the materials and circumstances of interest in this report, synergistic effects of this kind were not expected to be important, since ionization type radiation effects produce electrons and holes which are probably similar to those formed by ultraviolet light. There could be interaction effects if, for example, the ionizing radiation produces electrons and holes throughout the material. These become trapped to form trapped electrons and hole centers. Ultraviolet radiation may produce effects chiefly at certain sites in the material, to produce, for example, a trapped hole and free electrons which could preferentially destroy the hole centers produced by the ionizing radiation. Effects of this kind do not appear to have been reported for optical materials, but synergistic effects of electrons and ultraviolet light have been reported[14] for thermal control coatings of the type used on spacecraft, including a glass.

5. Effects of Vacuum

Many oxide and tungstate materials show enhanced colorizability when irradiated in vacuum. This is associated with loss of oxygen. An oxygen atoms is lost from the surface, which, in the crystal, had been an $O^{=}$ ion. There are two electrons left in the crystal which enter sites and form color centers. Since they are mobile, the coloration can occur throughout the bulk of crystal. This effect is most marked with radiation of low penetration,

such as soft electrons, ultraviolet photons, etc., and may thus be important in the present application.

6. Dependence on Dose and Dose Rate

Many of the effects described above are expected to depend on the total radiation dose administered and on the dose rate used.

A typical form for the curve of concentration of optically absorbing centers versus total radiation dose has an initial rapidly rising portion followed by a more slowly rising portion. In some materials, a saturation of the optical absorption is seen; in other cases, a decrease is observed at high doses. The saturation effects may arise from the finite concentration of an impurity necessary to form the center or from radiation annealing. A decrease may also be due to radiation annealing or to changes in the electronic occupation of the center being observed. At the relatively low doses to be used in this program, the function may be assumed to be linear, but measurements should be made at about the total dose level expected to be encountered. At very high doses, ionization effects may saturate and displacement effects become controlling, but these levels are not expected to be of any importance here.

Variation of optical absorption with the rate at which the dose is administered is also a common occurrence. Two types of such "dose rate effects" may be distinguished. In one, the effect is due merely to a spontaneous annealing, at the temperature of irradiation and measurement, of the degradation produced by irradiation. An amount of the degradation is lost, depending on the lapse of time between introduction of damage and measurement; if significant loss occurs during the irradiation time, there will plainly be a dose-rate effect. This process can be identified

by studying the further recovery that occurs after the end of irradiation. A second type of dose-rate effect occurs when there are two competing processes for damage formation, with different functional dependences on dose-rate, via such intermediate quantities as the instantaneous concentration of electrons and holes produced by the irradiation. At low dose-rates, this last type of mechanism is not expected to be important.

7. Simulation of the Space Environment

As indicated above, exact simulation of the space environment is not possible. Reasonable simulation for the purposes of this program can be made using the following considerations. First, the expected radiation exposure is evaluated using the Apollo mission profile. The overwhelming source of radiation is the passage through the trapped radiation belts, unless a solar flare is encountered. For electrons, essentially all the energy lost in passage in or through the window material is lost as ionization. The same applies to the protons which show any appreciable penetration. For 1 MeV protons in SiO_2 for example, the theory of Lindhard[15] shows that in excess of 90% of the energy is lost as ionization. As the proton slows down, the last portion of its energy is used chiefly in producing displacements.

Since ionization effects are, as shown below, of chief importance in the window materials considered in this program, and since they are so much more efficient energetically in producing optical changes than are displacement effects, simulation is best achieved on the basis of comparing ionization effects. A suitable experimental procedure is then to irradiate with the energetic particles, using energies that correspond to a typical range in the window material for the space radiation to be encountered.

The particulate radiations should be conducted in vacuum, to include any effect of oxygen loss. Proton irradiations should be conducted first, so as to produce any displacement effects (even if small) first, so that changes, in any centers formed by displacement effects, by subsequent ionization effects, can occur. Similarly, the irradiations with ultraviolet light should be at the same time as, or follow those with charged particles, to allow optical bleaching effects to occur.

8. Coloration of Glasses

The coloration of transparent materials by irradiation has been studied most intensively in crystalline materials, particularly the alkali halides where many specific defects - color centers - have been distinguished and have had their structure determined. An example is the F center, which is an electron trapped in a negative ion vacancy. Many other centers are due to trapped electrons or trapped holes.

Work on the coloration of glasses has concentrated, as far as fundamental studies are concerned, on fused silica SiO_2 glasses, to compare them with single crystal quartz on the one hand and with silicate glasses on the other. In addition, the effects of impurities have been examined.

Glasses have an inherently disordered structure but this need not correspond to "defects" in crystals. A formalism for describing the structure of glasses is provided by the network theory of Stevels.[16] This treats SiO_2 glass as an irregular array of SiO_2 tetrahedra, as compared to the various crystalline forms of SiO_2 which are built up of regular arrays of the SiO_2 tetrahedra. Each oxygen atom serves to bond ("bridge") two silicon atoms and the structure has large interstices. When metal oxides such as Na_2O are added to SiO_2 to form a silicate glass,

the excess oxygen ions are taken up by the network by the replacement of one briding oxygen ion by two non-bridging ions. The added metal ions enter in nearby interstitial positions to maintain charge neutrality. Similarly, an impurity such as aluminum may be incorporated into the network in place of a Si atom: to enter "substitutionally," charge neutrality must be conserved by the incorporation of an interstitial alkali metal ion, e.g., Na^+ or Li^+. This formalism enables many of the observations of effects of irradiation upon glasses to be systematized and has been used for example, to relate[17] such apparently diverse properties as the short wave limit of optical transmission for a glass and its colorability by ionizing radiation. The network defect formation has also been used[16] to relate the colors produced in different glass compositions.

In general, irradiation of a glass produces optical absorption over wide regions of the spectrum, generally more intense in the ultraviolet than in the infrared. This absorption can usually be decomposed into a number of broad bands. These bands are generally treated[18] as having a Gaussian shape, described by the expression

$$\alpha(E) = \alpha_m e^{-(4 \ln 2/U^2)(E-E_o)^2}$$

where E_o is the photon energy at the peak, U is the full width at half maximum, α_m the absorption at the maximum and $\alpha(E)$ the absorption for photons of energy E. The Gaussian shape is thought to arise from differences in the surroundings of centers of nominally the same kind, as well as from thermal broadening. The observed widths are large, with values of U being typically 0.5 to 2 eV. Sharp absorption lines would be expected to be produced by irradiation only for glasses doped with relatively large amounts of special impurities, such as rare earth ions, and do not appear

to have been reported. "Zero-phonon" absorption, which gives rise to sharp line absorption by certain color centers in crystals such as MgO has not been observed in glasses.

The concentration of color centers, e.g., trapped electrons producing an observed band of a certain intensity is given by Smakula's equation

$$Nf = 0.87 \times 10^{17} U\alpha_m \, n/(n^2 + 2)^2$$

where N is the concentration of centers per cm^3, f the oscillator strength of the center (usually not measured, but generally may be taken to be in the range 0.1 to 1) and α_m is the absorption coefficient at the peak. This relationship can be used to give a semi-quantitative feel for the number of trapped electrons, or of impurity atoms, involved in a given absorption.

Some of the absorption bands found in fused silica are associated with impurities and others with intrinsic sites in the pure SiO_2 network. The distinction has been made possible by the availability of very pure synthetic fused silicas such as Corning 7940. These are made by fusing synthetic silica powder made from chemically purified volatile compounds such as $SiCl_4$ and show no absoprtion bands in the visible when irradiated:[19,20] For example, a dose of 10^{16} 2 MeV electrons/cm^2 was stated[21] to produce no visible coloration.

An intense violet color is found in irradiated silicas of lower purity. Examples are glasses made from fused natural Quartz which contains uncontrolled impurities in the 0.1% range and show a typical "swirly" pattern of violet coloration, corresponding to distribution of impurity in the melting process, and Vycor, which contains impurities in the 0.01% range since it is made by fusing together the porous silica left after other oxides in a

glass are leached out chemically. Vycor shows an intense but uniform coloration on irradiation.[6] This violet color is associated with an absorption band at ~5300Å which is attributed to aluminum impurity. The process occurring has been definitely identified, for the band occurring at the same wavelength in single crystal quartz, as the ionization of substitutional Al ion by correlating[22,23,24] electron spin resonance measurements with the changes in optical absorption spectra produced by irradiation and bleaching.

In fused silica, this band has been shown[25] not to occur in material intentionally doped only with aluminum, or only with a univalent ion such as lithium but to be very intense if both Al and Li are added. This again supports the view that the effect is due to Al substituting for Si: the Li is needed to maintain charge neutrality. The role of impurities is also discussed by Byurganovskaya and Orlov.[26]

Absorption in the visible region produced in pure synthetic silicas by irradiation is very small and due chiefly to the long wavelength tails[27] of absorption bands produced in the ultraviolet and associated with centers produced in the pure SiO_2 network. Reactor irradiation is also stated by Levy[28] to give a very weak absorption band at about 6000Å.

The chief ultraviolet band is at 2150Å and is generally referred to as the C band. This band, which can become very intense and can have a tail in the visible,[27,28] can be formed by ionizing radiation in pure fused silica. The growth is slow but uniform with dose for Corning fused silica but may show an initial rapid rise, followed by slow growth for other silicas.[27] It can be bleached optically by ultraviolet light, but this bleaching may result in increased absorption at longer wavelengths.[27] Thermal annealing of this center was found by the same workers[27] to be

rapid and virtually complete at 350-400°C. They also studied neutron effects on Corning fused silica and find that the coloration is less easily annealed. Further, irradiation with neutrons followed by annealing at 700°C leaves the silica uncolored but more easily colorable by subsequent gamma irradiation,[27] suggesting that in this extreme case there is a cooperative effect between displacement and ionization effects. Levy[28] found a similar enhancement by neutron irradiation. He studied the efficiency with which the band is formed over the temperature range from -190°C to +170°C and found that the absorption produced falls with increasing irradiation temperature. Since he found appreciable loss of absorption on standing at room temperature after irradiation, it is not clear how much of this change with temperature is due to thermal annealing during irradiation. Arnold and Compton[29] also found a similar effect of temperature. Their studies extended down to 4°K. They compared the effects of irradiation on Corning 7940, which includes some OH impurity and Corning 7943, an "infrared" grade of synthetic fused silica from which water has been carefully removed. For each glass, they found a tenfold enchancement of the 2150 band on irradiating at 77°K rather than 300°K, and they found that 7943 showed about three times higher coloration at 2150 than 7940. 7940 showed a band at 2570Å on irradiating at 77°K, which was not found in 7943. The water impurity seems to reduce the colorability of fused silica but the mechanism is unknown. The same authors made a careful study of the mode of formation of the defect responsible for the 2150Å band. The dependence of formation rate on the energy of the electrons used for irradiation showed clearly that ionization-type, rather than displacement-type, processes are involved. This was confirmed by using X-rays, which cannot produce displacement effects but which did produce the 2150 absorption band, and continued to do so on

prolonged exposure, reaching estimated concentrations up to $\sim 5 \times 10^{19}$ per cm^3. The energy required to form the center was found to be ~5800 eV at 300°K if the oscillator strength is taken as unity. (The authors also implicitly assume that none are lost.) The center is not formed in crystalline quartz unless the structure is damaged by neutron bombardment.

These results taken as a whole indicate that this absorption band, the most important in pure fused silicas, is due to the breaking of a Si-O bond. The two atoms are thought to relax apart and to then form an electron trap. It is important to note that this defect, as well as those due to impurities, is formed by ionization-type processes. There are other absorption bands formed in the far ultraviolet[30] which also appear to be due to defects in the pure SiO_2 network and to be formed by ionization processes. It would also appear that the water impurity in synthetic fused silicas such as Corning 7940 is beneficial in reducing coloration, and that 7940 rather than 7943 should be used in a radiation environment. 7943 (but not 7940) was found to show an absorption band at 2150Å after exposure to ultraviolet light.[31]

The coloration of other glasses (borosilicate, aluminosilicate, etc.) is discussed in the general bibliographies.[1,2,4,6] While detailed studies have not been made, the coloration is found to be due to ionization effects. The growth curves, i.e., the optical absorption vs radiation dose, were studied by Levy.[18] Typically, a region of rapid growth occurs at low doses; this saturates at $\sim 3 \times 10^7$ rads and is followed by a slower linear increase with dose. Similar results are reported by Nelson and Crawford,[27] and by Byurganovskaya and Orlov,[26] who also point out that some absorption bands in technical glasses decrease upon irradiation. Effects on a number of different glasses are reported by Kreidl and Hensler.[32]

9. Other Effects on Glasses

a) Radioluminescence

Materials exposed to ionizing radiation emit light, from Cerenkov radiation and radioluminescence. However, the intensity of light emitted is a function of the instantaneous dose rate. Since this is low in the space environment, no interference with viewing is expected from this cause, even in the dark and during passage through the trapped radiation belts. High purity fused silica also shows lower radioluminescence in the visible than any other glass or transparent material investigated at General Atomic.[33]

b) Induced Fluorescence

Many glasses, not originally fluorescent, show induced fluorescence after irradiation, and this property has been used as a dosimeter. Even high purity fused silica shows this effect after neutron bombardment[34] ($< 5 \times 10^{17}$ n cm^2) and emits a red, orange, or green glow on exposure to ultraviolet light. This effect is not expected to be important because of the low exposure doses for displacement effects and because it is unlikely to interfere with normal viewing in daylight.

c) Antireflection Coatings

Doses of up to 10^{13} 30 MeV electrons/cm^2 have been shown at General Atomic[35] to have no effects on multi-layer dielectric coatings of the type used for reflective and antireflective coatings.

d) Thermoluminescence

After irradiation, glasses can store energy which can be released as a burst of light on the first subsequent increase in temperature. Thermoluminescence (TL) of various types of fused silicas has been discussed in detail by Arnold.[36] The TL of Corning fused silica is reported by him to

be easily measurable on heating to 90°C after exposure to a low dose of X-rays at room temperature. Ultraviolet light can cause a similar effect. Lell,[25] on the other hand, reports no TL from apparently similar material after exposure to high doses of radiation. The importance of TL is thus difficult to estimate, since it depends on knowing the rate of temperature rise that may be experienced. Since this is unlikely to be large during dark viewing period occurring after irradiation at a low temperature (all these conditions are necessary) it is felt that TL is unimportant.

e) Changes in Refractive Index

The refractive index and the optical absorption are related for any system by the Kramers-Kronig relation. The refractive and dispersive properties of transparent materials are dominated by the contribution from the intense absorption bands found at the ultraviolet transmission limit. It is thus generally assumed that changes in refractive index, produced by irradiation and associated with the comparatively weak absorption bands introduced, must be negligibly small. That this is not the case has recently been demonstrated by workers[37] at Frankford Arsenal and NBS, who showed that gamma or electron irradiation of several common glasses can produce increases or decreases of up to 2×10^{-4} in the index of refraction, for doses of up to 10^{15} 2 MeV electrons. Presumably the contribution to the refractive index is appreciable, even for relatively weak absorption bands, at frequencies near the absorption band because of the factor $(\omega^2 - \omega_o^2)$ in the denominator of the Kramers-Kronig relation, where ω is the frequency of light at which the refractive index is being considered, and ω_o is the frequency of the peak of the absorption band concerned.

The only attempt at quantitative measurement and interpretation of the change of refractive index due to a color center is in an unpublished paper by Noble[38]; he finds a fractional change in index of refraction $\Delta n/n$ of about $10^{-2}\alpha$ where α is the absorption coefficient (per cm). This change was sufficient to produce marked changes in the reflectance (the quantity that he measured).

III. EXPERIMENTAL

1. Samples

After discussions with personnel of the Vehicle Design Group of Grumman Aircraft, the materials to be utilized in this study were determined to be UV grade, fused silica (Corning 7940), aluminosilicate glass (Corning 1723) and Vycor (Corning 7913). The latter represents a late substitution by Apollo Project personnel for the originally selected Plexiglas.

After an unusually long delivery delay, four prisms and eight "window" samples of each material were fabricated to the dimensions shown in Figure 1. The prisms were utilized in measuring the index of refraction while the "window" samples were used to measure transmission. The thicknesses of the transmission samples were selected to conform to the best available data (as of December, 1965) on the thicknesses of the comparable materials utilized in the Apollo window sandwich.

The transmission samples were coated by Optical Coating Laboratory, Inc. in accordance with Apollo specifications (OCLI Spec. 11-001) and the scheme denoted by Figure 2. The prisms were coated on one side with a reflective layer of platinum. Liquid Bright Platinum Paint No. 5 manufactured by the Hanovia Liquid Gold Division of Engelhard Industries was

SPECIFICATIONS OF PRISMS AND SAMPLE WINDOWS

NUMBER :

	FUSED SILICA (U.V. GRADE) C-7940, TOP GRADE	ALUMINO SILICATE C - 1723	VYCOR C - 7913
PRISMS	4	4	4
WINDOWS	6	6	6

SIZE AND FINISH

PRISMS

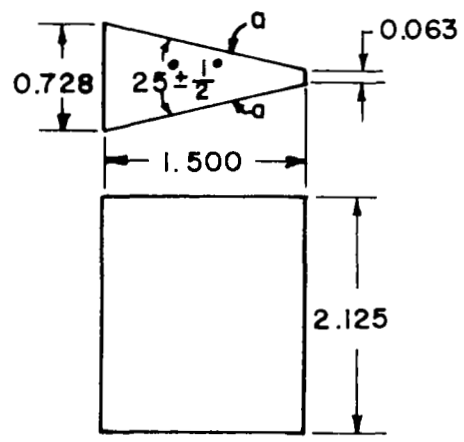

WINDOWS

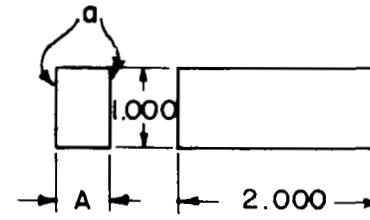

MATERIAL	A IN
C-7940	0.700
C-1723	0.230
C-7913	0.125

SIDES "a" TO BE PLANO WITHIN $\lambda/4$ AND OPTICAL FINISH OF $\lambda/4$, λ = Na D-LINE OTHER SURFACES UNFINISHED.

FIG. 1 : WINDOW AND PRISM DIMENSIONS

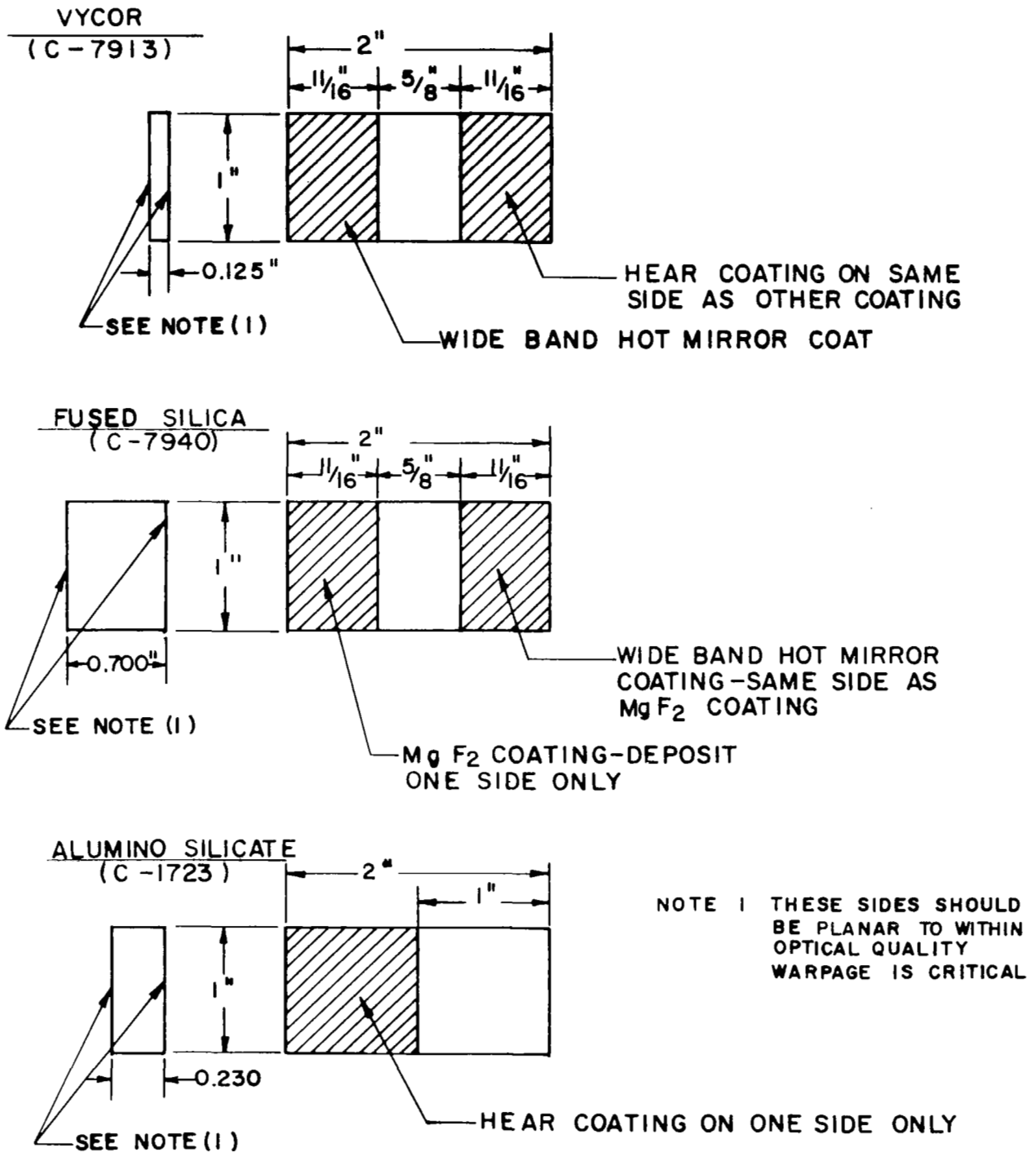

FIG. 2 : COATING ARRANGEMENT-WINDOW SAMPLES

sprayed on one face of the prism with a Paasche Airbrush, after which the coating was cured at high temperature. Platinum was selected to withstand the temperature cycling required in measuring the refractive index.

Figure 2 shows the manner in which the transmission samples were coated by OCLI. Three types of coatings are utilized in the fabrication of the Apollo window and were evaluated during the course of this study: (1) A single layer magnesium fluoride anti-reflectance coating, (2) a multi-layer blue-red reflection coating and (3) a high-efficiency reflection reducing coating (per North American Aviation, Inc., specification MA 0201-0415, revision C, dated 15 April 1965 and private conversations with Mr. D. Morelli of Optical Coating Laboratory, Inc.). The first of these coatings is used on the outer surface of the outer window, the second type on the inner surface of the outer window and the third type is used on both surfaces of the two inner windows. All coatings were guaranteed to conform to Apollo specifications by OCLI. It should be noted that according to North American specifications all coatings are designed for use at an incidence of 45^{o} while the transmission measurements made in the laboratory were at an incidence angle of 90^{o}.

2. Irradiation Facility

The contribution of the Space Science Laboratory Radiation Physics Group of General Dynamics Convair to this study consisted of simulating the radiation environment to which the Apollo materials would be subjected during the performance of a typical mission to the moon and return.

The Dynamitron Accelerator provided beams of electrons and protons at an appropriate energy and flux density to simulate the space environment. High intensity mercury arc lamps were used to provide the solar-ultraviolet radiation pattern.

Brief descriptions of the Dynamitron Accelerator used for the tests, estimates of the particle flux (electrons and protons), the experimental arrangement, etc. are presented below.

a. Accelerator Electrical Design

As shown in Figure 3, the basic circuit of the Dynamitron is a set of cascaded rectifiers capacitively coupled to a powerful r-f oscillator with a frequency of 300 kc. Two large electrodes just inside the cylindrical outer tank draw power from the oscillator and induce an r-f potential in a set of corona rings just inside the electrodes. Thus, direct current flows through the stack of rectifiers to establish a large DC potential at the output.

One advantage of operating at radio frequencies is that the Dynamitron requires no large capacitors to store energy between cycles and the output is smoothed. Consequently, static energy storage is not significantly greater than in electrostatic machines; accidental spark breakdowns are not violent and do not damage rectifiers or beam tube.

A large toroidal coil is connected in parallel with the driving electrodes; electrodes and coil function as a resonant tank circuit.

The driving r-f oscillator is a conventional (and highly reliable) modified Hartley type. The unit is separately housed in an air-tight, water-cooled enclosure and connected by cable to the DC generator, which contains the oscillator tank circuit (coil and electrodes). A high-pressure gas dielectric (SF_6) between resonant circuit and rectifiers provides DC insulation and r-f coupling. Along the axis of the system runs an evacuated acceleration tube, which for electron acceleration has a tungsten cathode at its high voltage terminal. For positive ion accelera

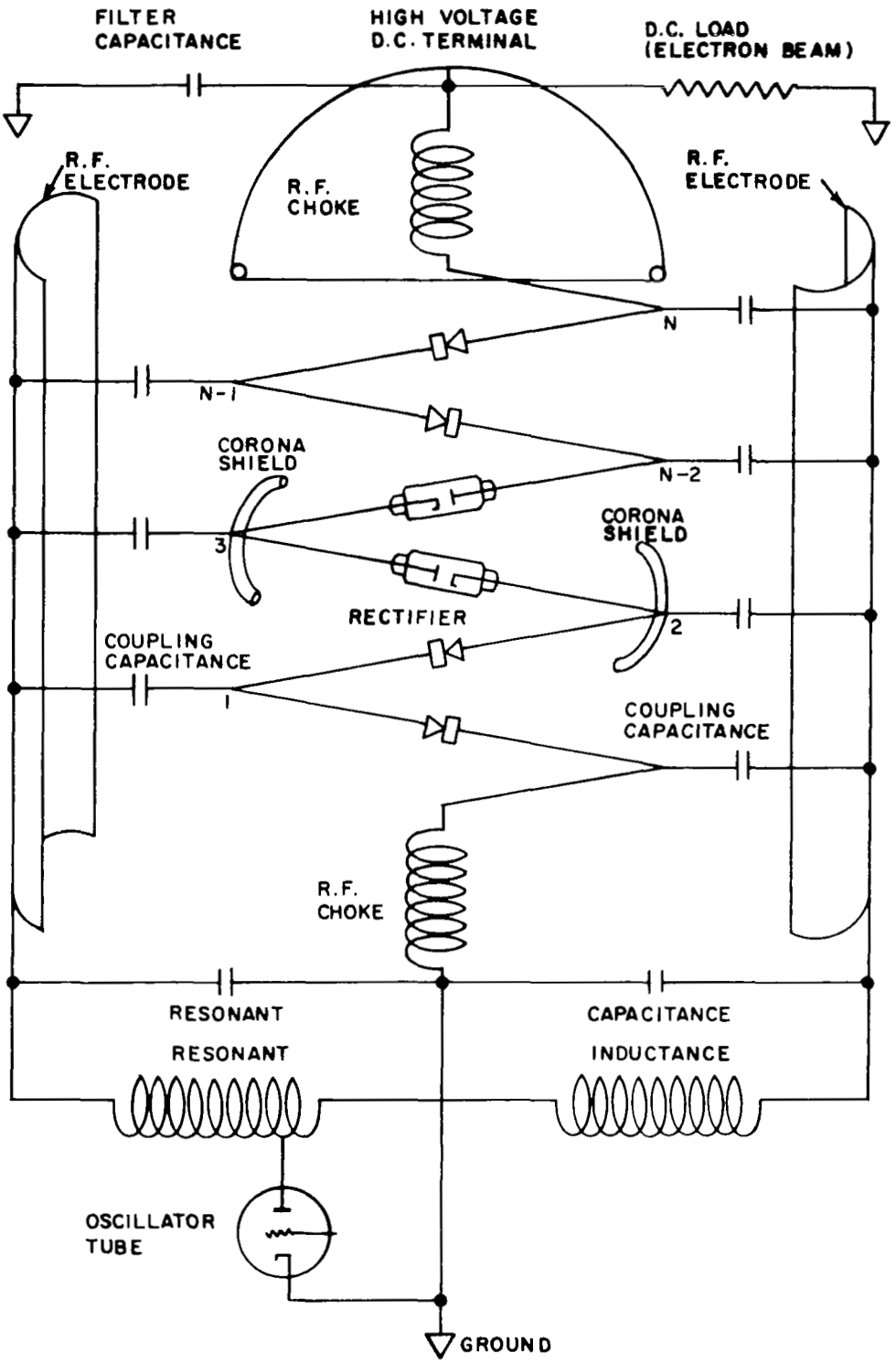

FIG. 3 : DYNAMITRON ACCELERATOR

tion the potential is reversed.

For production of protons, a universal ion source of our design[39] was substituted for the commercial source provided by Radiation Dynamics, Inc.

b. Accelerator Experimental Arrangement

A block diagram showing the experimental arrangement is shown in Figure 4. The electron or proton beam at the required energy is extracted from the accelerator and after traversing a beam tube approximately 7 ft long, is deflected through 90^{o} by an analyzing magnet into an ultra high vacuum chamber which houses the window material to be bombarded. This chamber is maintained at an operating pressure of under 8×10^{-8} Torr by a Varian ion pump.

The ultra high vacuum section is isolated from the power vacuum in the magnet chamber by an aluminum foil. In addition to maintaining a differential of two orders of magnitude in pressure, the aluminum foil also transmits the high energy proton and electron beam through it. The kinetic energy and current degradation experienced in passing through the foil are of course much greater for the protons than for the electrons. Thus, for electrons, the beam has to be extracted from the accelerator at 1.025 MeV to permit degradation down to the desired value of 1 MeV energy at the target sample. (The energy degradation was estimated by integrating the individual losses through five separate aluminum foils of equal thickness that are equivalent in total thickness to the actual foil used.) Likewise, for protons, the foil thickness was 1.1×10^{-3} inches and the initial beam energy 2 MeV. Calculations are given below to estimate the operating current required to get the suggested particle flux to the target materials.

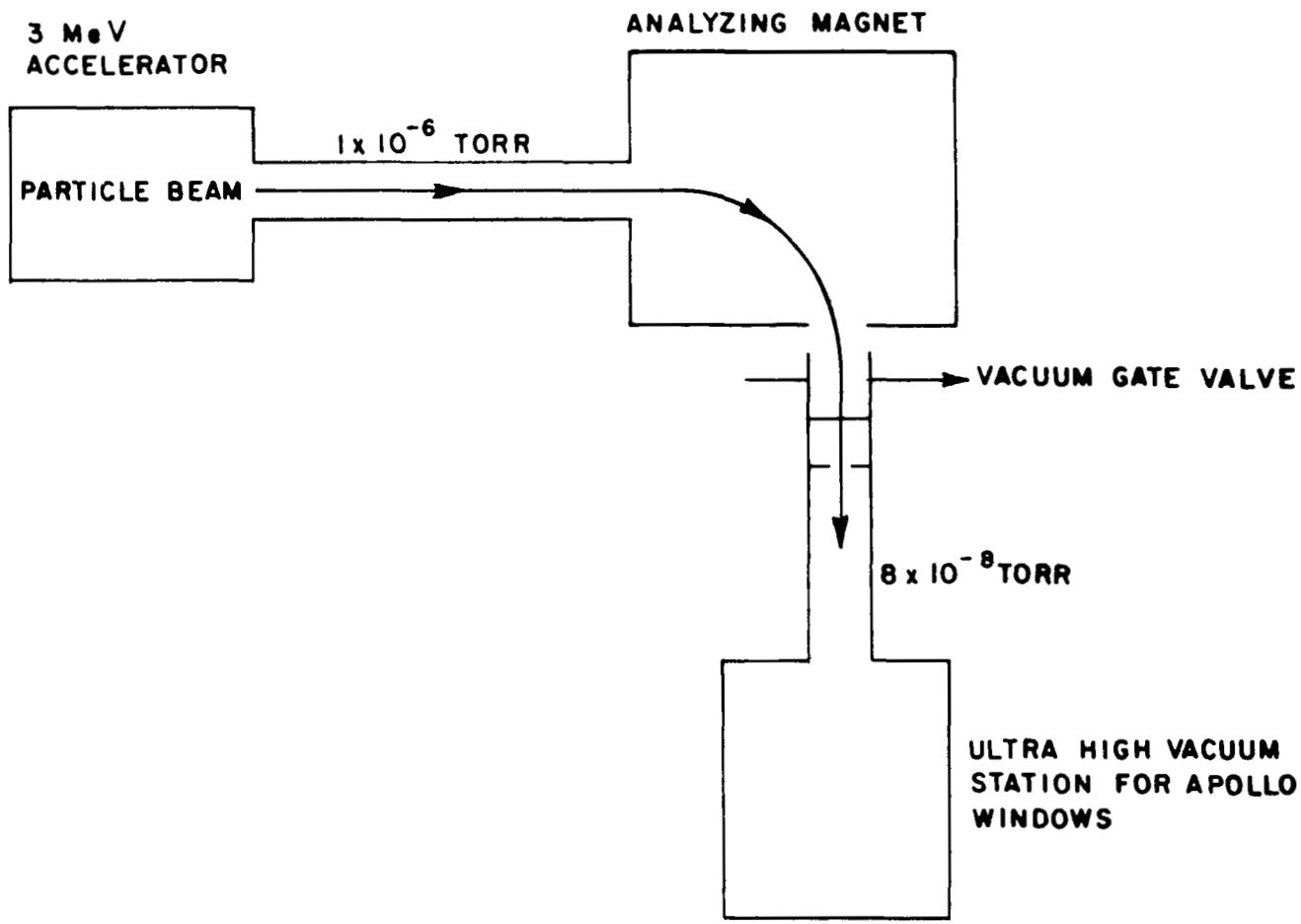

FIG. 4 : EXPERIMENTAL ARRANGEMENT– DYNAMITRON ACCELERATOR

c. Estimation of Particle Bombardment Time

Proton flux desired $p = 3 \times 10^{10}/cm^2/sec$

Total charge $= p \times e = 3 \times 10^{10} \times 1.6 \times 10^{-19}$

$= 4.8 \times 10^{-9}$ Coul/cm^2

Beam size $= 3\frac{1}{8}$" dia; $A = 49.5\ cm^2$

$Q_{Total} = 49.5\ cm^2 \times 4.8 \times 10^{-9}$ Coul/cm^2

$= 2.38 \times 10^{-7}$ Coulombs.

Maximum available proton current $= 1.55 \times 10^{-10}$ amp.

Duration of bombardment, $t = \dfrac{2.38 \times 10^{-7}}{1.55 \times 10^{-10}}$

$= 1580$ secs.

Utilizing the same technique the electron bombardment time was calculated. The available current was 6.6×10^{-8} amp. Bombardment time to obtain the desired total flux of $2.5 \times 10^{12}/cm^2/sec$ = 300 secs.

d. Beam Collimation and Alignment

The primary electron beam after passing through the aluminum foil is scattered into a large cone, resulting in a considerable fraction of the current hitting the walls of the beam tube instead of the target. The beam spread was considerably reduced by inserting an aperture. This collimating aperture was found to be unnecessary for the beam of protons.

e. The Particulate Radiation Environment

The beam energy density calculated above was based on the calculated radiation environment to which the Apollo materials would be subjected while on a model Apollo trajectory obtained from the Apollo Experiments Guide, 15 June 1965. The calculation assumed an inclination

of 30° between earth orbital trajectory and the equator. As shown in Table I a nominal two earth orbits on exit and reentry was assumed.

The calculated particulate radiation levels which would be encountered by Apollo in passing through the radiation belts are contained in Tables II and III. The integrated proton flux was calculated to an earth altitude of 24,000 N.M. while the integrated electron flux was calculated to an altitude of 18,000 N.M. The calculation was performed for exiting passage only and doubled to simulate exit and reentry. This results in a higher (more conservative) dosage since earth exit trajectories will result in longer dwell times within the radiation belts than the reentry trajectory.

The electron dose was calculated from data prepared by Aerospace Corporation as of 31 January 1966 and presents the projected 1968 electron environment. Above 6,000 N.M. altitude these values represent median values but can fluctuate up or down by a factor of 5 to 10. The proton data is from the same source and is current as of 15 May 1965. These values should be stable with time except for solar cycle changes which also effect the electron data.

The particulate radiation associated with a solar particle event (solar flare) consists predominantly of protons with energies lying between 1 MeV and a few GeV. The values used in this study are contained in Table IV and represent the worst conditions that could be found for any thirty day period on record.

Galactic cosmic rays are a negligible contribution to the radiation environment. Solar wind contributions are also probably negligible by comparison to the other radiation phenomena since energies encountered are from 1 to 5 kilovolts although one could encounter a number of densities in amounts such as 10^{14} to 10^{15} particles.

Table I

Assumed Mission Trajectory Characteristics Summary
Apollo-Saturn 500 Series Mission

Phase Description	Elapsed Time (Hours) (Approx)	Altitude Nautical Miles	Velocity ft/sec	Radial Velocity (NM/hr)
Liftoff	0	0	1,340	→500
Earth Orbit Insertion	0.2	100	25,580	→2.14
Begin Translunar Injection on Second Orbit	3.0	106	25,555	→610
Begin Coast to Transposition	3.1	167	35,621	→8,627
Jettison S-IV B and Begin Coast to Lunar Orbit Insertion	3.8	6,206	21,994	
Begin Lunar Orbit Insertion	64.3	103*	8,431	
LEM/CSM Separation on Second Orbit	68.1	83.1*	5,279	
Begin Coast to Initiation of Powered Descent	68.4	83.1*	5,178	
Begin Powered Descent	69.4	49,534 ft*	5,587	
Touchdown	69.5	0*	3.6	
Begin Powered Ascent on 20th CSM Orbit	104.3	0*	15	
Begin Docking	105.3	82.9*	5,276	
Begin Lunar Orbit Coast to Transearth Injection	105.7	83.9*	5,279	
Jettison LEM	106.2	83.4*	5,282	
Begin Transearth Coast	109.2	83.4*	8,013	
Jettison SM	198.0	2,447	28,160	
Entry	198.3	380,760 ft	36,048	
Earth Landing	198.6	0	25	

*Lunar altitude (measured above the landing site radius).

Flight azimuth of 500 series missions = 72 degrees.
Earth parking orbit = 1 to 3 revolutions - nominal is 2 revs.
Translunar phase lasts 60-80 hours.

Table II

Protons (to 24,000 NM Altitude)

Energy (MeV)	# Encountered on Exit From Earth Orbit (prot/cm^2)	# Encountered on Exit and Reentry (prot/cm^2)
4 to 15	9.178×10^8	1.836×10^9
15 to 30	3.729×10^7	7.458×10^7
30 to 50	6.451×10^6	1.290×10^7
above 50	1.715×10^6	3.430×10^6

Table III

Electrons (to 18,000 NM Altitude)

Energy (MeV)	# Encountered on Exit From Earth Orbit (elect/cm^2)	# Encountered on Exit and Reentry (elect/cm^2)
0 -0.25	4.309×10^{12}	8.618×10^{12}
0.25-0.50	7.637×10^{11}	1.528×10^{12}
0.50-0.75	1.765×10^{11}	3.530×10^{11}
0.75-1.00	6.394×10^{10}	1.279×10^{11}
1.00-1.25	3.211×10^{10}	6.422×10^{10}
1.25-1.50	1.731×10^{10}	3.462×10^{10}
1.50-1.75	1.039×10^{10}	2.078×10^{10}
1.75-2.00	6.086×10^9	1.216×10^{10}
2.00-2.25	3.771×10^9	7.542×10^9
2.25-2.50	2.320×10^9	4.640×10^9
2.50-2.75	1.451×10^9	2.902×10^9
2.75-3.00	9.230×10^8	1.846×10^9
3.00-3.25	5.934×10^8	1.187×10^9
3.25-3.50	3.855×10^8	7.710×10^8
3.50-3.75	2.554×10^8	5.108×10^8
3.75-4.00	1.713×10^8	3.426×10^8
4.00-4.25	1.176×10^8	2.352×10^8
4.25-4.50	8.205×10^7	1.641×10^8
4.50-4.75	5.880×10^7	1.176×10^8

Table III (Cont.)

Electrons (to 18,000 NM Altitude)

Energy (MeV.)	# Encountered on Exit From Earth Orbit (elect/cm^2)	# Encountered on Exit and Reentry (elect/cm^2)
4.75-5.00	4.163×10^7	8.326×10^7
5.00-5.25	3.234×10^7	6.468×10^7
5.25-5.50	2.568×10^7	5.136×10^7
5.50-5.75	2.006×10^7	4.012×10^7
5.75-6.00	1.692×10^7	3.384×10^7
6.00-6.25	1.389×10^7	2.778×10^7
6.25-6.50	1.221×10^7	2.442×10^7
6.50-6.75	1.099×10^7	2.198×10^7
6.75-7.00	9.510×10^6	1.902×10^6
7.00- ∞	1.651×10^8	3.302×10^8

Table IV

Estimated Integral Flux (prot/cm^2) for Dates Shown

Date	E > 100 MeV	30 ≤ E ≤ 100	10 ≤ E ≤ 30
10 July 1959	1.4×10^8	8.6×10^8	3.36×10^9
14 July 1959	1.0×10^8	1.2×10^9	6.10×10^9
16 July 1959	1.3×10^8	7.8×10^8	2.26×10^9
Total for July 1959	3.7×10^8	2.84×10^9	1.172×10^{10}

f. Ultraviolet Irradiation

The General Electric AH-6 lamps used to simulate the UV environment were calibrated using a Cary 14 Spectrophotometer, an integrating sphere, and a GE 6.6A/T4Q/1C/-200W tungsten-iodine lamp calibrated by N.B.S.[41,42] (See Figures 5, 6, 7, and 8). The calibrated tungsten-iodine lamp was positioned 43 cm from a one inch diameter opening in the integrating sphere to reproduce the distance at which the lamp was originally calibrated. The integrating sphere was used to insure that the entrance slit of the spectrophotometer was uniformly illuminated, and to insure that the difference in shape and size between the standard lamp and the AH-6 did not introduce errors.

The lamp and sphere were enclosed completely to prevent light from any other sources from entering the sphere. The internal walls of the enclosure were painted with flat-black paint to prevent reflected light from the source from entering the sphere. Only direct illuminations were recorded.

The intensity of illumination for the calibrated lamp was measured for wavelengths from 0.22μ to 0.40μ. The conditions of the original calibration, specifically current and orientation, were duplicated and the resulting intensity was recorded on a strip chart. The AH-6 lamp was then placed at the same position and its intensity measured on the same strip chart over the same wavelength band. Knowing the irradiance of the calibrated lamp as a function of wavelength (from N.B.S. data accompanying the lamp), and the ratio of intensities as a function of wavelength (from the strip chart), the irradiance of the AH-6 lamp was determined for all wavelengths from 0.22 to 0.4μ. The relationship is described by the equation

WITH TRANSFER OPTICS AND

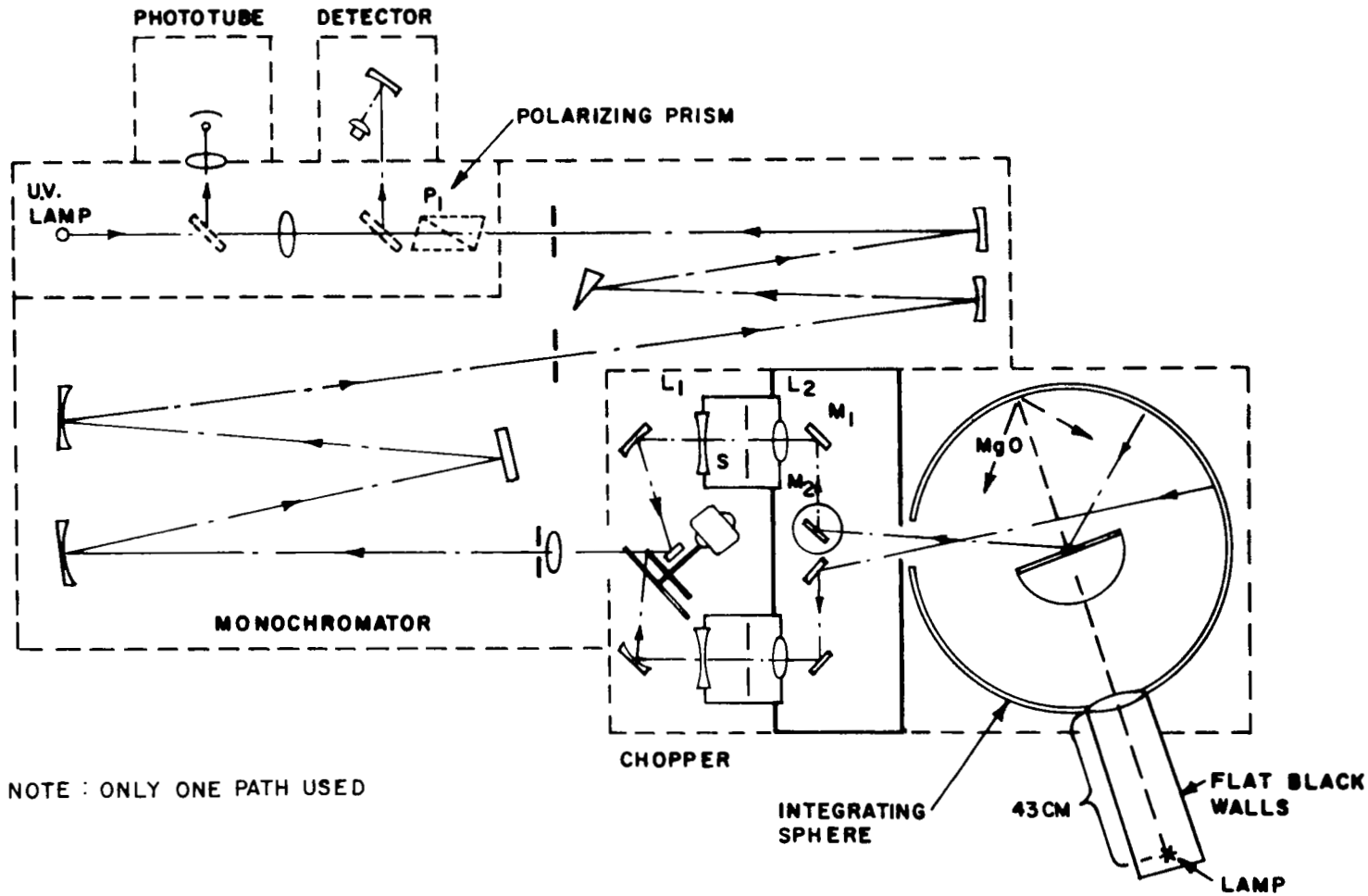

FIG. 6 : OPTICAL SCHEMATIC OF CARY MODEL 14 AND INTEGRATING SPHERE ATTACHMENT

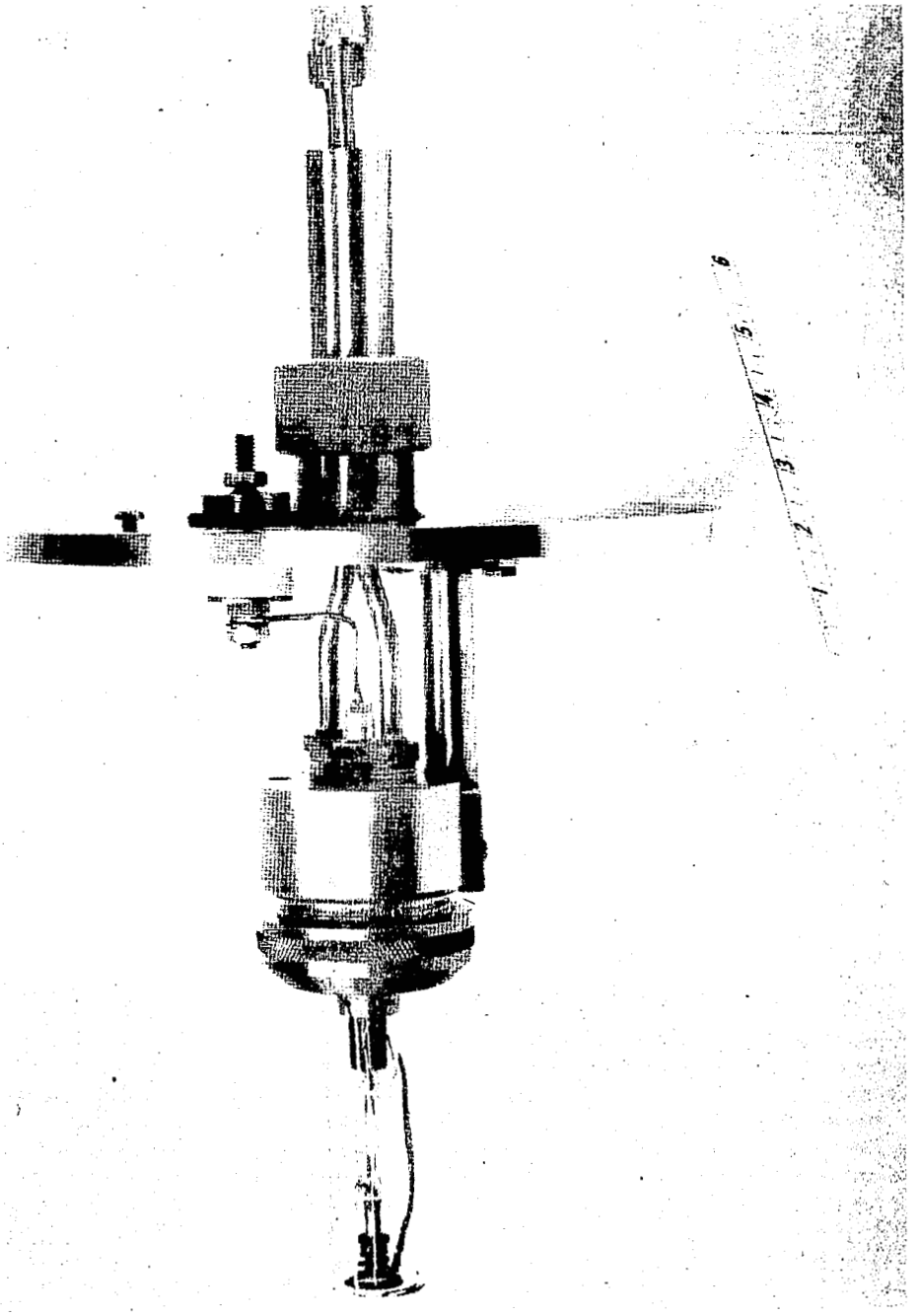

FIG. 7 : WATER-COOLED GENERAL ELECTRIC AH-6 HIGH INTENSITY MERCURY ARC SOURCE WITH QUARTZ MANTLE AND VELOCITY TUBE, ADAPTED TO VACUUM OPERATION

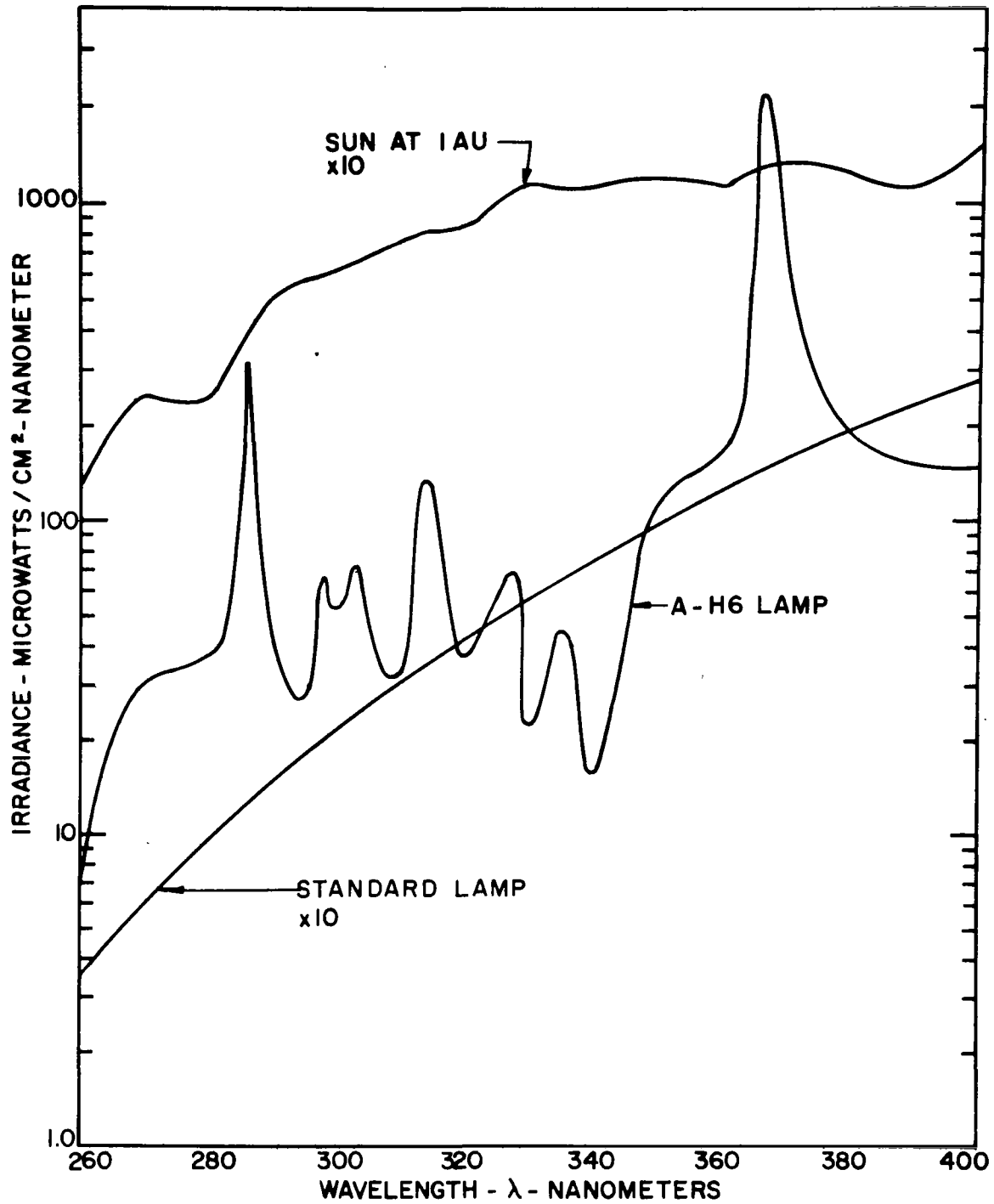

FIG. 8: MERCURY ARC CALIBRATION CURVE

$$\left(\text{Irradiance}_{\text{A-H6}}\right)_{\lambda} = \left(\text{Irradiance}_{\text{N.B.S.}} \times \frac{\text{Intensity}_{\text{A-H6}}}{\text{Intensity}_{\text{N.B.S.}}}\right)_{\lambda}$$

In turn, this irradiance was compared wavelength for wavelength with the irradiance of the sun. For ease of calculation, the irradiance for both the sun and the lamp was summed in small bands ($\Delta\lambda$) and then the bands were compared (see Table V), a technique which eliminates the need for a computer calculation.

The total irradiation of the lamp in the 0.22 to 0.40μ spectrum divided by the total irradiation of the sun for the same range gives an equivalent sun value for the lamp. However, in the study of the effects of radiation on materials, the energy of the interacting photons are important as well as the total number of photons, and the energies of the photons, of course, vary with the wavelengths. Thus one milliwatt per cm^2 of 0.3μ radiation is not the same as one milliwatt per cm^2 of 0.2μ radiation as far as the deterioration of materials is concerned. It is because of this effect that radiations of wavelengths greater than 0.4μ are essentially ignored. Also, spectral mismatches exist between the sun and the lamp being used to simulate the sun. Hence, the lamp spectrum is not a simple multiple of the solar spectrum. The real equivalency between the lamp and the sun would thus vary depending upon the effects being measured and the nature of photon energies with respect to those effects. Since these relationships are not known, the real equivalency cannot be determined. However, for those effects which exhibit a lower frequency cutoff or threshold level, it can be assumed that any effect seen with a low energy photon will occur with a higher energy photon. Thus, if the averaging of the radiation energy of the lamp is done in such a way that

Table V. Calculated Equivalent Sun Hours from G.E. AH-6 Lamp

Wavelength Band Micron	Lamp Irradiation (1) Watts/cm^2	Sun Irradiation (2) Watts/cm^2	Lamp/Sun	% of Sun's Power in Band	ES x Fraction of Sun's Power in the Band	Average Quantum Energy in the Band, ev
.22 - .24	0.0063	0.000098	64.286	0.78	0.50	5.39
.24 - .26	0.0437	0.000154	283.766	1.22	3.46	4.96
.26 - .28	0.0387	0.000434	89.171	3.44	3.07	4.59
.28 - .30	0.0705	0.001008	69.940	7.99	5.59	4.28
.30 - .32	0.1320	0.001442	91.540	11.43	10.45	4.00
.32 - .34	0.0627	0.002156	29.082	17.09	4.97	3.76
.34 - .36	0.0331	0.002338	14.790	18.53	2.74	3.54
.36 - .38	0.1179	0.002548	46.272	20.20	9.35	3.35
.38 - .40	0.0412	0.002436	19.913	19.31	3.85	3.18
	0.5461	0.012614		99.99	43.98	

(1) At a distance of 2.5 inches from lamp

(2) At one Astronomical unit

Ratio of watts/cm^2 over spectrum = $\frac{0.5461}{0.012614}$

= 43.29

the energy associated with the higher energy photons is always used to fill in the gaps in the spectrum for the lower energy photons, a minimum equivalent sun value will be established. The 43 to 44 equivalent sun value (ES) calculated in Table V for an effective lamp distance of 2.5 inches meets this minimum value requirement, at least within the chosen wavelength bands used in the calculation. The column "Lamp/Sun" in Table V indicates how the ES value may vary if specific effects were limited to specific ranges of wavelengths. These ES values would be more appropriate where the cutoff frequency was high, or where resonance or peak absorption was occurring.

An assumption was made that the entire ultraviolet range was essentially effective, and that the ES value could be essentially represented by a ratio of total irradiance. With this assumption, the ES value at a distance of 8.5 inches, the actual working distance of the lamps, was calculated to be approximately 3.75. With two lamps being used, a total of 7.5 ES would yield approximately an ES value of 7 on a surface tipped at $22\frac{1}{2}^{o}$.

These mercury arc lamps are not identical with respect to their intensities, and degrade with age. Variances as large as 20% would be expected due to these causes. Because of these potential errors, small factors such as transmission losses through the vacuum chamber windows were not calculated. The larger errors were kept to a minimum by replacing the lamps approximately every 24 hours.

g. *Sample Chamber*

A major factor in the design of this facility has been the ultraviolet irradiance of the sample. The flux density of the particle beam is essentially constant with increasing distance from the source

since the beam is parallel, but the UV radiation proceeds from a point source and its power density decreases as the inverse square of the distance from the source.

The initial aim was to create a UV device with an acceleration factor of 10 which would permit the completion of a 30 day equivalent exposure in 3 days. The belief was that such an acceleration would not introduce irradiation rate effects into the degradation mechanism nor would it violate the accelerator's minimum current level in supplying the necessary particulate flux density.

As an alternative to the use of the GE mercury arc as a UV source, tungsten-iodine lamps were investigated since they operate at very high temperatures and emit significant quantities of UV radiation, the spectrum of which is a smooth continuum similar to that of the sun. However, calculations of their UV irradiance indicated the necessity for using a large number of these lamps at short distances from the target, making it impossible to achieve simultaneous particulate and UV irradiation. The final decision was to use 2 mercury-arc lamps at a distance of approximately 8.5 inches from the sample target as discussed in Section III, 2.f.

In the ideal case the particulate and UV radiations should strike the samples simultaneously and from the same direction but the constraints imposed upon a laboratory simulation obviate this procedure since one radiation beam would have to be transmitted through the other beam's source in such case. If the UV source was of sufficient power to permit its removal an appreciable distance from the target or if it radiated a parallel beam, both beams could be caused to impinge normally on the

samples. But for currently available UV sources these criteria are not met. To cause both beams to impinge on the window sample as close to perpendicularity as possible, it was decided to have each beam strike the sample with an incident angle of $22\frac{1}{2}^{o}$ off the normal, as illustrated in Figure 9.

The sample holder was designed with eight positions, six of which hold prism and window samples (each position holds a prism and coated window sample of a different material), one of which is for the Faraday cup and the last holding three uncoated window samples to be irradiated end-on for a transverse damage test. The sample wheel in the chamber is shown in Figure 10. Figure 11 presents a plan and side view of the rotating sample holder. No fabrication problems were encountered in building the sample holder dish, which was made of aluminum to reduce the load on the cantilevered shaft.

Two high pressure mercury arc lamps, General Electric A-H6 were mounted external to the vacuum system, approximately 8.5 inches from the sample target (Figure 7). Mounting the lamps externally permitted lamp replacement during a test run without interruption or subjection of the samples to atmospheric pressures (Figure 12).

The ultraviolet beam was directed through a window in the vacuum chamber. The window was G.E. Type 106, UV transparent quartz (greater than 90% transmission down to 0.2μ). As noted, the beam impinged upon the specimen at an angle of 22.5^{o} from normal.

The arrangement of number, type, distance and angle resulted in an equivalent sun value of approximately 7. (Section III, 2.b. discusses the determination of the equivalent sun value and its relation to the simulation of actual space environment.) Each lamp was individually controlled and

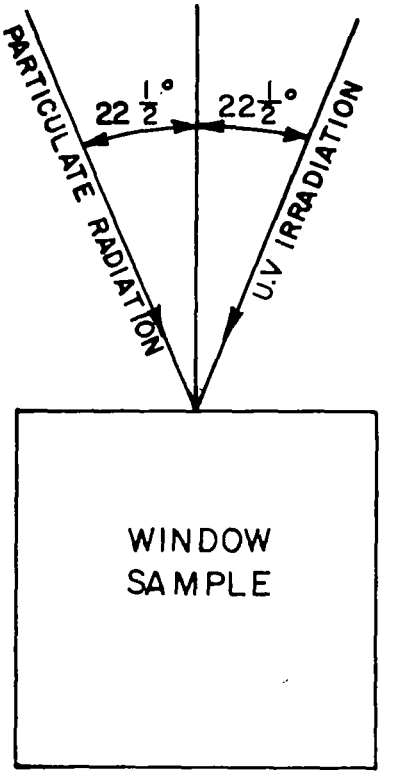

FIG. 9 : SCHEMATIC REPRESENTATION OF RADIATIONS INCIDENT ON WINDOW SAMPLES

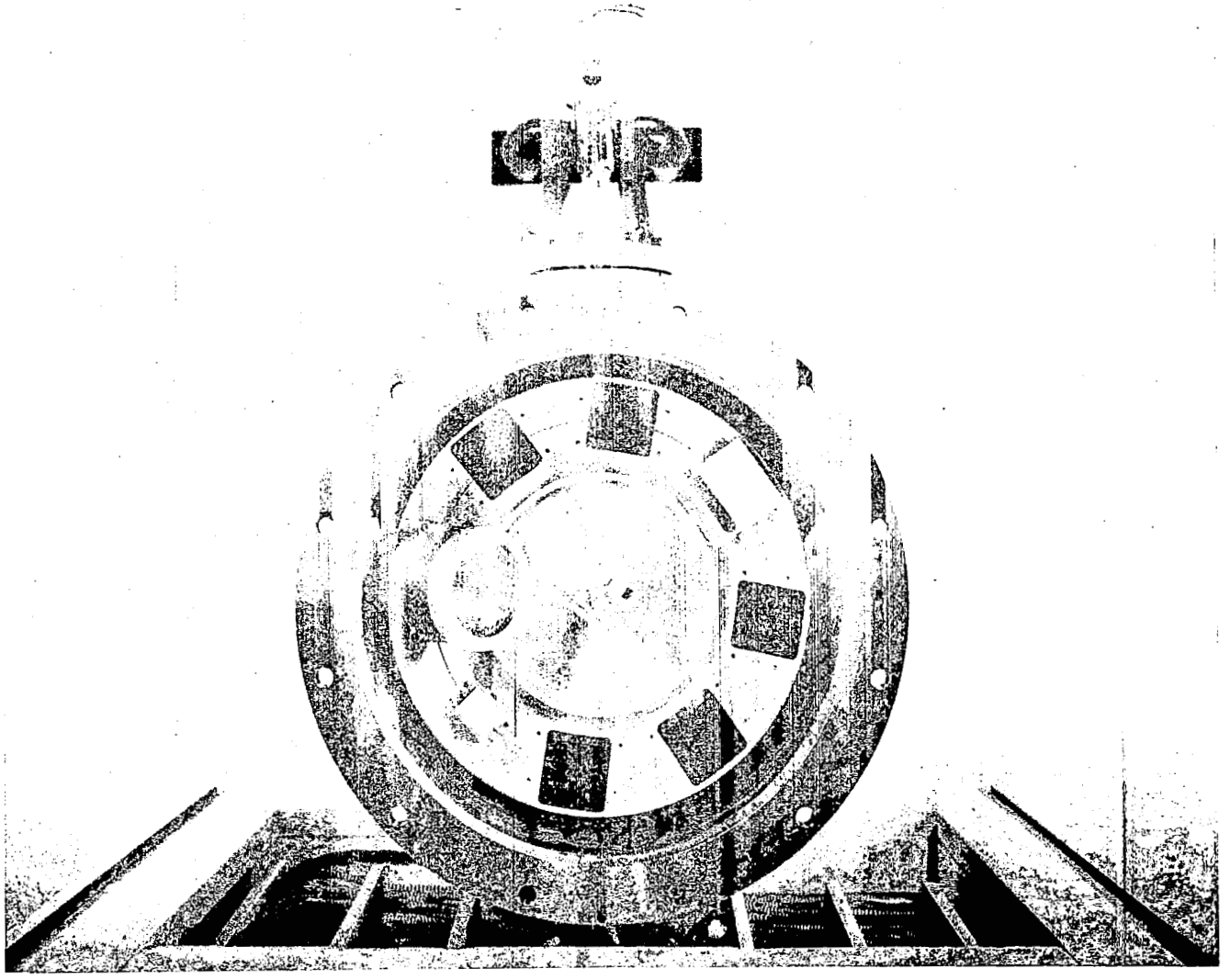

FIG. 10 : SAMPLE WHEEL IN CHAMBER

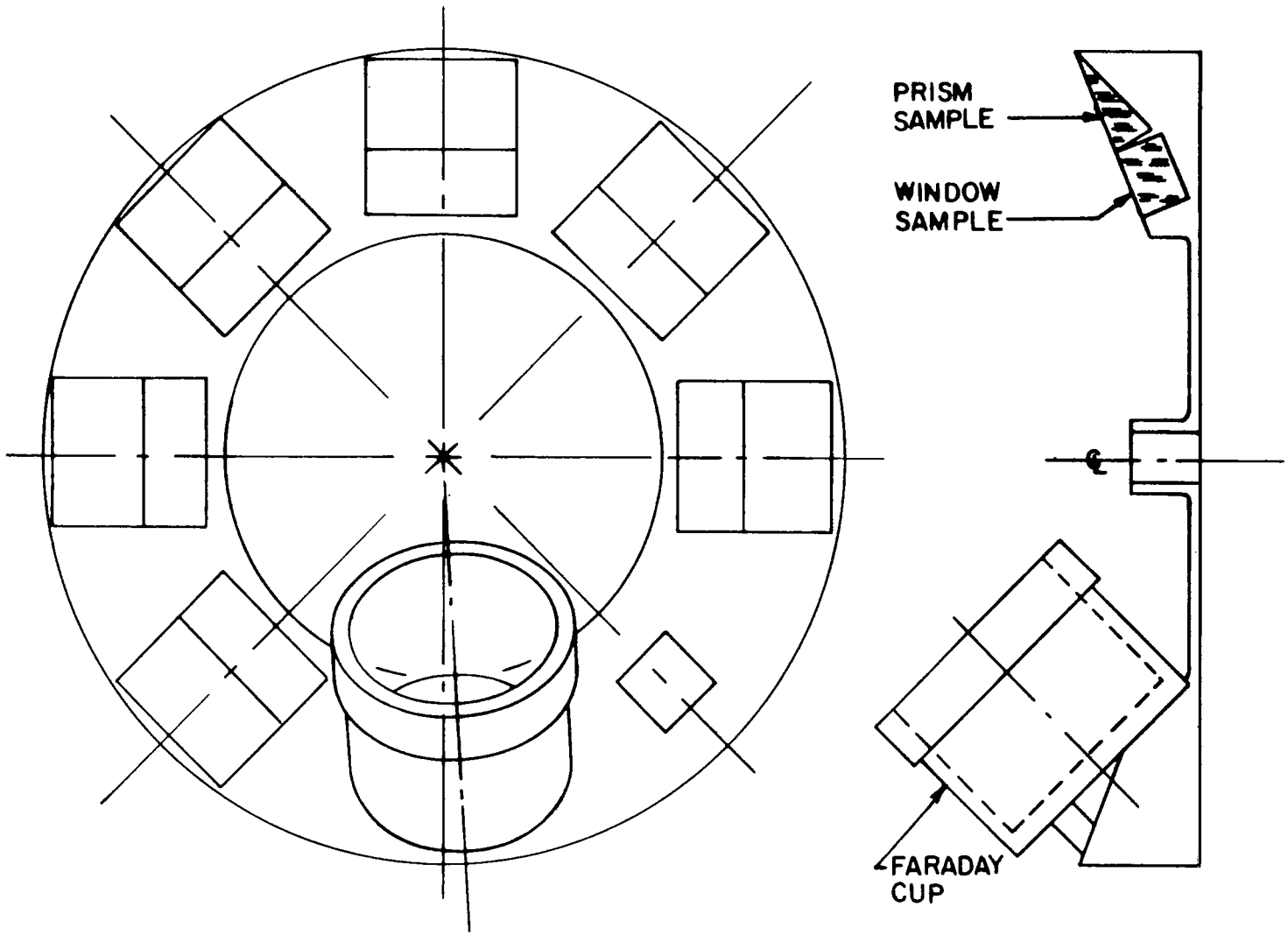

FIG. II : ROTATING SAMPLE HOLDER

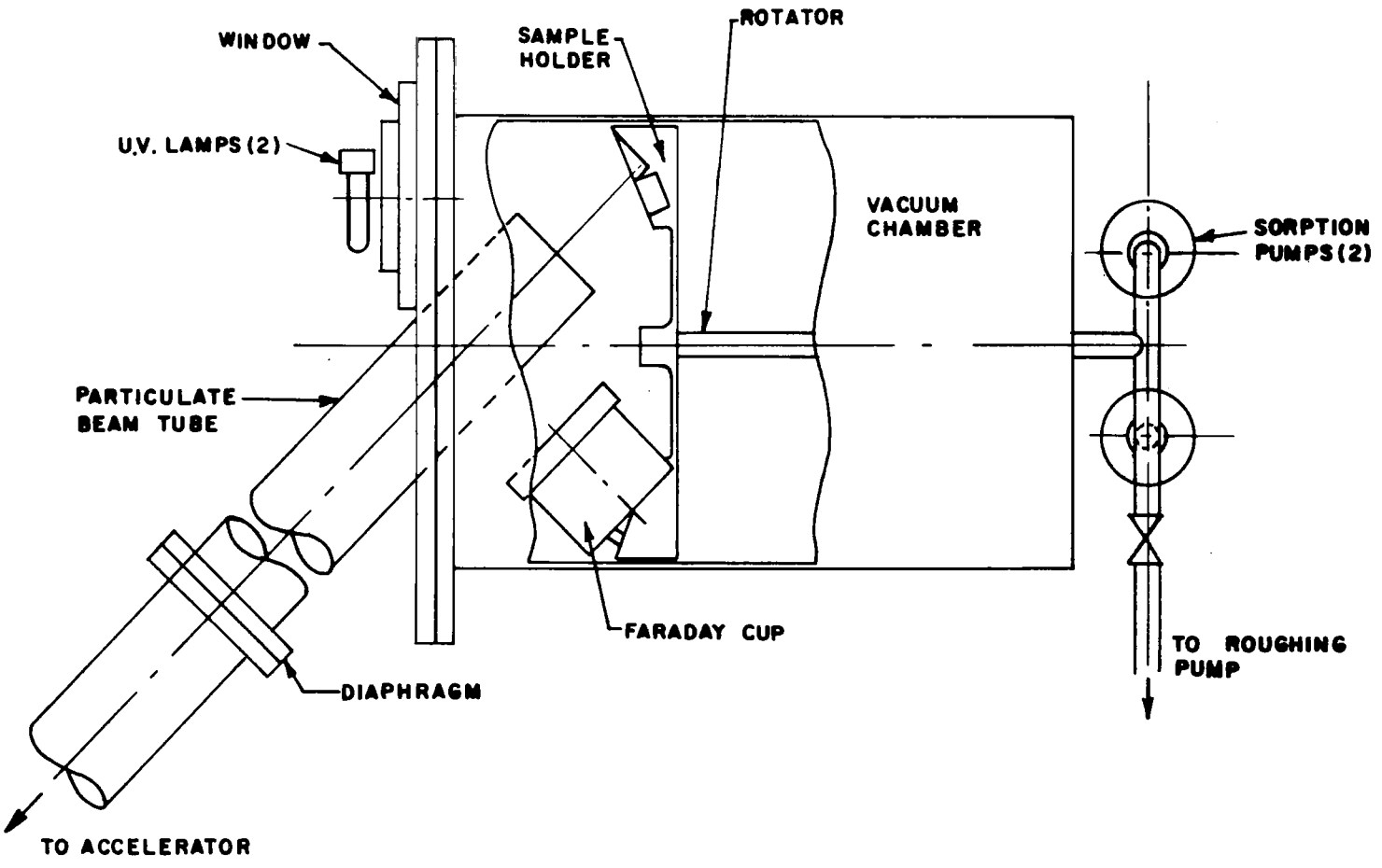

FIG. 12 : SAMPLE CHAMBER SCHEMATIC

they were assumed to be point sources of light at the distances being used.

The vacuum system for the facility was a 400 liter/sec Varian ion pump with a 12 x 18 inch stainless steel chamber (see Figure 13). Except for teflon coated wire leads for the Faraday cup and Viton "O" rings on the isolation valve, all materials in the chamber were low vapor pressure inorganics (metals or glass). Rough pumping was done by the Dynamitron pumps. A common fore pump was used to obviate a differential pressure across the aluminum foil window, which could cause its rupture. After the absolute pressure was reduced below the rupture pressure of the foil, the connecting roughing line was closed and a liquid N_2 sorption pump completed the rough pumping. The pressure at which transition was made from mechanical to adsorption pumping was sufficient to prevent pump oil from migrating into the chamber and into the samples. The ultimate vacuum capability with the ion pump was in the 10^{-10} torr range.

3. Index of Refraction Measurements

a. Method

The index of refraction of uncoated Apollo window materials was measured using the minimum deviation technique. Measurements were made to determine the apex angle of the prism and the minimum deviation angle as a function of wavelength. These measurements were made at room temperature and elevated temperatures on non-irradiated samples and at room temperature on irradiated samples.

A collimated beam is incident on the sample prism. The collimator is adjusted so that the entrance and exit slit are in coincidence. The prism is rotated until the coated face is perpendicular to the incident

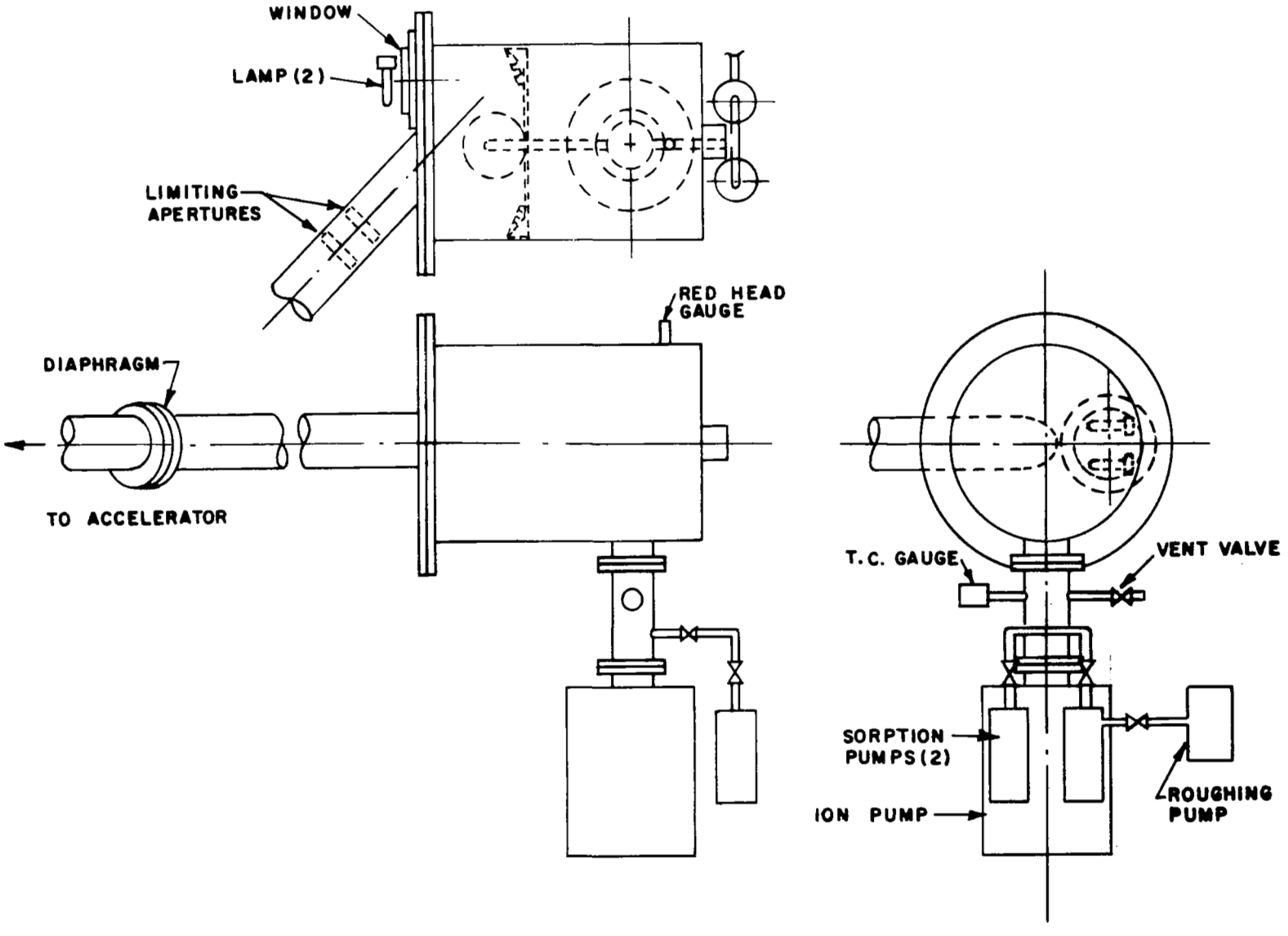

FIG. 13 : PUMPING ARRANGEMENT

beam in which position the energy emerging from the exit slit is a maximum. The prism is then rotated until the uncoated face is perpendicular to the incident beam and another maximum obtained. The angular difference between these two positions of the prism is the apex angle θ of the prism.

Next the prism is rotated until energy of wavelength λ is a maximum at the exit slit. In this position, incident energy of wavelength λ enters the entrance slit, is collimated, is refracted at the uncoated prism face, is reflected at normal incidence at the coated prism face, is refracted again at the uncoated face, and retraces the incident path, emerging at the coincident exit slit (Figure 14). The angular difference between this position and the position at which the uncoated face is perpendicular to the incident beam is the minimum deviation angle ϕ.

From Snell's law we have

$$n_\lambda = \frac{\sin \phi_\lambda}{\sin \theta} \quad .$$

b. The Apparatus

A Perkin-Elmer model 112UG grating spectrometer was modified and used as the collimator. To obtain coincidence between the entrance and exit slits, the optical path length from the collimating parabola to the exit slit had to be lengthened. This was accomplished by inserting two mirrors (M_1 and M_3) in the optical path from the exit slit to the parabola (Figure 15). Only half the entrance and exit slits are used. Incident energy enters the upper half of the entrance slit, passes over mirror M_1, and is reflected and collimated by the parabola M_2. After reflection at the sample, the collimated beam is focused by the parabola and is reflected by M_1 and M_3 onto the exit slit. Parabola M_2 is adjusted to focus the

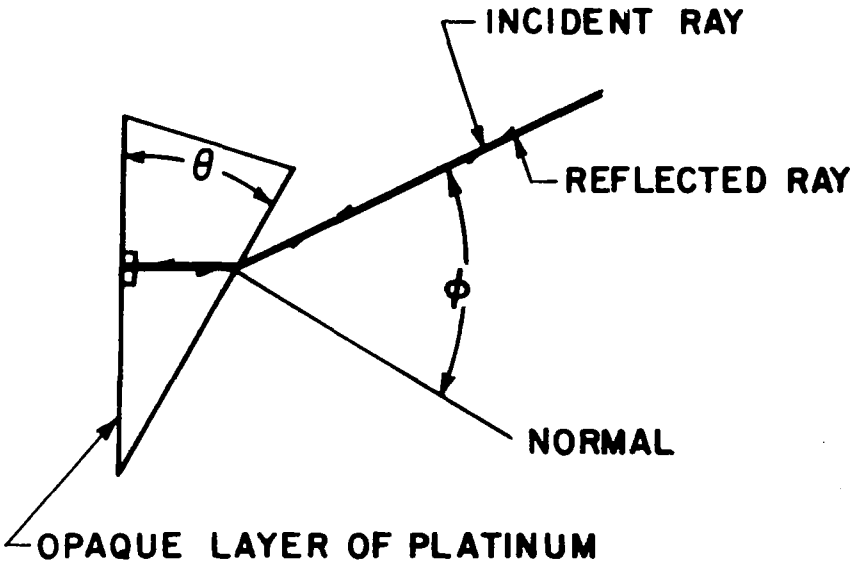

FIG. 14 : RAY DIAGRAM AND PRISM GEOMETRY

entrance slit simultaneously on itself and on the exit slit, and the angular positions of M_1 and M_3 are adjusted so the entrance and exit slits are in coincidence. This adjustment is made as follows. The parabola M_2 is slightly tilted to permit a fraction of the energy returning to M_1 to pass over the top of M_1. When an optical flat is positioned perpendicular to the collimated beam, the energy passing over M_1 forms an image of the entrance slit at the entrance slit, and the portion reflected by M_1 forms an image of the entrance slit at the exit slit. M_1 and M_3 are adjusted so that when the image at the entrance slit is in coincidence with the entrance slit, the image at the exit slit is in coincidence with the exit slit. The grating is removed from the instrument and the grating drive is not used for the angular measurements.

To accommodate high temperature measurements, a water cooled cylindrical vacuum tank containing a concentric insulated heater core was used. The heater was made of platinum wire. A fused silica window at one end of this tank permitted the collimated beam to enter and leave. The axis of the tank is parallel to the collimated beam. The sample prism is mounted on a holder within the heater core. The holder was made of Grade A LAVA manufactured by the American Lava Corporation. This material was chosen for its low thermal coefficient of expansion, (about the same as that of Apollo window materials) its low thermal conductivity, and its mechanical strength at high temperatures. The shaft of the prism holder is coupled to a copper drive shaft which passes through the bottom of the cylindrical vacuum tank through an O-ring seal. The vertical (rotational) axis of the prism holder is perpendicular to the axis of the tank. The angular position of the prism was controlled by a precision rotary table coupled to the prism holder shaft. An Imperial No. 8216 ultra precision rotary table

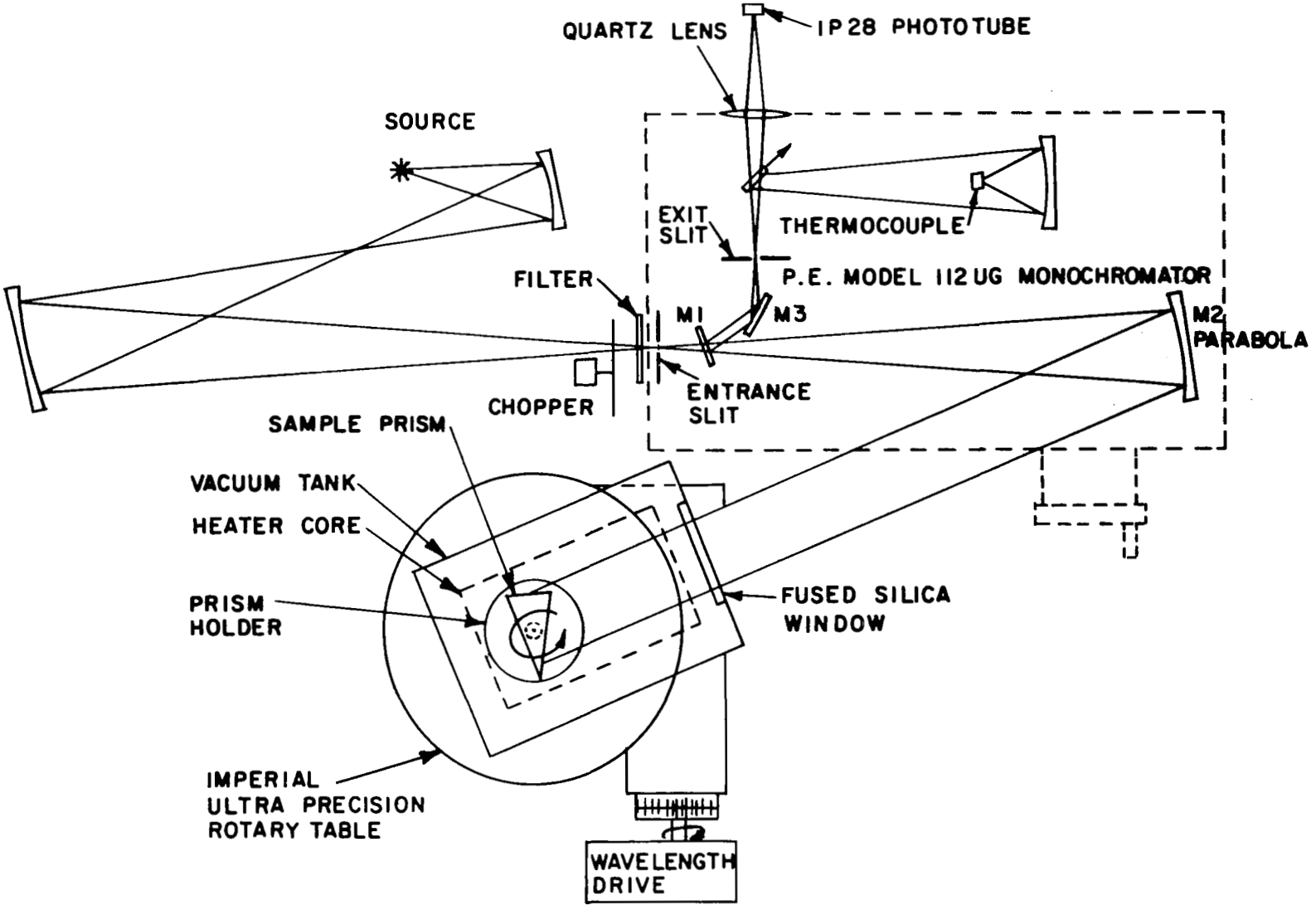

FIG. 15 : MODIFIED PERKIN ELMER 112UG MONOCHROMATOR AND ROTARY TABLE FOR REFRACTIVE INDEX MEASUREMENTS

with an indexing accuracy of ±5 seconds was employed.

The three angular positions (coated face, uncoated face, and refraction angle) were determined as follows. The wavelength drive assembly for a Perkin-Elmer Model 12 spectrometer was modified by substituting a drive motor whose speed is 1/4 rpm. The modified drive assembly was coupled to the drive of the rotary table. The reduced speed of the drive resulted in a scale of approximately 2 seconds of arc per millimeter paper travel of the Leeds and Northrup recorder used with the Perkin-Elmer spectrometers. Further, the drive speed was sufficiently slow to permit reading the rotary table angular position on its vernier dial every second of arc. Ten second markers were placed on the recording chart by manually operating the pip-marker switch on the wavelength drive assembly while observing the vernier dial. The detector output was processed in the manner commonly used with the Perkin-Elmer Model 12 spectrometer.

The prism position was manually adjusted to the angle at which the coated face was approximately perpendicular to the collimated beam. The drive assembly was then engaged and the prism was slowly scanned through the angle at which its coated face was perpendicular to the beam. When perpendicular, the energy emerging from the exit slit is a maximum with resultant maximum pen deflection. In this manner we obtain a recording similar in appearance to a spectrometer recording with angular calibration superimposed by the manually energized 10 second pip-markers. A similar recording is obtained for the uncoated prism face. For all wavelengths less than 2 microns, the spectral lines of a General Electric AH-4 mercury lamp with envelope removed were used for wavelength calibration. The spectrum was scanned by the drive assembly with added calibration markers resulting in a recorder trace similar to that of a conventional prism spectrometer. Above 2 microns, narrow band interference filters, in

conjunction with a globar source, were used for the wavelength calibration. From 0.2 to 0.6 microns a 1P28 phototube was used as the detector. Above 0.6 microns a thermocouple detector with CsBr window was used. The angular positions of the prism faces and refraction angle were determined from the center of the peaks on the recorder trace. Linear interpolation was used between the 10 second markers.

A thermocouple was installed on the inside of the heater wall close to the prism. This thermocouple was calibrated by installing a second thermocouple in a hole drilled through a sample prism, and measuring prism temperature versus heater wall thermocouple temperature. Platinum-Platinum +10% Rhodium thermocouples were used with a $0^{o}C$ reference junction. A Leeds and Northrup type K-3 Universal Potentiometer was used to measure thermocouple emf.

c. Experimental Error

A statistical analysis of all data taken was used to determine the experimental error. Both a systematic and non-systematic error were encountered.

The non-systematic error arises from random noise in the detectors and amplifiers, from temperature fluctuations in the sample and instrument, from vibration, and from statistical fluctuations in the rotary table readout. An analysis of 178 coated face measurements showed a Gaussian distribution with a standard deviation $\sigma_c = 2.28$ seconds of arc. Similarly for the uncoated face, 179 measurements resulted in a standard deviation $\sigma_{uc} = 2.62$ seconds. For the refraction angle 87 measurements resulted in a standard deviation $\sigma_r = 3.47$ seconds. In reducing the data, the estimated error is $\sigma_d = 0.50$ seconds. The effective error resulting from the observer manually

energizing the pip-marker at 10 second intervals is estimated to be $\sigma_o = 0.20$ seconds.

The systematic error was determined by comparing the results of reproducibility measurements. Twenty-three such comparisons were made. Reproducibility in the index of refraction for a given prism under the same environmental conditions was found to range from -62 to +59 x 10^{-5}. The 23 values obtained within this range are not Gaussian distributed, as expected. The mean absolute deviation $\overline{|\delta_n|}$ for these 23 measurements is 21 x 10^{-5}. A study of the data indicated that this value is more indicative of the experimental systematic error than the standard deviation and so was used. The systematic error arises principally from the extreme difficulty encountered in resetting and maintaining the prism fixed with respect to the optical axis of the instrument. Small vibration, temperature changes, expansion of the prism holder with temperature, change in parabola focus with prism and sample cell window temperature, and rotary table accuracy all contribute to this error.

As shown in Table VI, the estimated experimental error in refractive index $\delta_n = 23.2 \times 10^{-5}$.

4. Transmittance Measurements

a. Method

All room temperature transmittance measurements were made on a Cary Model 14 spectrophotometer from 0.2 to 2.5 microns and on a Beckman IR4 spectrophotometer from 2.5 to 15 microns. In the overlapping spectral range, 2 to 2.5 microns, of these two instruments differences in transmittance of ±8% were observed.

TABLE VI

Error in Refractive Index Measurements

$\overline{|\delta_n|}$ = mean absolute deviation in n 21×10^{-5}

$\sigma_c = 2.28"$ $\quad \sigma_\phi = (\sigma_r^2 + \sigma_{uc}^2 + \sigma_d^2)^{\frac{1}{2}} = 4.38"$

$\sigma_{uc} = 2.62"$ $\quad \sigma_\theta = (\sigma_c^2 + \sigma_{uc}^2 + \sigma_o^2)^{\frac{1}{2}} = 3.51"$

$\sigma_r = 3.47"$

$\sigma_n = n(\cot \phi\ \sigma_\phi + \cot \theta\ \sigma_\theta)$ 9.7×10^{-5}

$\sigma_d = 0.50"$

$\sigma_o = 0.20"$ $\quad n \simeq 1.5$

$\phi \simeq 37^\circ$

$\theta \simeq 25^\circ$

Experimental Error $\quad \delta_n = 23.2\times10^{-5}$

The Apollo window transmittance samples are thick samples. The thicknesses used were: fused silica, Corning Code 7940-1.784 cm; Vycor, Corning Code 7913-0.378 cm; aluminosilicate glass, Corning Code 1723-0.595 cm. When a thick sample is placed in the sample beam of a spectrophotometer, it materially affects the beam geometry. In general, spectrophotometers use a focused rather than a collimated beam in the sample compartment. The refracting properties of a thick sample alter the beam geometry and the resulting measured transmittance. Spectrophotometer manufacturers attempt to minimize the thick sample effect by incorporating optical systems which are relatively insensitive to the change in beam geometry caused by a thick sample. The optical systems employed vary from manufacturer to manufacturer and one expects different measured values of transmittance depending upon the particular instrument used.

Elevated temperature measurements were made using a single pass system in which a focused beam was employed. The sample was alternately moved in and out of the beam. The beam was passed through a Perkin-Elmer Model 12 prism monochromator and the ratio of the intensity measured with the sample in and out of the beam was initially taken as the transmittance of the sample at a particular wavelength.

Early in the program it was established that the thick samples used were drastically affecting the measured transmittance values. Measurements at a given wavelength were not reproducible within 10% in transmittance. The position of the sample in the beam and the angle of the sample normal to the beam axis were critical.

Neither time nor funds permitted the design and construction of a new vacuum tank-heater core for use with the spectrophotometers used at room

temperature. Alternatively, it was decided to refer all measurements to those made at room temperature with the spectrophotometers.

b. High Temperature Transmittance Apparatus

The optical schematic of the high temperature transmittance apparatus is shown in Figure 16. The vacuum tank contains a heater core in which the transmission sample is placed. The tank slides along its axis on machined ways. The tank axis is perpendicular to the incident beam axis. The tank may be positioned along its axis to enable measurement of the beam intensity at a given wavelength for the following conditions (Figure 17): (1) I_1 - intensity through tank windows, (2) I_2 - intensity through tank windows and uncoated sample in tank, (3) I_3, I_4 - intensity through tank windows and coated sample in tank (one or two coatings depending on particular sample). It was determined that the incident beam intensity I was sufficiently stable over the short time required to make a set of measurements at a given wavelength.

A Perkin Elmer Model 99 monochromator with calcium fluoride prism was used as the wavelength determining element. This monochromator was calibrated by conventional means. A 1P28 phototube was used as the detector for wavelengths less than 0.6 microns. For the longer wavelengths a thermocouple detector with CsBr window was employed. The detector output was processed in the normal manner for this monochromator and intensity was read directly from the strip chart recorder. In the UV region of the spectrum, a Beckman No. 8333 hydrogen discharge lamp was used as a source. In the visible and infrared region, a General Electric DXW, 1000 watt, Sun Gun was used. These are continuum sources and the wavelength at which a given measurement was made was determined by the monochromator drum setting.

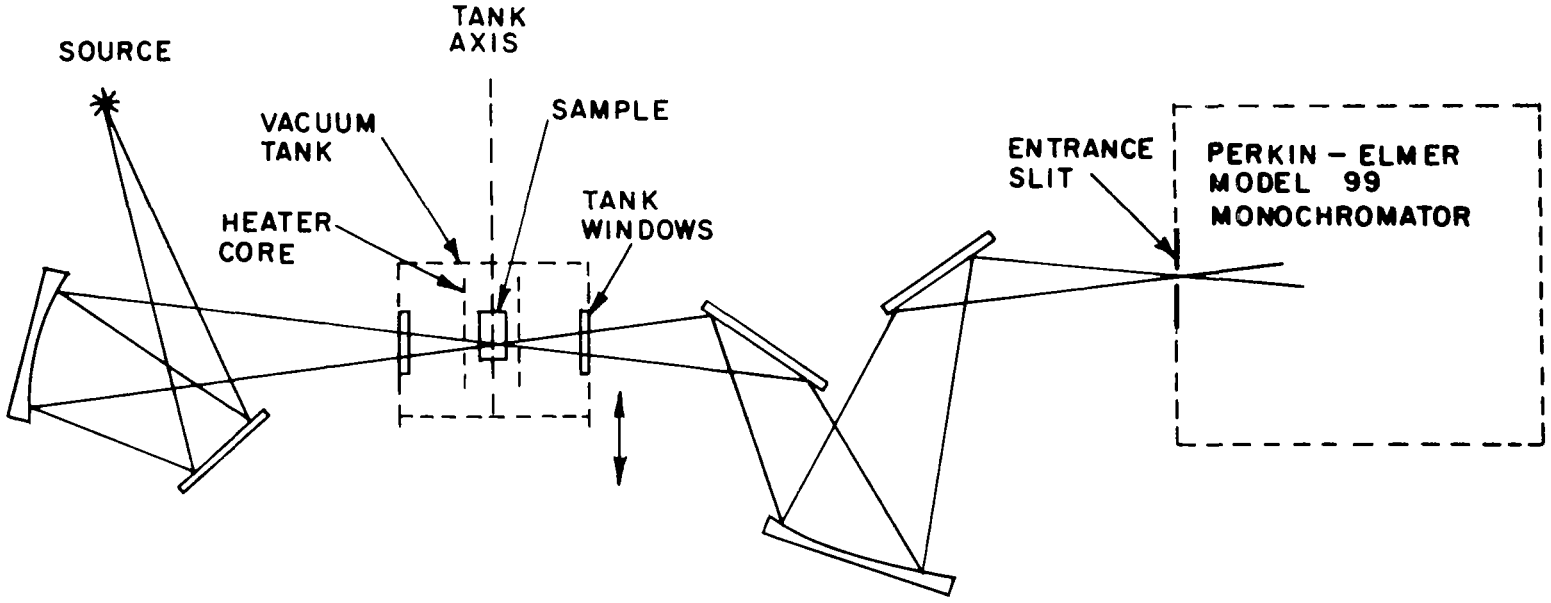

FIG. 16 : OPTICAL SCHEMATIC– HIGH TEMPERATURE TRANSMITTANCE APPARATUS

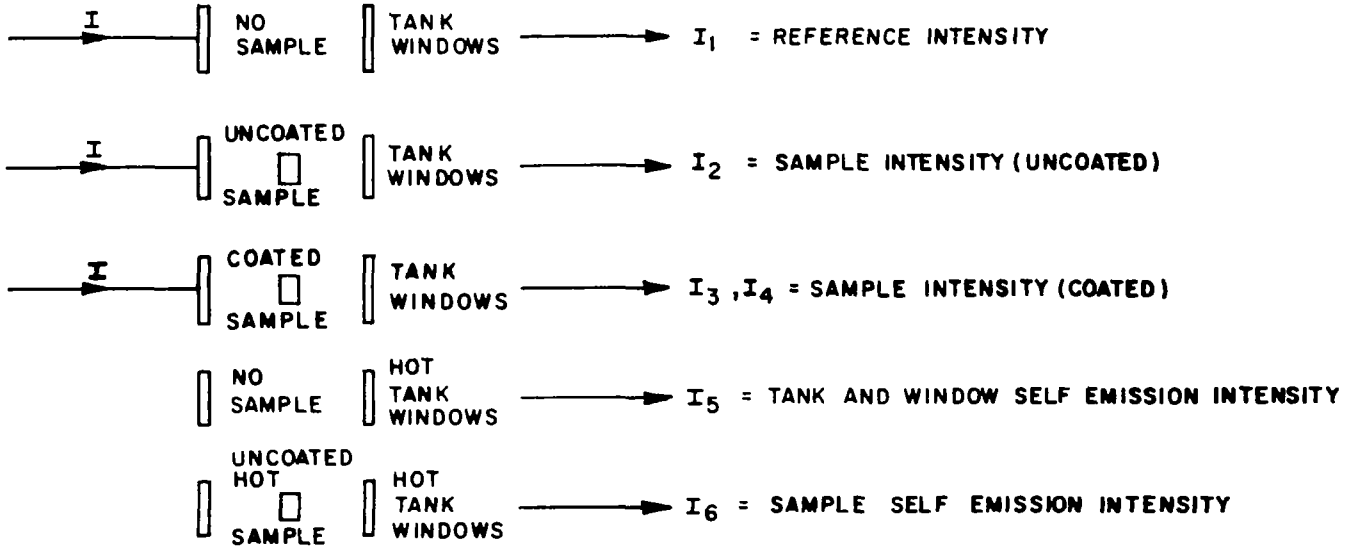

FIG. 17 : BEAM INTENSITY MEASUREMENTS WITH HIGH TEMPERATURE TRANSMITTANCE APPARATUS

c. High Temperature Sample Transmittance

Sample and reference intensities were measured first at room temperature. Then the tank sample was brought up to temperature T and the intensity measurements were repeated. In addition, sample and reference self emission intensities, I_5 and I_6 (Figure 17), were measured. From these measurements, sample transmittance at temperature T, referred to the room temperature Cary 14 and Beckman IR4 measurements, could be determined.

The procedure which follows for computing the hot sample transmittance is necessary because as the sample is heated to a temperature T, several effects occur. At high sample temperatures, the tank window temperature rises appreciably changing their transmittance at a given wavelength. In addition, geometrical changes may occur in the system as a result of window warpage or bending and expansion in the tank and external reference structure. Finally, at high temperatures both the windows and sample emit energy, particularly in the infrared. This energy must be removed from the sample transmitted intensity and from the reference intensity (no sample in beam) to obtain a true value for the sample transmittance.

Though it was originally planned to chop the incident beam ahead of the vacuum tank to eliminate self emission, it was found that stray light was a major consideration in the model 99 monochromator when its internal chopper was not employed. Time prohibited utilization of a double chopping scheme with a high speed chopper at the source, associated amplifier and detector, in addition to the model 99 internal chopper.

The hot sample transmittance was computed in the following way. Primed quantities refer to intensities measured when the sample and tank were hot. Unprimed quantities refer to measured intensities with tank and sample at room temperature. Intensities are those designated in Figure 17.

When the tank and sample are at elevated temperature, the measured sample transmittance is

$$T_S' = \frac{(I_2' - I_6')}{(I_1' - I_5')} \quad . \tag{1}$$

Here self emission has been subtracted from both the hot sample intensity and the hot reference intensity. It is assumed that changes in tank window transmittance and geometry affect both sample and reference beams equally.

With the system at room temperature, the measured sample transmittance is

$$T_S = \frac{I_2}{I_1} \quad . \tag{2}$$

But this value must equal the room temperature values obtained with the Cary 14 and Beckman IR4 spectrophotometers. The system correction factor is therefore the ratio T_R/T_S where T_R is the transmittance measured at room temperature with the spectrophotometers. The corrected value of the hot sample transmittance is then given by

$$T_\lambda' = \frac{T_S'}{T_S} T_R = \left(\frac{I_2' - I_6'}{I_1' - I_5'} \right) \frac{I_1}{I_2} T_R \quad . \tag{3}$$

For the coated samples, I_3' and I_4', are substituted for I_2' in (3). This simple relation was programmed for computer calculation of the high temperature sample transmittance as a function of wavelength.

d. Experimental Error

The experimental error for the Cary 14 and Beckman IR4 room temperature transmittance measurements was found as follows. Five samples of Corning Code 7940 fused silica were cut from the same piece of raw material and processed identically. Room temperature transmittance measurements

were made on all five samples. The mean value of T_λ at each wavelength and the deviation from this mean for each sample was computed. A statistical analysis of this data indicated a Gaussian distribution with standard deviation $\sigma_\lambda = 0.54\%$. Noise on the spectrophotometer traces is estimated to result in an observation error in reading the transmittance values whose standard deviation is $\sigma_o = 0.2\%$.

From the index of refraction measurements, it is possible to calculate the maximum possible sample transmittance as a function of wavelength. This value T_{max} is arrived at by considering that only reflection at the sample-air interfaces affects transmission. Absorption in the sample is assumed zero. Under these conditions

$$T_{max} = \frac{16n^2}{(1+n)^4} \quad .$$

In the transparent (visible) region of the spectrum, the Cary 14 transmittance values were found to be consistently 0.5% higher than T_{max}. This systematic error is most probably due to the thick sample effect.

For the room temperature transmittance measurements the estimated experimental error is therefore

$$+0.5 \pm 0.58\% \quad .$$

In the case of the high temperature transmittance measurements, an additional error arising from inaccuracies in the measurement of the intensities in equation (3) must be considered. Taking the variation of (3) with respect to all quantities one has

$$\frac{\delta T'_\lambda}{T'_\lambda} = \frac{\delta T_R}{T_R} + \frac{\delta I_1}{I_1} - \frac{\delta I_2}{I_2} + \frac{\delta I'_2 - \delta I'_6}{I'_2 - I_6'} - \frac{\delta I'_1 - \delta I'_5}{I'_1 - I'_5} \quad . \tag{4}$$

Below 2 microns (self emission was only found in the infrared beyond 2 microns), normalizing the reference to 1, $I_1 \simeq I_1' \simeq 1$, $I_2' \simeq I_2 \simeq T_R$, $T_\lambda' \simeq T_R$ and $I_5' = I_6' = 0$. In this region (4) becomes

$$\delta T_\lambda' \simeq (\delta T_R - \delta I_2 + \delta I_2') + T_R(\delta I_1 - \delta I_1'), \quad \lambda < 2 \text{ microns} \quad . \qquad (5)$$

The intensity measurements made with the high temperature transmittance apparatus have an estimated standard deviation $\sigma_I = 0.50\%$. Using this value for the δI in (5) one has

$$\delta T_\lambda' \simeq +.5 \pm .9\% \text{ min } (T_R = 0)$$
$$\delta T_\lambda' \simeq +.5 \pm 1.5\% \text{ max } (T_R = .9) \quad .$$

Above 2 microns, $I_1 \simeq I_1' \simeq 1$, $I_2' - I_6' \simeq T_R$, $T_\lambda' \simeq T_R$, $I_1' - I_5' \simeq 0.9$. Under these conditions (4) becomes

$$\delta T_\lambda' = (\delta T_R - \delta I_2 + \delta I_2' - \delta I_6') + T_R[\delta I_1 - 1.1(\delta I_1' - \delta I_5')], \quad \lambda > 2 \text{ microns.} \qquad (6)$$

Using $\delta I = \sigma_I = 0.50\%$, one obtains

$$\delta T_\lambda' \simeq +.5 \pm 1.1\% \text{ min } (T_R = 0)$$
$$\delta T_\lambda' \simeq +.5 \pm 1.9\% \text{ max } (T_R = .9) \quad .$$

It was observed that the self emission intensity of some of the coated samples was apparently greater than that of the uncoated sample in the region $\lambda > 2.5$ microns. This results in an impossibly high transmittance of the coated sample. In these cases, the coated sample transmittance was adjusted to correct for the increased emittance of the coating. Adjusted values are indicated by an asterisk in the results.

The experimental error in sample transmittance is summarized in Table VII.

TABLE VII

Error in Transmittance Measurements

Systematic error in room temperature measurements	+ 0.50%
Nonsystematic error in room temperature measurements	σ_λ = 0.54%
Observation error in room temperature measurements	σ_o = 0.20%
Experimental error in room temperature measurements	δT = +.5±.6%

Systematic error in high temperature measurements	+ 0.50%
Standard deviation in intensity measurements	σ_I = 0.50%
Standard deviation in reference transmittance	σ_R = 0.60%

Experimental error in high temperature measurements

$\delta T'_\lambda$ = +.5 ± .9% min (T_R = 0)	λ < 2 microns
$\delta T'_\lambda$ = +.5 ± 1.5% max (T_R = .9)	
$\delta T'_\lambda$ = +.5 ± 1.1% min (T_R = 0)	λ > 2 microns
$\delta T'_\lambda$ = +.5 ± 1.9% max (T_R = .9)	

5. Extinction Coefficient Calculations

The extinction coefficient as a function of wavelength and temperature was calculated for Apollo window materials from the experimentally determined values of refractive index and transmittance. The relation

$$T = \frac{(1 - R)^2}{e^{\alpha t} - R^2 e^{-\alpha t}} \tag{11}$$

connects the transmittance T, reflectance R, sample thickness t and absorption coefficient α. The reflectance of a material of refractive index n is given by

$$R = \left(\frac{1 - n}{1 + n}\right)^2 . \tag{12}$$

Assuming that $\exp(\alpha t) >> R^2 \exp(-\alpha t)$, which is equivalent to neglecting interreflections, (11) becomes

$$T = (1 - R)^2 e^{-\alpha t} . \tag{13}$$

Solving for αt one has

$$\alpha t = \ln\left[\frac{(1 - R)^2}{T}\right] = \ln\left[\frac{16n^2}{T(1 + n)^4}\right] . \tag{14}$$

Because of interreflections, the value of αt thus obtained is somewhat too small. A computer is programmed to increase αt in small steps until a value of αt is found which satisfies (11). Finally the extinction coefficient K is found from αt by the relation

$$K = \frac{(\alpha t)\lambda}{4\pi t} . \tag{15}$$

The quantities T and n have been measured as a function of λ and the thickness t of the samples was also measured.

This method of determining extinction coefficient suffers from the same drawback encountered when one calculates absorptance from reflectance. That is, a small error in reflectance, when the reflectance is high, results in a large error in absorptance. Similarly, when the transmittance is high, a small error in transmittance results in a large error in extinction coefficient. The situation here is considerably worse than encountered in the reflectance-absorptance analogy as we here deal with a logarithmic function. From (14) and (15) one finds for the fractional variation in K

$$\frac{\delta K}{K} = \frac{\left[2\left(\frac{n-1}{n+1}\right)\frac{\delta n}{n} + \frac{\delta T}{T}\right]}{\ell n\left[\frac{16n^2}{T(1+n)^4}\right]} + \frac{\delta\lambda}{\lambda} - \frac{\delta t}{t} \quad . \tag{16}$$

The contribution of the last two terms is very small. However, in the transparent region of the sample, the argument of the logarithm is $\simeq 1$ (no absorption, only reflection) which means the denominator of the first term is very small of the order 10^{-2} to 10^{-3}. The error in the refractive index measurements was shown to be very small, of the order 10^{-4}, and contributes little to the first term. But, the error in sample transmittance measurements was shown to be much larger, of the order 10^{-2}. One easily sees that errors in K of 100% are indeed obtained under these conditions. In fact, a 40% error in K in the high transmission region requires a precision in the determination of T of about 0.1%. In contrast an error of .01% in n results in an error of only .004% in K.

In summary, the computed values of extinction coefficient must be viewed with caution. In the ultraviolet and infrared regions, where the sample transmittance is low, the error in K is small, 1 to 2%. However, in the visible region, where sample transmittance is a maximum the error in K may be several hundred percent. In those cases (visible region of

spectrum) where the observed transmittance T was greater than the maximum possible transmission $16\ n^2(1+n)^4$ based on refractive index, the value of T was reduced so as to be slightly below this maximum possible value. This is necessary to insure that the argument of the logarithm is greater than unity or a negative extinction coefficient (impossibility) results. The reduction in the observed value of T was always within experimental error.

IV. RESULTS AND CONCLUSIONS

1. Refractive Index

The results of the refractive index measurements are given in Tables VIII through XIII. For fused silica, within experimental error, the room temperature results before irradiation, Table VIII, agree well with those of Malitson.[43] The rate of change of n with temperature for fused silica lies between the values given by Malitson[43] and L. Prod'homme[44] and within experimental error agrees well. The linear change in refractive index with temperature for fused silica as reported by L. Prod'homme[44] is verified. Values of n and $(dn/dT)/^{\circ}C$ for non-irradiated aluminosilicate glass and Vycor are given in Tables IX and X. An attempt was made to measure the refractive index of Corning code 1723 aluminosilicate glass at $826^{\circ}C$. This is above the annealing point, $710^{\circ}C$, for this glass and deformation of the prism rendered the measurement impossible. The rate of change of refractive index with temperature was not found to be constant for the Vycor sample over the $800^{\circ}C$ temperature range considered. Though containing a very high percentage of fused silica, the difference in this characteristic from that of the fused silica sample is probably due to impurities present in Vycor.

Measured values of refractive index before and after the 30 day space equivalent irradiation for the three materials are presented in Tables XI through XIII. Within experimental error, no change of refractive index as a result of the 30 day irradiation can be concluded. This is not surprising as the expected magnitude of the change in refractive index due to radiation exposure is about 1/4 the experimental error.[37] Certainly one may conclude that no change in refractive index due to irradiation occurred to the 3rd decimal place for any of the materials tested. Further refractive index measurements on irradiated samples either at higher temperatures or after shorter exposures were deemed unnecessary as a consequence of the 30 day exposure results.

Only a very slight darkening of the fused silica and Vycor prisms was noticed after the 30 day irradiation. Charged particle discharge patterns, Lichtenberg figures, were clearly visible in the aluminosilicate glass sample only.

2. Transmittance

Figures 18 through 28 present the results of the room temperature transmittance measurements made with the Cary 14 and Beckman IR-4 spectrophotometers. These figures were reduced from tracings of the spectrophotometer recordings. One observes a sizeable reduction in transmittance of all three materials in the ultraviolet region of the spectrum and very little change in the infrared region. The lowered transmittance of the coated samples after irradiation follows that of the uncoated samples indicating that the increased absorption results mainly due to changes in the bulk material rather than the coatings. Little visible darkening was noted in any

of the irradiated samples. Charged particle discharge tracks were noted only in the aluminosilicate glass sample which had been subjected to the 30-day space equivalent irradiation dose.

The results of the high temperature transmittance measurements for non-irradiated and irradiated samples are presented in Tables XIV through XIX. Measurements were made at 526°C and 826°C for all samples. One must view with caution the results for the coated samples. The anti-reflectance coatings begin to deteriorate in the neighborhood of 550°C and 10^{-4} mm Hg. This deterioration manifests itself in color changes in the coatings and flaking off of the coatings from the bulk sample. The degree of deterioration is a function of time at a given temperature and pressure. No attempt was made during the course of transmittance measurements to bring all samples to the measurement temperature in a uniform manner, nor to hold the samples at a given temperature for the same period of time. Therefore, the results of the transmittance measurements for a coated sample, depend upon the state of the coating at the time the measurement was made. One cannot correlate the resultant transmittance at 826°C, for example, between an irradiated and non-irradiated coated material, as the state of the coating may be quite different. Further, attempts to correlate the measured transmittance at 526°C and 826°C for a coated sample suffer the same difficulty.

The results of all the transmittance measurements agree qualitatively with what one would expect. The effect of ionizing radiation in lowering the transmittance in the ultraviolet region is clearly demonstrated. The lowering of transmittance in the infrared region as temperature is increased is also evident. Since no attempt was made to separate the effects of irradiation by ultraviolet photon, electrons, and protons, one can only view the

gross effects of the radiation exposure. Increased optical absorption in the ultraviolet resulting from ionizing radiation lowers the transmittance in the UV and visible region of the spectrum, but apparently the increased absorptance of the ultraviolet bands is not sufficiently high to affect refractive index. Because the high temperature transmittance measurements were made at specific wavelengths rather than over the entire transmission band, it was not possible to verify the shifts in the infrared absorption bands reported by Edwards.[45] However, the decrease in transmittance with temperature at the UV band edge and in the infrared is clearly demonstrated.

3. Extinction Coefficient

The extinction coefficients for the Apollo window materials as a function of temperature are given in Tables XX through XXV. Values are given for both non-irradiated and the 30-day space equivalent irradiated samples. The extinction coefficient was computed for the uncoated sample only as this constant has no meaning for a coated sample. Measured values of transmittance and refractive index were used for the computation.

TABLE VIII. Fused Silica-Corning Code 7940, Ultraviolet Grade-Refractive Index vs. Temperature, Non-Irradiated.

λ Microns	n 26°C	n 471°C	(dn/dT)/°C x 10^6	n 828°C	(dn/dT)/°C x 10^6
0.23021	1.52034	1.52908	+ 19.6	1.53584	+ 19.3
0.23783	1.51496	1.52332	+ 18.8	1.52985	+ 18.6
0.2407	1.51361	1.52201	+ 18.9	1.52832	+ 18.3
0.2465	1.50970	1.51774	+ 18.1	1.52391	+ 17.7
0.24827	1.50865	1.51665	+ 18.0	1.52289	+ 17.8
0.26520	1.50023	1.50763	+ 16.6	1.51351	+ 16.5
0.27528	1.49615	1.50327	+ 16.0	1.50899	+ 16.0
0.28035	1.49425	1.50143	+ 16.2	1.50691	+ 15.8
0.28936	1.49121	1.49818	+ 15.7	1.50358	+ 15.4
0.29673	1.48892	1.49584	+ 15.6	1.50112	+ 15.2
0.30215	1.48738	1.49407	+ 15.1	1.49942	+ 15.0
0.3130	1.48462	1.49126	+ 14.9	1.49641	+ 14.7
0.33415	1.48000	1.48633	+ 14.2	1.49135	+ 14.1
0.36502	1.47469	1.48089	+ 14.0	1.48563	+ 13.6
0.40466	1.46978	1.47575	+ 13.4	1.48033	+ 13.2
0.43584	1.46685	1.47248	+ 12.7	1.47716	+ 12.9
0.54607	1.46028	1.46575	+ 12.3	1.47004	+ 12.2
0.5780	1.45899	1.46429	+ 11.9	1.46870	+ 12.1
1.01398	1.45039	1.45562	+ 11.8	1.45960	+ 11.5
1.12866	1.44903	1.45426	+ 11.8	1.45820	+ 11.4
1.254*	1.44772	1.45283	+ 11.5	1.45700	+ 11.6
1.36728	1.44635	1.45140	+ 11.4	1.45549	+ 11.4
1.470*	1.44524	1.45031	+ 11.4	1.45440	+ 11.4
1.52452	1.44444	1.44961	+ 11.6	1.45352	+ 11.3
1.660*	1.44307	1.44799	+ 11.1	1.45174	+ 10.8
1.701	1.44230	1.44733	+ 11.3	1.45140	+ 11.3
1.981*	1.43863	1.44361	+ 11.2	1.44734	+ 10.9
2.262*	1.43430	1.43933	+ 11.3	1.44306	+ 10.9
2.553*	1.42949	1.43450	+ 11.3	1.43854	+ 11.3
3.00*	1.41995	1.42495	+ 11.2	1.42877	+ 11.0
3.245*	1.41353	1.41893	+ 12.2	1.42243	+ 11.1
3.37*	1.40990	1.41501	+ 11.5	1.41915	+ 11.5

$\delta n = 23 \times 10^{-5}$

$\delta(dn/dT) = 0.7 \times 10^{-6}$

*Wavelength determination by narrow band interference filters.

TABLE IX. Aluminoscilicate Glass-Corning Code 1723-Refractive Index vs. Temperature, Non-irradiated.

λ Microns	n $28^{\circ}C$	n $526^{\circ}C$	$(dn/dT)/^{\circ}C \times 10^{6}$
0.36502	1.57093	1.57645	+ 11.1
0.40466	1.56405	1.56914	+ 10.2
0.43584	1.56000	1.56487	+ 9.8
0.54607	1.55100	1.55548	+ 9.0
0.5780	1.54928	1.55366	+ 8.8
1.01398	1.53854	1.54260	+ 8.2
1.12866	1.53699	1.54101	+ 8.1
1.36728	1.53419	1.53814	+ 7.9
1.470*	1.53292	1.53687	+ 7.9
1.52452	1.53224	1.53619	+ 7.9
1.660*	1.53078	1.53476	+ 8.0
1.701	1.53014	1.53408	+ 7.9
1.981*	1.52648	1.53044	+ 8.0
2.262*	1.52245	1.52643	+ 8.0
2.553*	1.51778	1.52181	+ 8.1
2.665*	1.51578	1.51998	+ 8.4

$\delta n = 23 \times 10^{-5}$

$\delta(dn/dT) = 0.7 \times 10^{-6}$

*Wavelength determination by narrow band interference filters

TABLE X. Vycor-Corning Code 7913, Optical Grade-Refractive Index vs. Temperature, Non-irradiated.

λ Microns	n 28°C	n 526°C	(dn/dT)/°C x10^6	n 826°C	(dn/dT)/°C x10^6
0.26520	1.49988	1.50799	+ 16.3	1.51438	+ 18.2
0.28936	1.49074	1.49831	+ 15.2	1.50418	+ 16.8
0.29673	1.48851	1.49587	+ 14.8	1.50164	+ 16.5
0.30215	1.48694	1.49423	+ 14.6	1.49990	+ 16.2
0.3130	1.48416	1.49121	+ 14.2	1.49679	+ 15.8
0.33415	1.47949	1.48622	+ 13.5	1.49158	+ 15.2
0.36502	1.47415	1.48065	+ 13.1	1.48570	+ 14.5
0.40466	1.46925	1.47547	+ 12.5	1.48027	+ 13.8
0.43584	1.46628	1.47234	+ 12.2	1.47708	+ 13.5
0.54607	1.45960	1.46544	+ 11.7	1.46992	+ 12.9
0.5780	1.45831	1.46407	+ 11.6	1.46849	+ 12.8
1.01398	1.44968	1.45526	+ 11.2	1.45924	+ 12.0
1.12866	1.44831	1.45373	+ 10.9	1.45779	+ 11.9
1.254*	1.44677	1.45222	+ 10.9	1.45627	+ 11.9
1.36728	1.44554	1.45095	+ 10.9	1.45504	+ 11.9
1.470*	1.44422	1.44965	+ 10.9	1.45370	+ 11.9
1.52452	1.44356	1.44896	+ 10.8	1.45306	+ 11.9
1.660*	1.44206	1.44750	+ 11.0	1.45157	+ 11.9
1.701	1.44137	1.44677	+ 10.8	1.45088	+ 11.9
1.981*	1.43750	1.44291	+ 10.9	1.44702	+ 11.9
2.262*	1.43298	1.43839	+ 10.9	1.44258	+ 12.0
2.553*	1.42825	1.43373	+ 11.0	1.43824	+ 12.5

$\delta n = 23 \times 10^{-5}$

$\delta(dn/dT) = 0.7 \times 10^{-6}$

*Wavelength determination by narrow band interference filters.

TABLE XI. Fused Silica-Corning Code 7940, Ultraviolet Grade-Effect of 30 Day Space Equivalent Irradiation on Refractive Index.

λ Microns	n $26^{o}C$ Non-irradiated	n $26^{o}C$ irradiated 30 day dose	Δn $\times 10^{5}$
0.23021	1.52034	1.52037	+ 3
0.23783	1.51496	1.51502	+ 6
0.2407	1.51361	1.51363	+ 2
0.2447	1.51081	1.51075	- 6
0.2465	1.50970	1.50974	+ 4
0.24827	1.50865	1.50869	+ 4
0.26520	1.50023	1.50028	+ 5
0.2700	1.49839	1.49831	- 8
0.27528	1.49615	1.49616	+ 1
0.28035	1.49425	1.49429	+ 4
0.28936	1.49121	1.49123	+ 2
0.2930	1.49021	1.49023	+ 2
0.29673	1.48892	1.48895	+ 3
0.30215	1.48738	1.48741	+ 3
0.3130	1.48462	1.48460	- 2
0.33415	1.48000	1.47997	- 3
0.36502	1.47469	1.47473	+ 4
0.40466	1.46978	1.46981	+ 3
0.43584	1.46685	1.46689	+ 4
0.54607	1.46028	1.46025	- 3
0.5780	1.45899	1.45900	+ 1
1.01398	1.45039	1.45040	+ 1
1.12866	1.44903	1.44901	- 2
1.254*	1.44772	1.44760	- 12*
1.36728	1.44635	1.44633	- 2
1.470*	1.44524	1.44513	- 11*
1.52452	1.44444	1.44445	+ 1
1.660*	1.44307	1.44296	- 11*
1.701	1.44230	1.44228	- 2
1.981*	1.43863	1.43859	- 4*
2.262*	1.43430	1.43426	- 4*
2.553*	1.42949	1.42939	- 10*
3.00 *	1.41995	1.41962	- 33*
3.245*	1.41353	1.41351	- 2*
3.37 *	1.40990	1.40997	+ 7*

$\delta n = 23 \times 10^{-5}$

*Wavelength determination by narrow band interference filters.

TABLE XII. Aluminosilicate Glass-Corning Code 1723-Effect of 30 Day Space Equivalent Irradiation on Radiative Index

λ Microns	n $26^{\circ}C$ Non-irradiated	n $26^{\circ}C$ Irradiated 30 day dose	Δn $\times 10^{5}$
0.33415	1.57836	1.57851	+ 15
0.36502	1.57093	1.57108	+ 15
0.40466	1.56405	1.56421	+ 16
0.43584	1.56000	1.56014	+ 14
0.54607	1.55100	1.55111	+ 11
0.5780	1.54928	1.54943	+ 15
1.01398	1.53854	1.53866	+ 12
1.12866	1.53699	1.53712	+ 13
1.36728	1.53419	1.53430	+ 11
1.52452	1.53224	1.53233	+ 9
1.660*	1.53078	1.53101	+ 23*
1.701	1.53014	1.53024	+ 10
1.981*	1.52648	1.52669	+ 21*
2.262*	1.52245	1.52266	+ 21*
2.553*	1.51778	1.51805	+ 27*
2.665*	1.51578	1.51609	+ 31*

$\delta n = 23 \times 10^{-5}$

*Wavelength determination by narrow band interference filters.

TABLE XIII. Vycor-Corning Code 7913, Optical Grade-Effect of 30 Day Space Equivalent Irradiation on Refractive Index

λ Microns	n $28^{\circ}C$ Non-irradiated	n $28^{\circ}C$ Irradiated 30 day dose	$\Delta n \times 10^5$
0.26520	1.49988	1.50013	+ 25
0.28936	1.49074	1.49093	+ 19
0.29673	1.48851	1.48869	+ 18
0.30215	1.48694	1.48707	+ 13
0.3130	1.48416	1.48426	+ 10
0.33415	1.47949	1.47964	+ 15
0.36502	1.47415	1.47426	+ 11
0.40466	1.46925	1.46932	+ 7
0.43584	1.46628	1.46637	+ 9
0.54607	1.45960	1.45969	+ 9
0.5780	1.45831	1.45843	+ 12
1.01398	1.44968	1.44984	+ 16
1.12866	1.44831	1.44838	+ 7
1.254*	1.44677	1.44690	+ 13*
1.36728	1.44554	1.44565	+ 11
1.470*	1.44422	1.44437	+ 15*
1.52452	1.44356	1.44365	+ 9
1.660*	1.44206	1.44219	+ 13*
1.701	1.44137	1.44145	+ 8
1.981*	1.43750	1.43762	+ 12*
2.262*	1.43298	1.43307	+ 9*
2.553*	1.42825	1.42835	+ 10*

$\delta n = 23 \times 10^{-5}$

*Wavelength determination by narrow band interference filters.

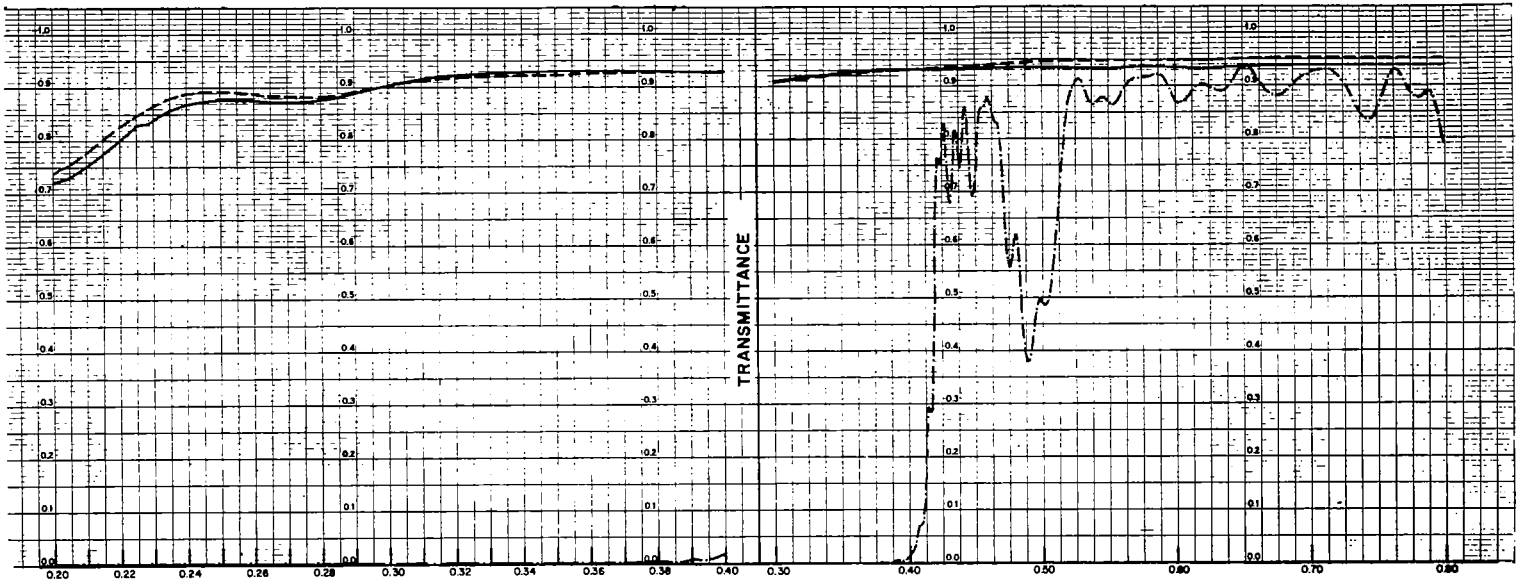

FUSED SILICA – CORNING CODE 7940, U.V. GRADE – TRANSMITTANCE AT 26°C, SAMPLE THICKNESS 1.784 CM

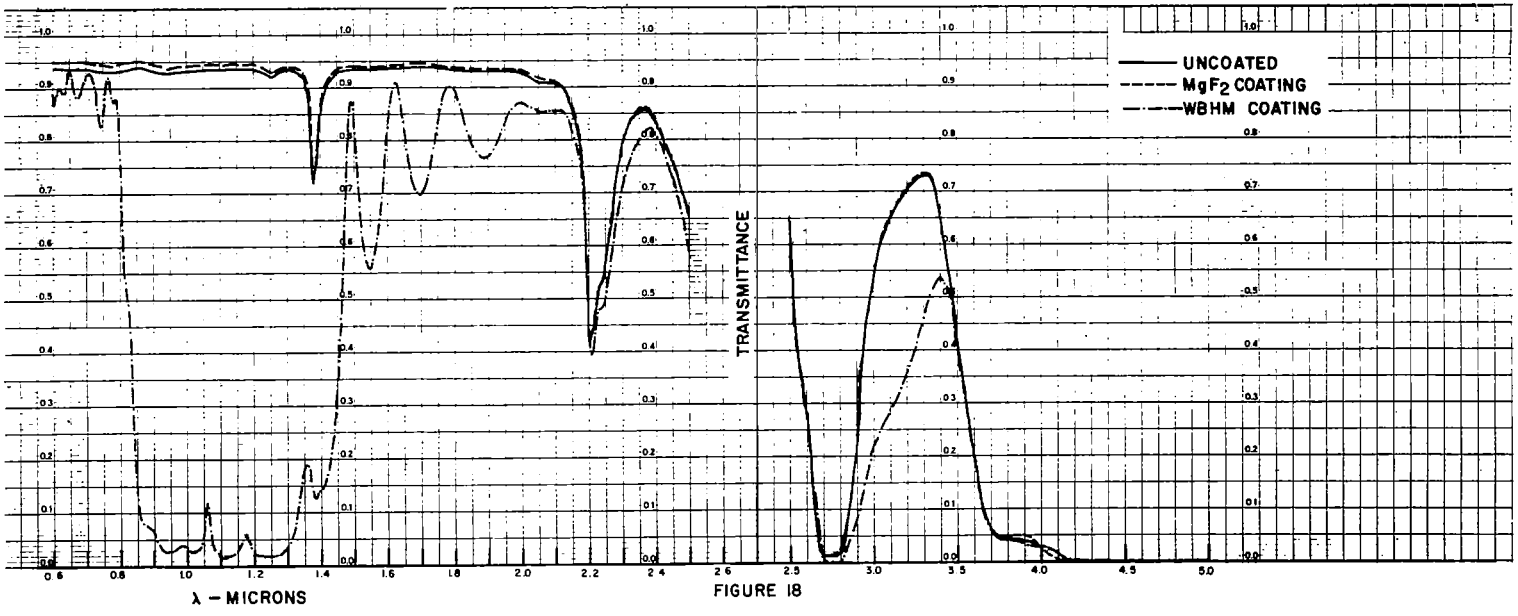

FIGURE 18

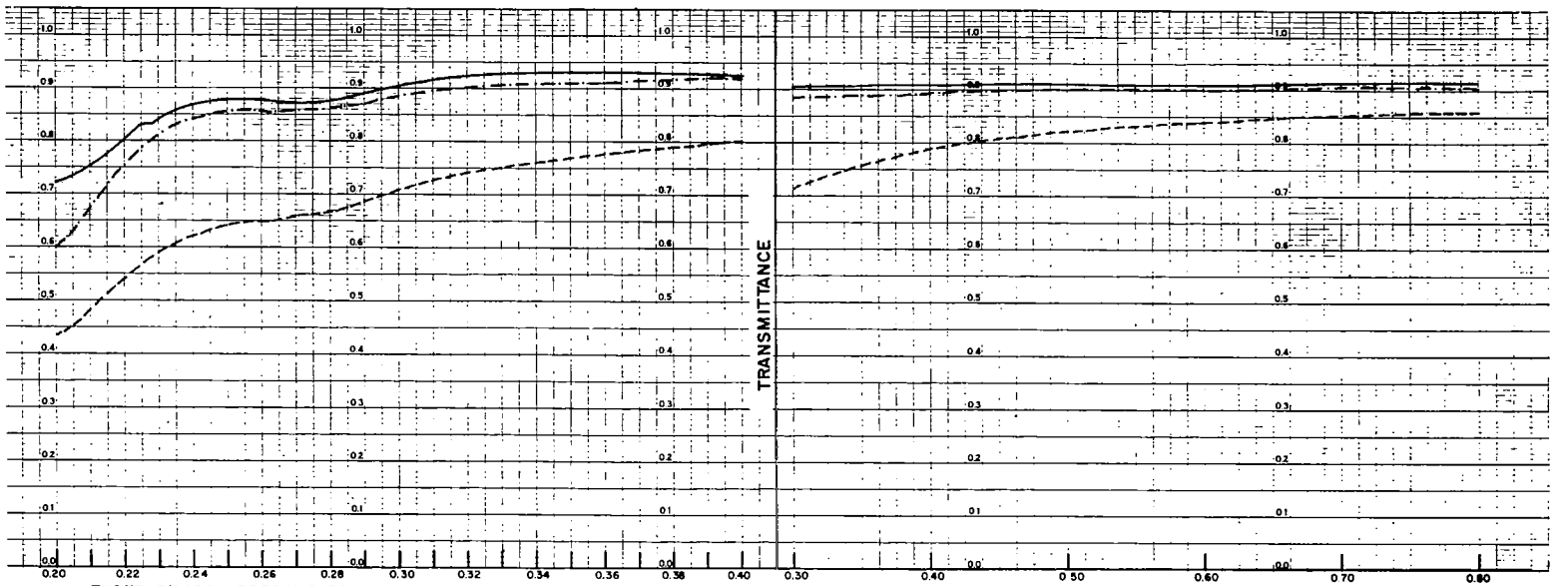

FUSED SILICA – CORNING CODE 7940, U.V. GRADE – EFFECT OF IRRADIATION ON TRANSMITTANCE AT 26°C, UNCOATED SAMPLE, SAMPLE THICKNESS 1.784CM

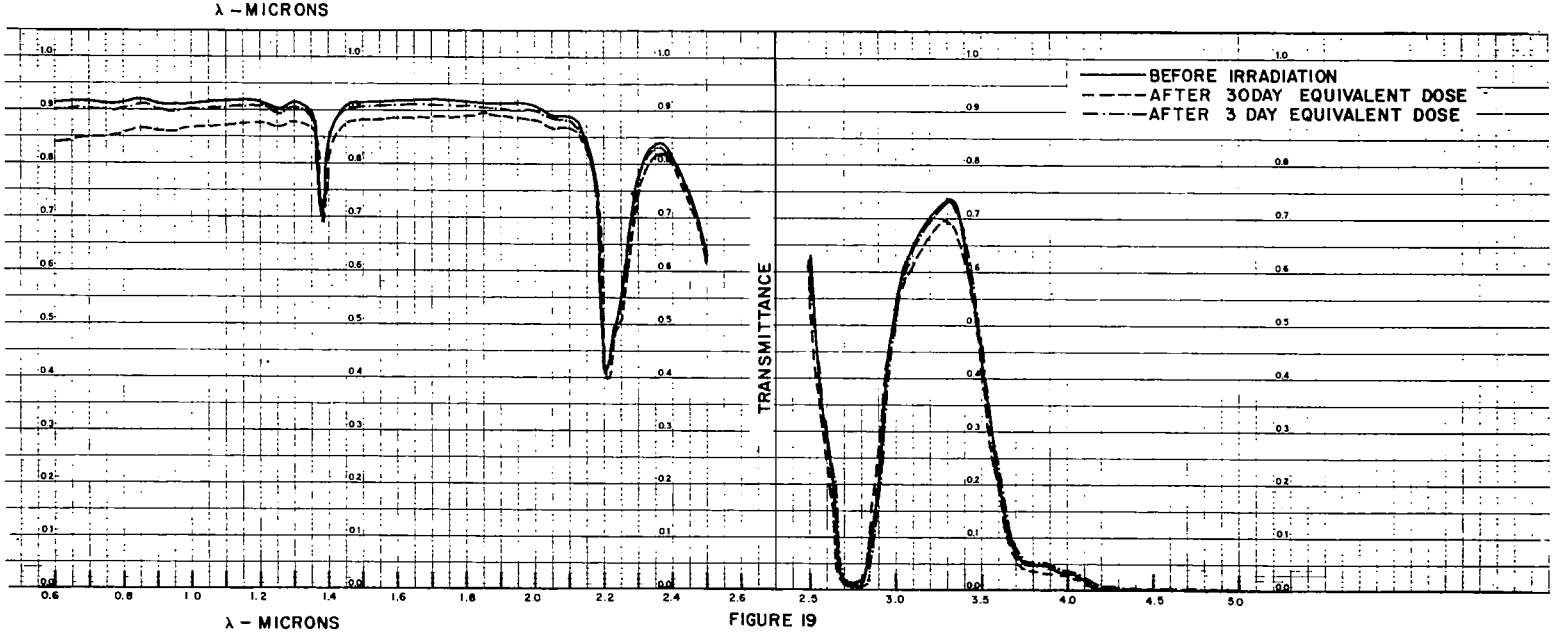

FIGURE 19

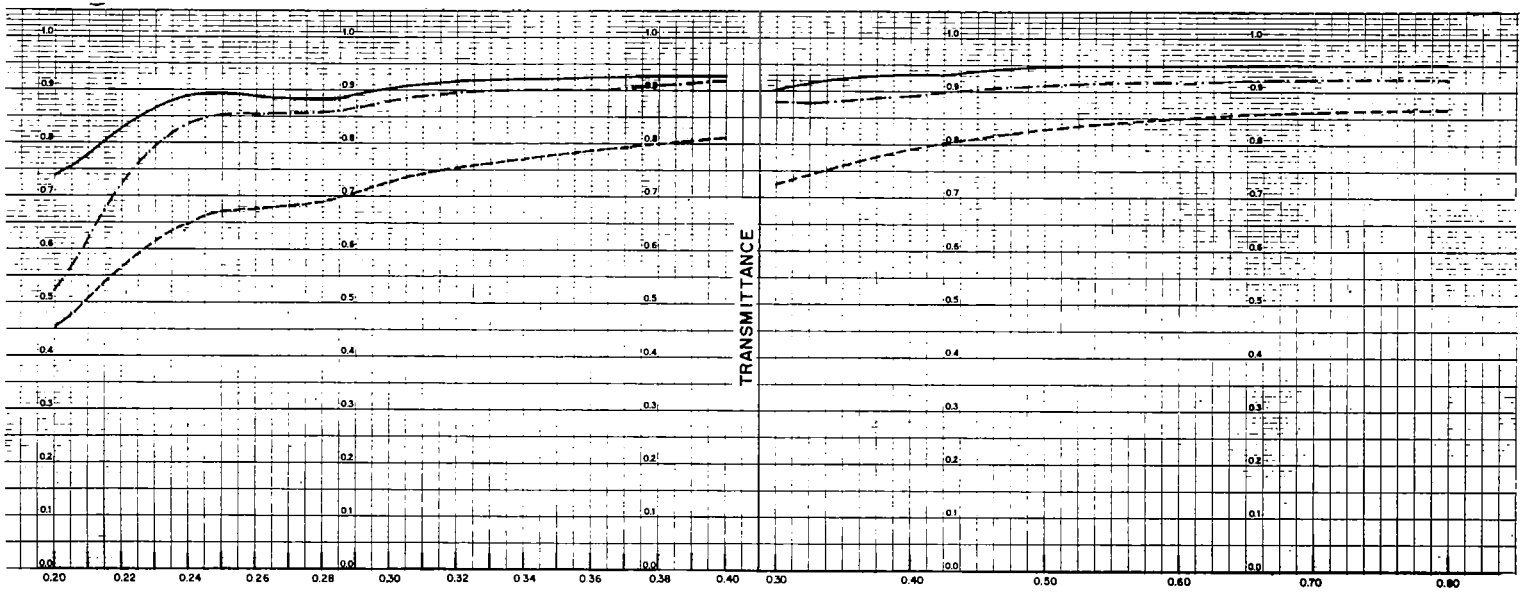

FUSED SILICA-CORNING CODE 7940, U.V.GRADE-EFFECT OF IRRADIATION ON TRANSMITTANCE AT 26°C . MgF_2 COATING, SAMPLE THICKNESS L784CM

λ - MICRONS

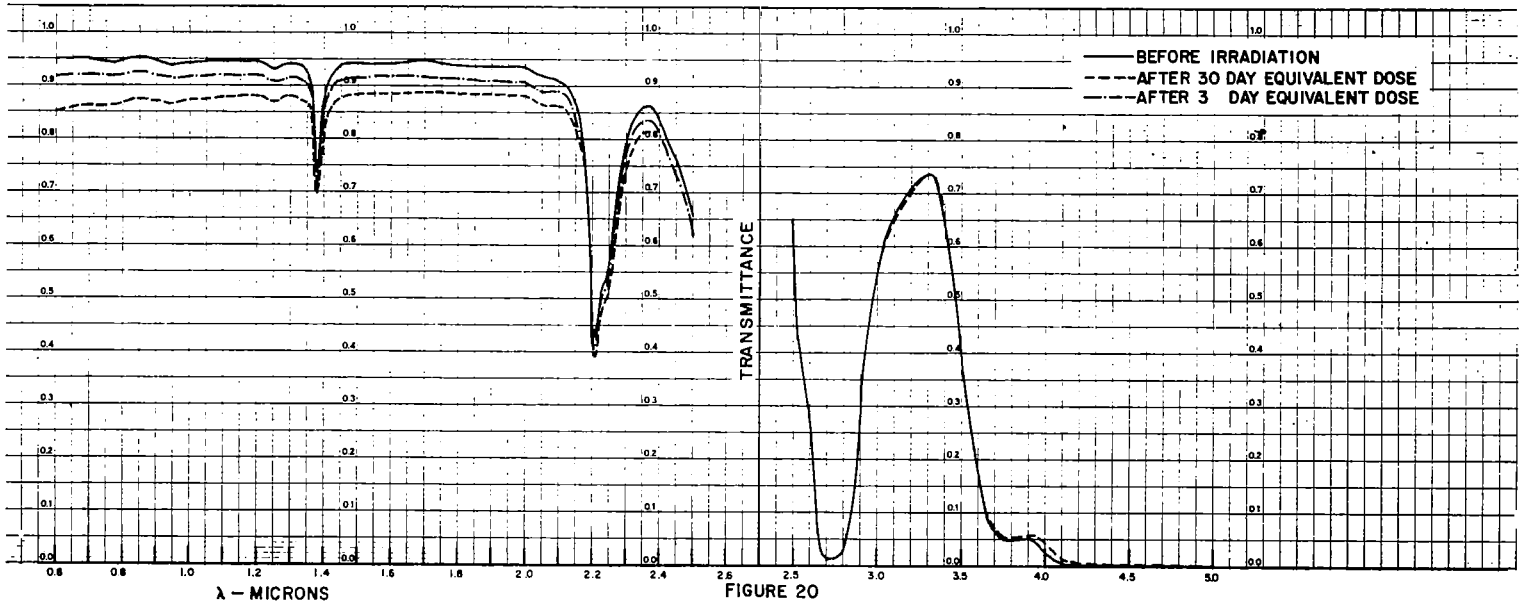

λ - MICRONS

FIGURE 20

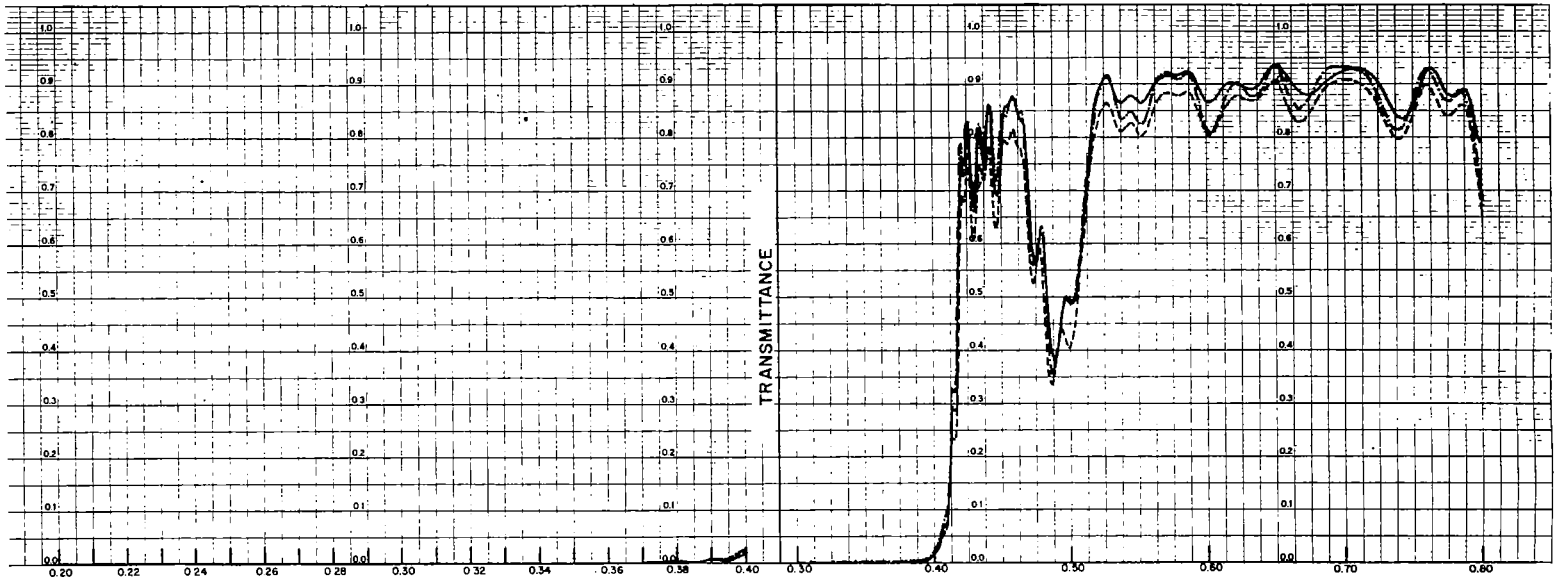

FUSED SILICA–CORNING CODE 7940, U.V. GRADE – EFFECT OF IRRADIATION ON TRANSMITTANCE AT 26°C . WBHM COATING, SAMPLE THICKNESS 1.784CM

λ – MICRONS

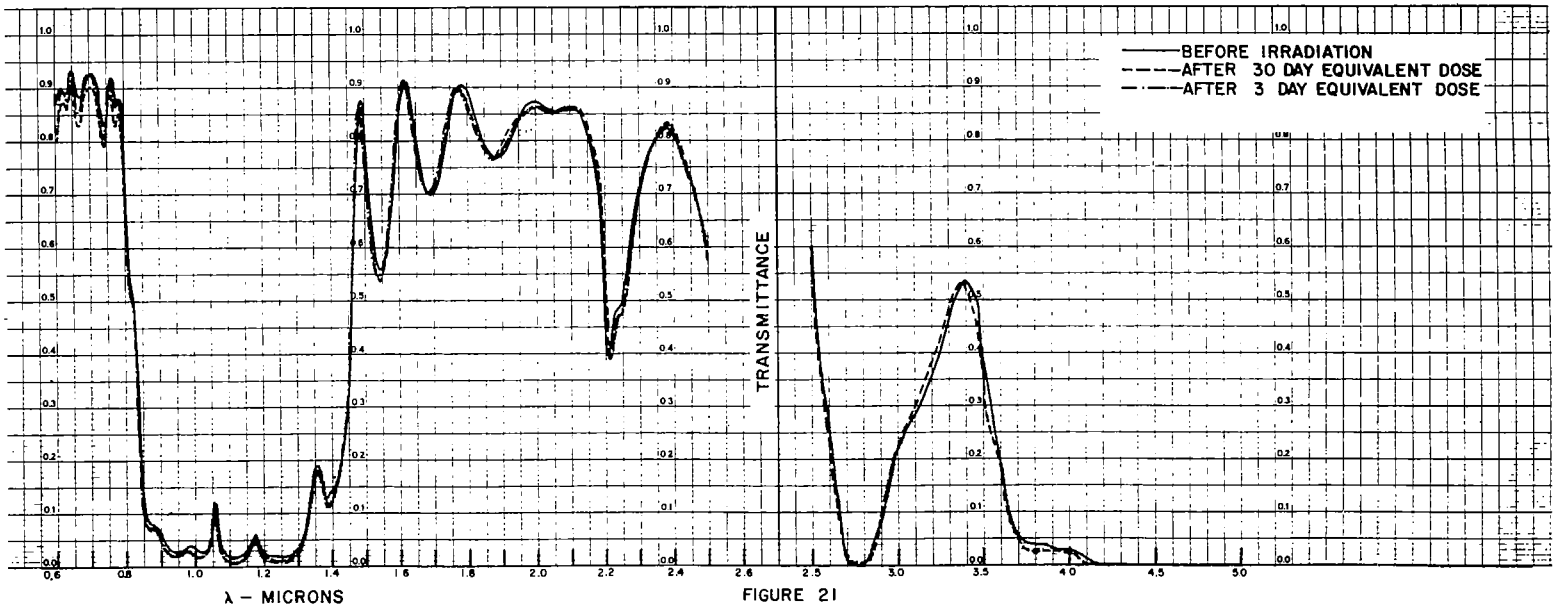

λ – MICRONS

FIGURE 21

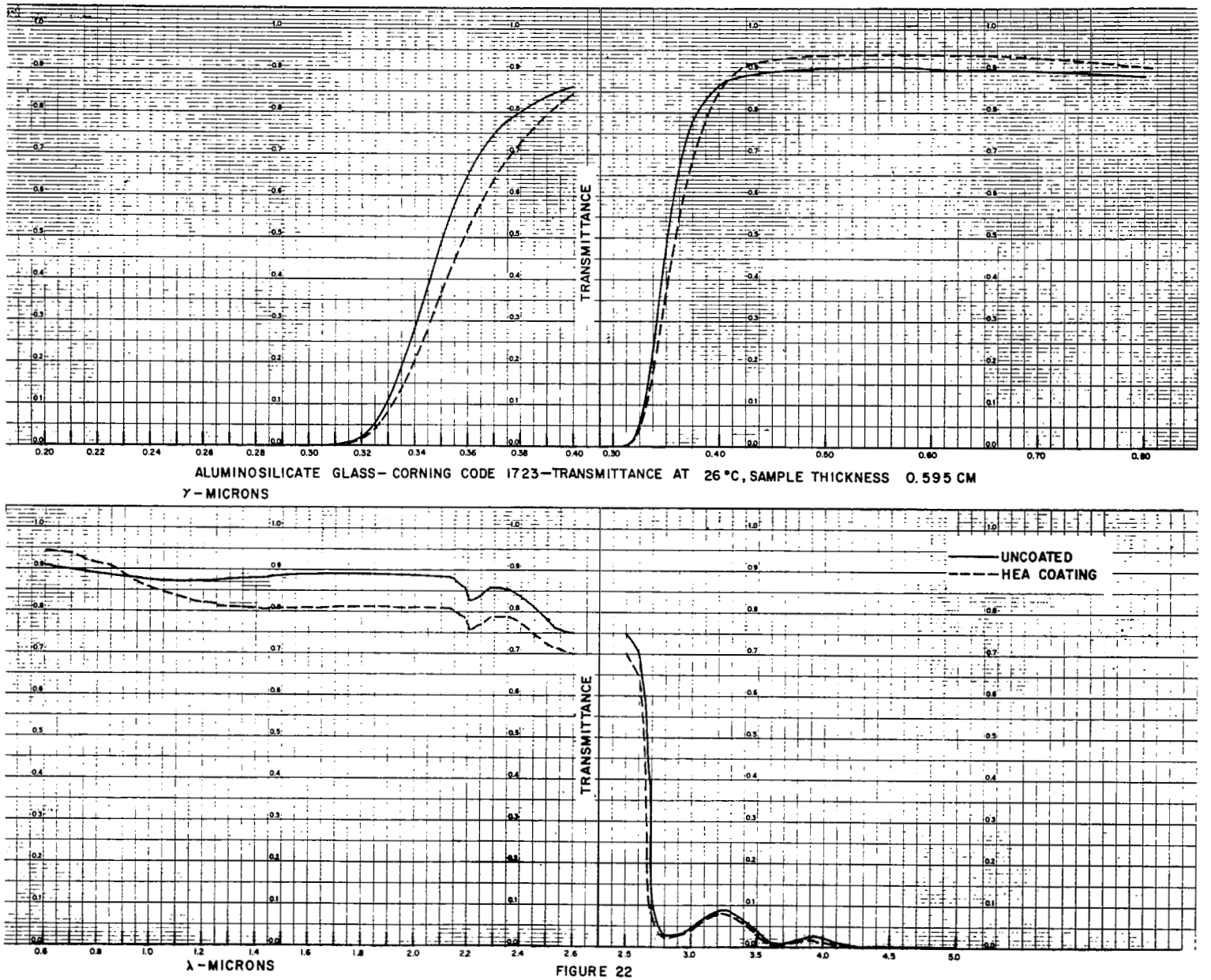

ALUMINOSILICATE GLASS- CORNING CODE 1723—TRANSMITTANCE AT 26 °C, SAMPLE THICKNESS 0.595 CM

FIGURE 22

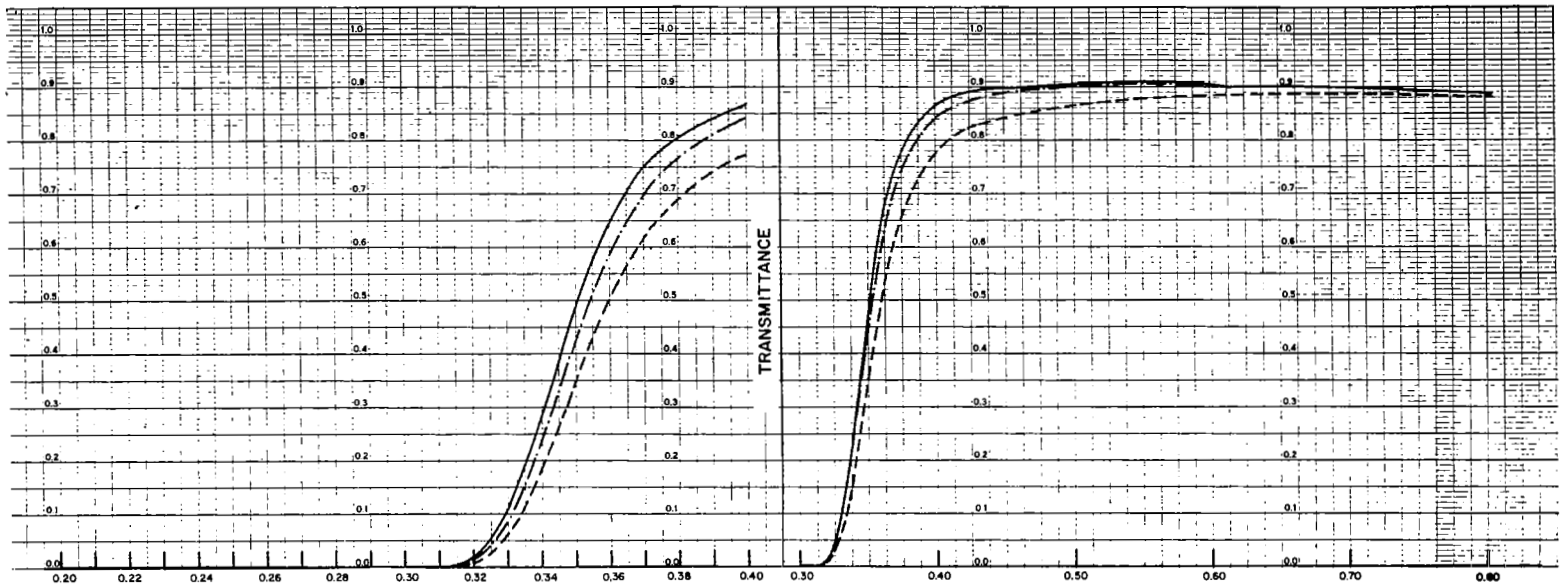

ALUMINOSILICATE GLASS – CORNING CODE 1723 – EFFECT OF IRRADIATION ON TRANSMITTANCE AT 26 °C, UNCOATED SAMPLE, SAMPLE THICKNESS 0.595 CM

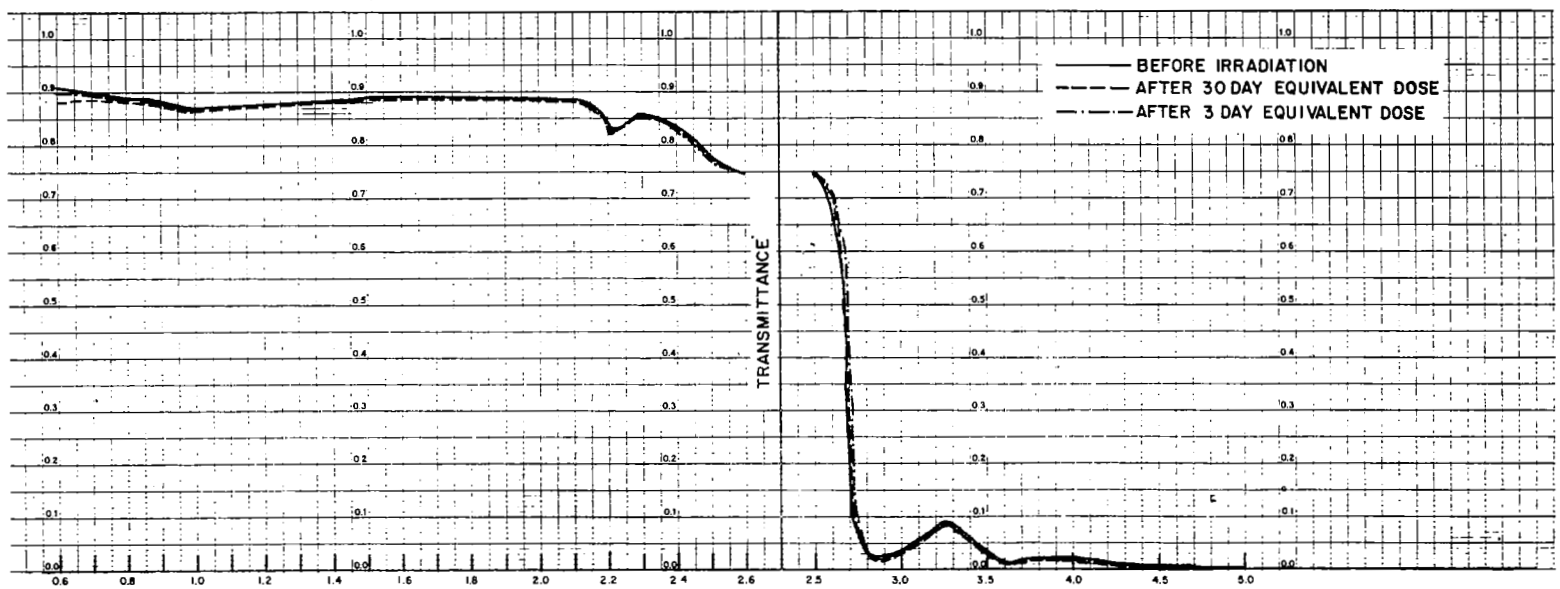

FIGURE 23

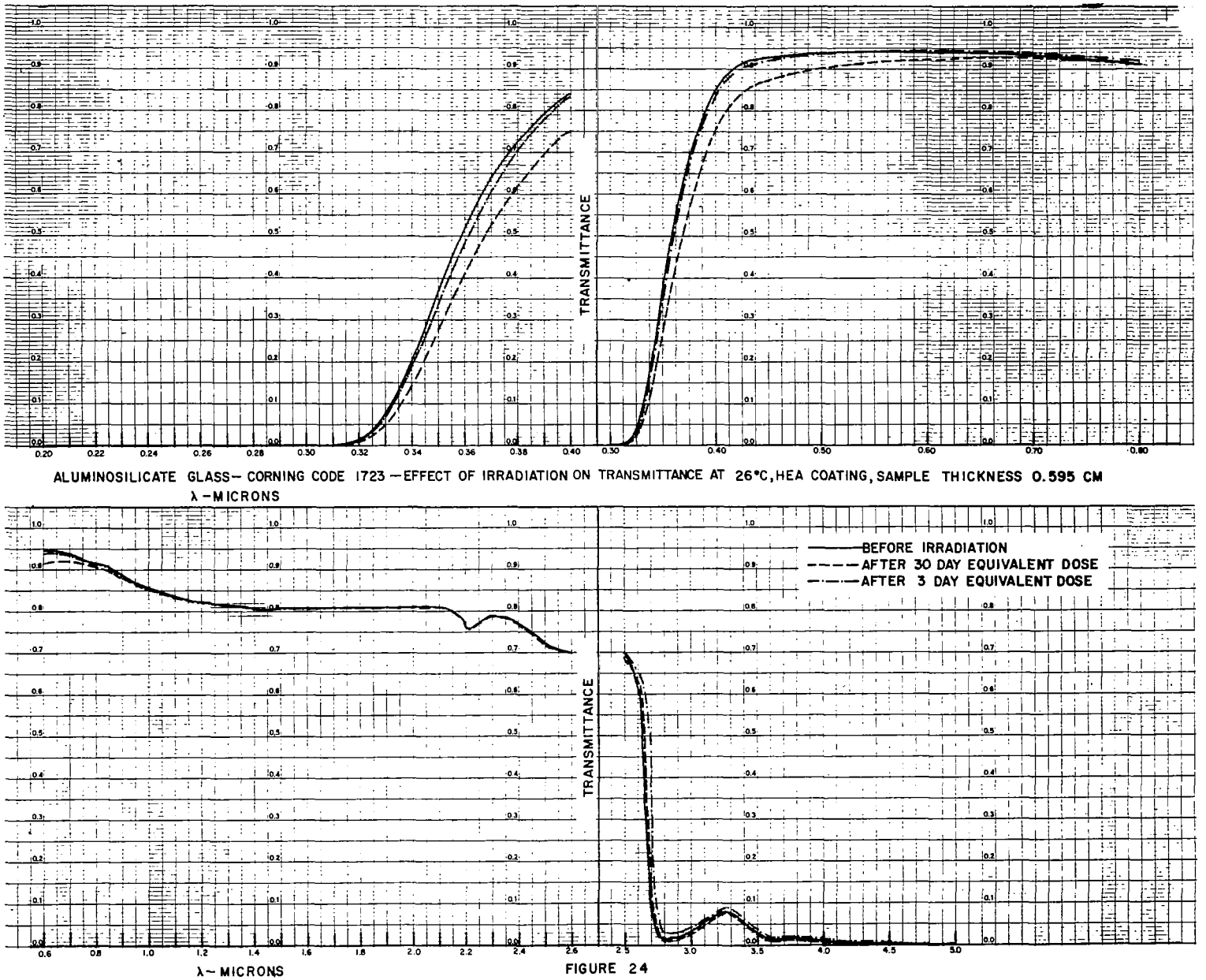

ALUMINOSILICATE GLASS- CORNING CODE 1723 - EFFECT OF IRRADIATION ON TRANSMITTANCE AT 26°C, HEA COATING, SAMPLE THICKNESS 0.595 CM

FIGURE 24

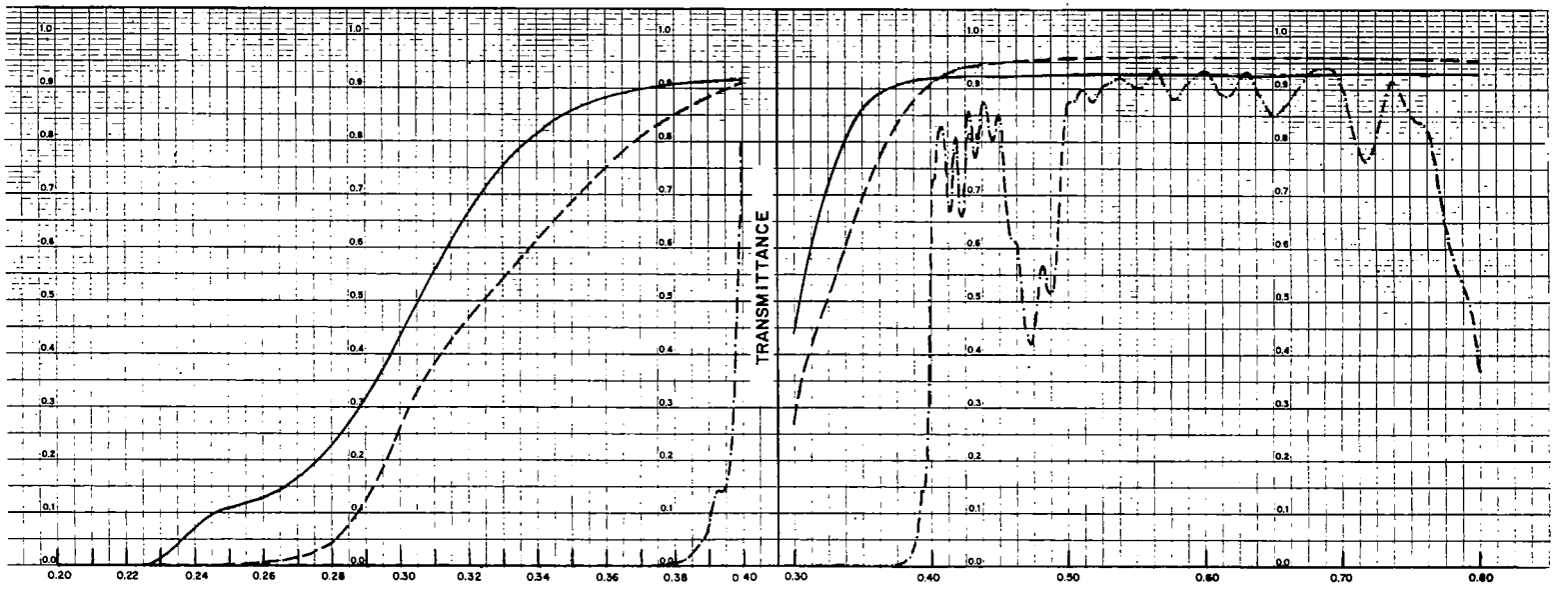

VYCOR – CORNING CODE 7913 –TRANSMITTANCE AT 26°C, SAMPLE THICKNESS 0.378 CM

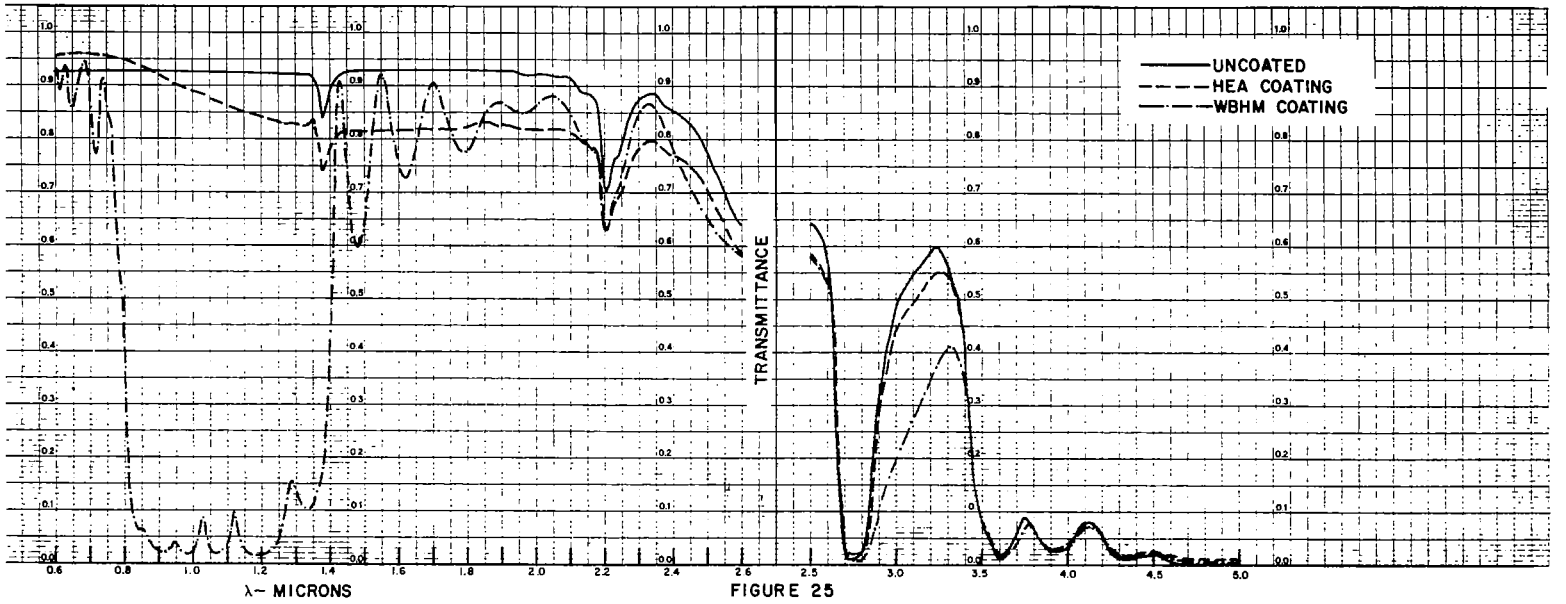

FIGURE 25

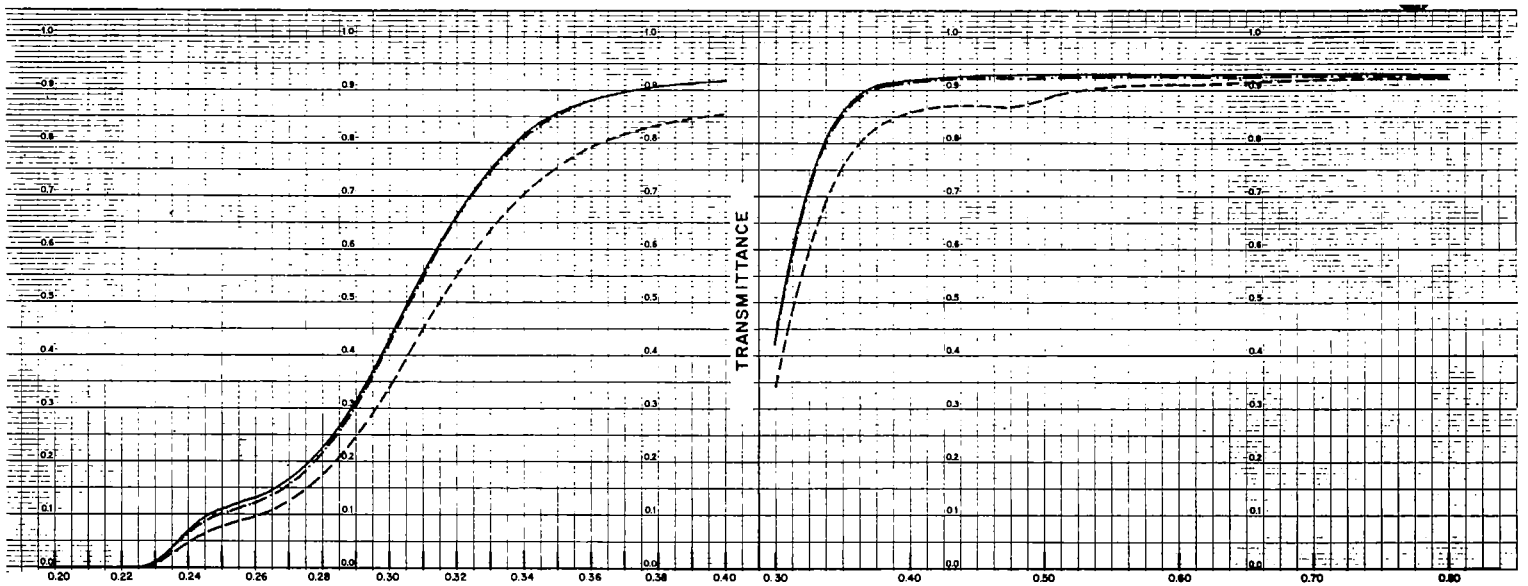

VYCOR – CORNING CODE 7913 – EFFECT OF IRRADIATION ON TRANSMITTANCE AT 26°C UNCOATED SAMPLE, SAMPLE THICKNES 0.378 CM

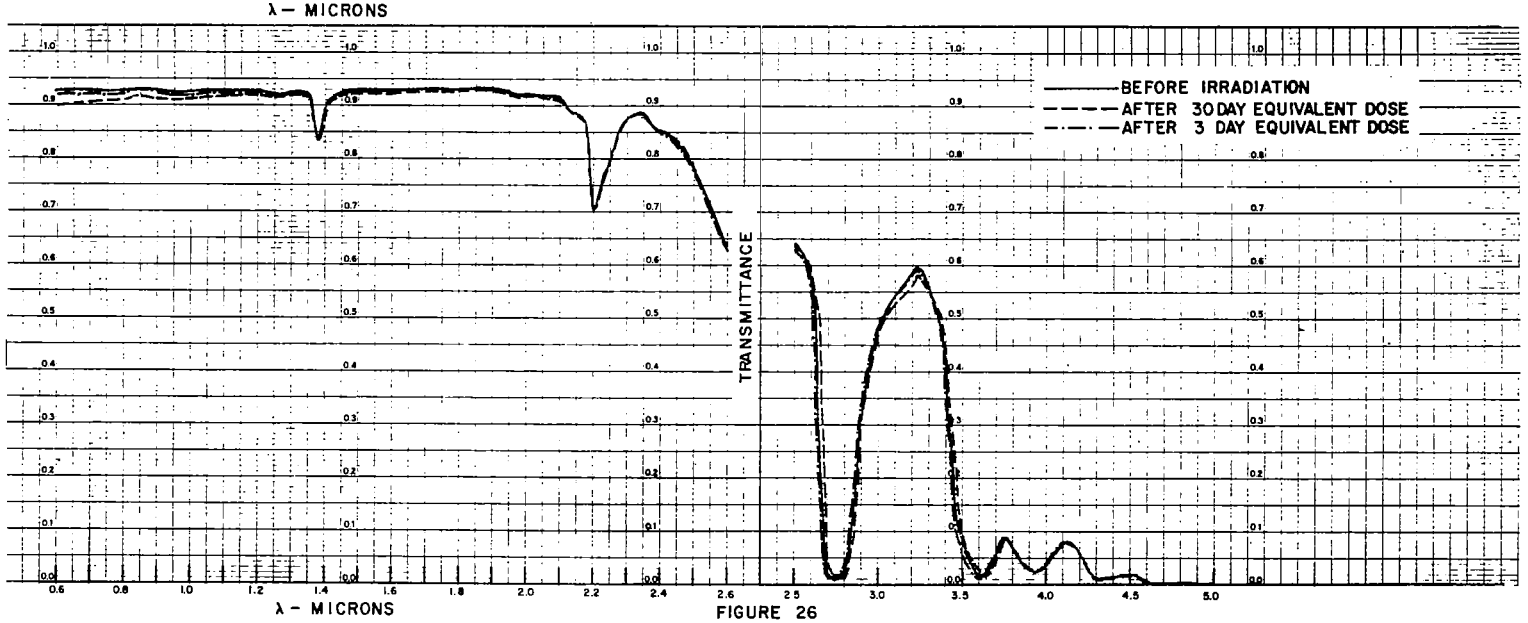

FIGURE 26

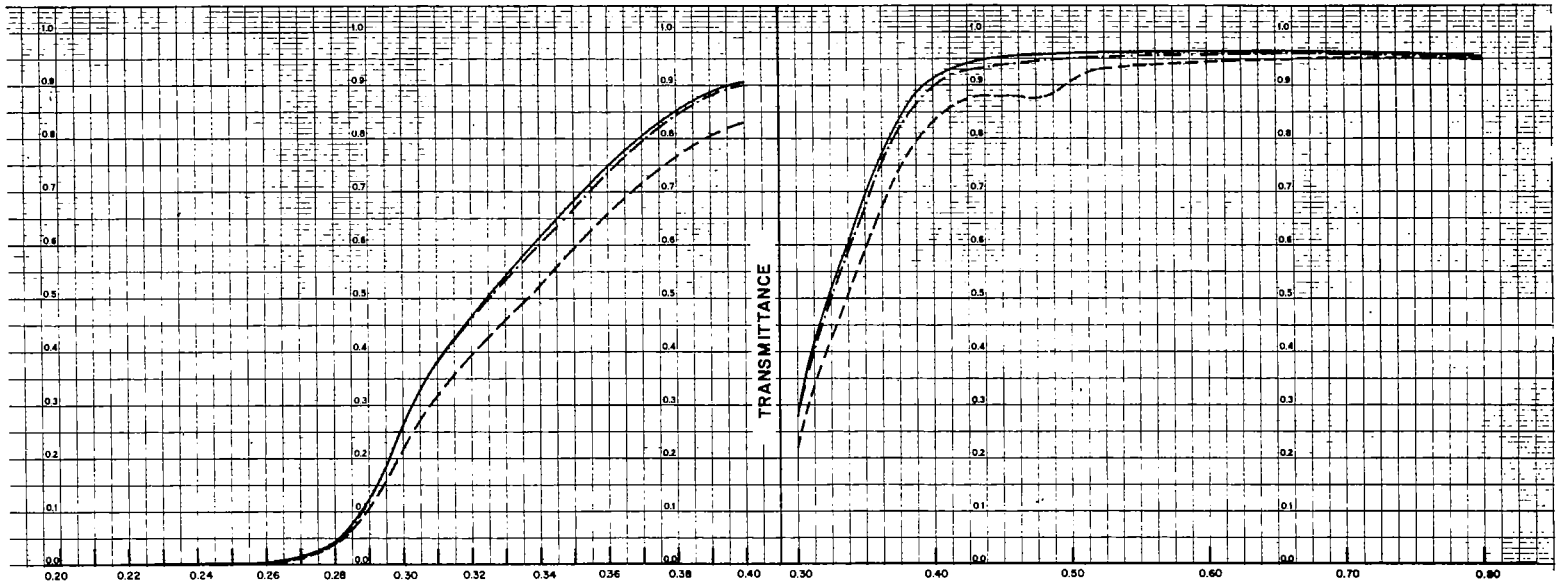

VYCOR – CORNING CODE 7913 – EFFECT OF IRRADIATION ON TRANSMITTANCE AT 26°C, HEA COATING, SAMPLE THICKNESS 0.378 CM

λ – MICRONS

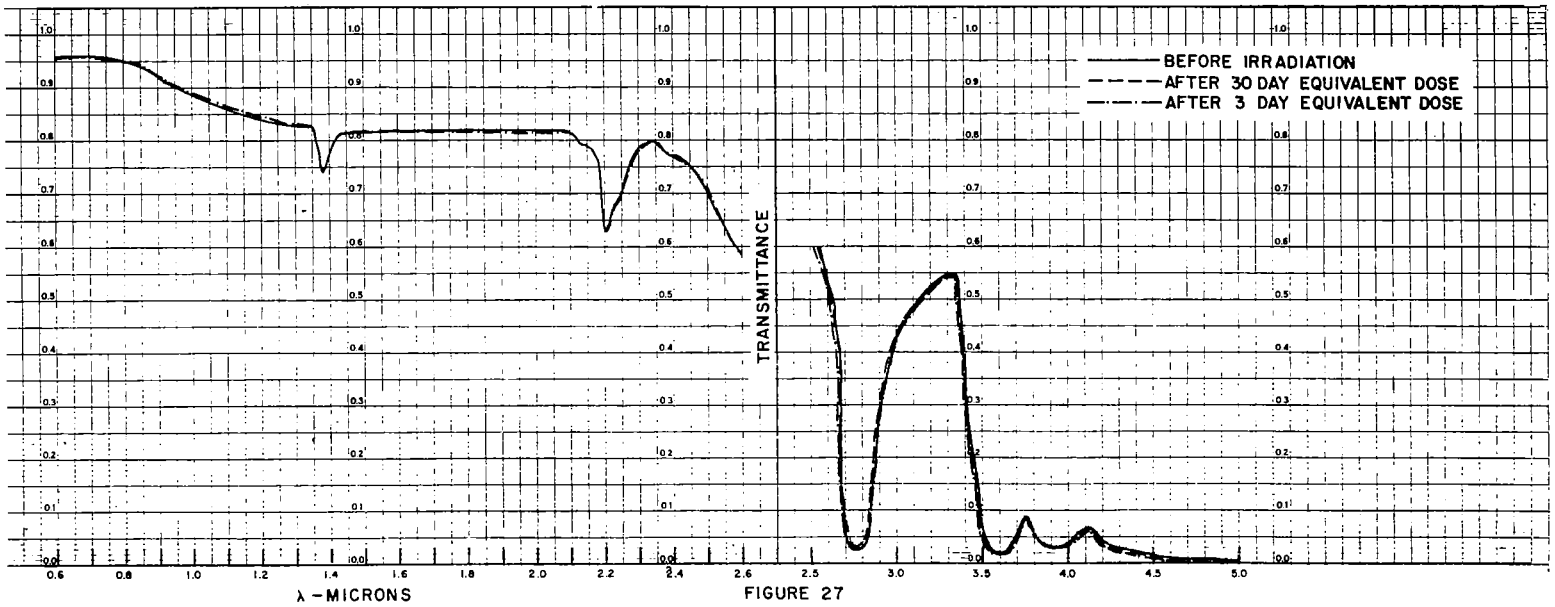

FIGURE 27

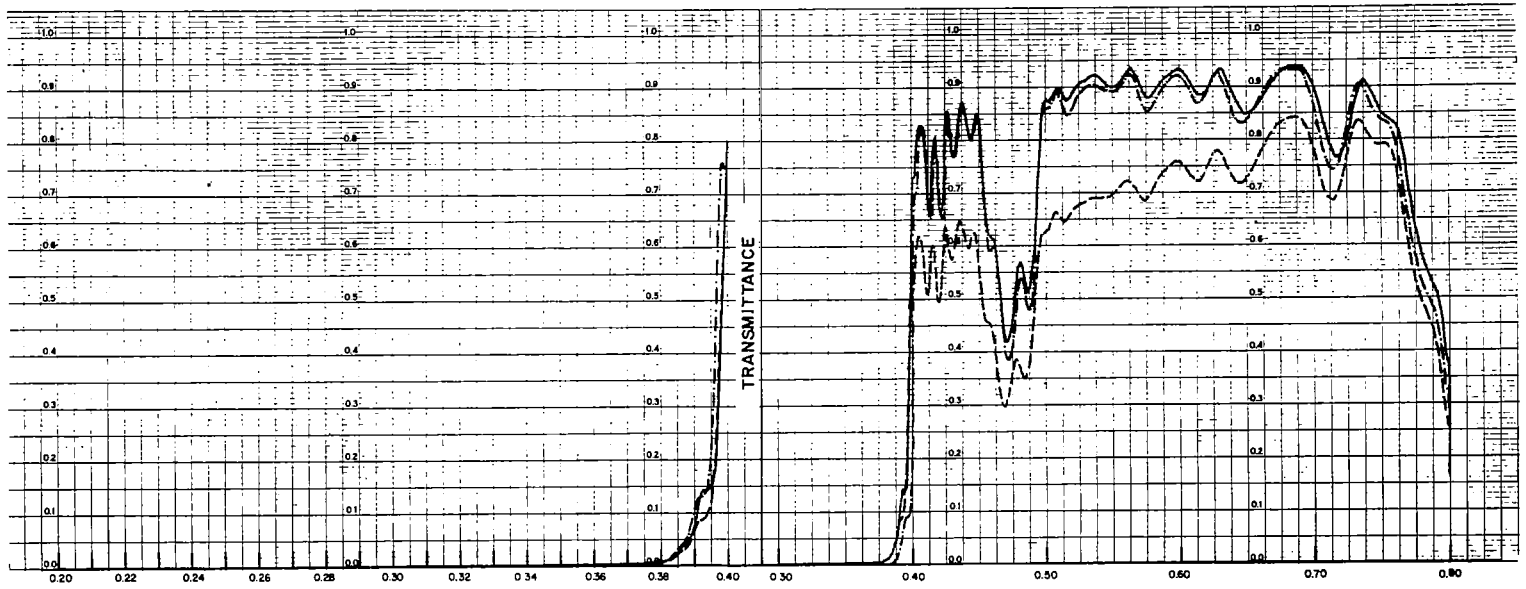

VYCOR—CORNING CODE 7913—EFFECT OF IRRADIATION ON TRANSMITTANCE AT 26 °C, WBHM COATING, SAMPLE THICKNESS 0.378 CM

λ – MICRONS

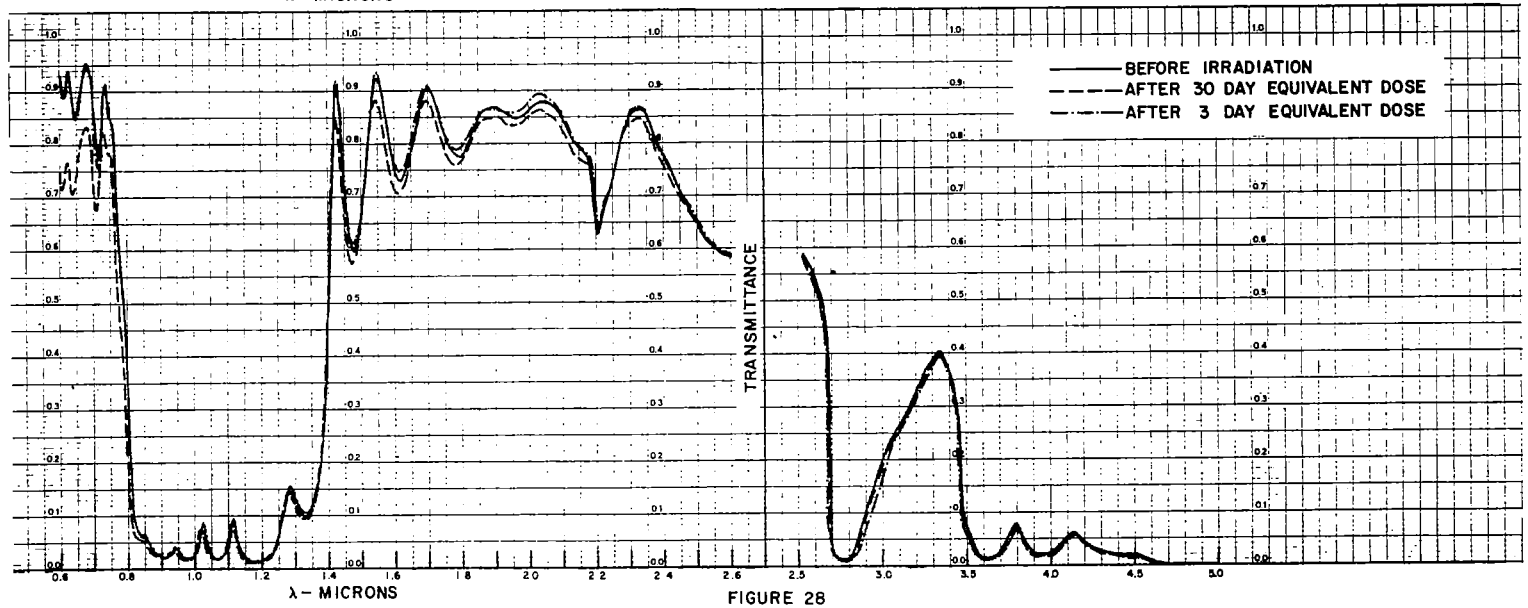

λ – MICRONS

FIGURE 28

TABLE XIV. Fused Silica-Corning Code 7940, Ultraviolet Grade-Transmittance vs. Temperature, Non-irradiated

λ	Uncoated T	Uncoated T	Uncoated T	MgF_2 Coating T	MgF_2 Coating T	MgF_2 Coating T	WBHM Coating T	WBHM Coating T	WBHM Coating T
Microns	26°C	526°C	826°C	26°C	526°C	826°C	26°C	526°C	826°C
0.2303	84.0	82.4	84.8	86.2	83.5	60.0	0	0	0
0.2379	86.3	85.6	86.1	88.5	84.4	62.8	0	0	0
0.2407	86.4	86.7	84.4	88.7	86.1	63.8	0	0	0
0.2447	87.1	86.6	86.2	89.0	86.0	65.3	0	0	0
0.2465	87.5	86.3	85.2	89.0	85.1	67.4	0	0	0
0.2480	87.4	85.5	85.8	89.1	84.9	66.4	0	0	0
0.2653	87.2	88.2	88.6	88.5	87.6	72.6	0	0	0
0.2700	87.3	87.8	88.4	88.5	87.2	72.3	0	0	0
0.2753	87.4	88.0	87.9	88.3	86.8	73.4	0	0	0
0.2805	87.5	88.3	87.7	88.3	86.5	75.6	0	0	0
0.2968	90.0	91.1	89.4	90.0	88.7	77.8	0	0	0
0.3023	90.6	89.3	90.1	90.1	87.6	79.4	0	0	0
0.3127	90.7	90.4	90.5	91.5	88.6	81.3	0	0	0
0.3133	91.7	91.3	91.0	91.6	89.6	81.9	0	0	0
0.3342	92.5	92.5	92.0	92.3	90.2	79.2	0	0	0
0.3651	92.6	92.0	91.8	92.4	91.4	88.0	0	0	0
0.4048	92.7	91.7	94.4	93.4	91.7	84.6	5.2	2.3	0
0.4358	92.8	92.3	92.3	94.1	92.8	78.8	78.7	48.7	7.8
0.5461	92.9	92.0	93.4	94.9	93.2	73.6	87.6	66.9	26.8
0.5771	93.0	92.0	92.6	95.1	92.6	74.0	91.6	72.5	22.6
0.5792	93.0	93.4	92.4	95.1	94.0	72.2	91.6	73.4	23.7
1.014	92.5	91.9	91.6	93.4	93.5	88.1	2.0	1.1	2.0
1.129	92.6	91.5	91.2	93.5	92.5	91.2	1.2	0	0.5
1.368	86.0	86.0	85.2	86.0	86.5	85.6	14.6	10.5	1.8
1.530	92.7	91.3	91.2	93.3	91.3	92.7	57.1	44.6	9.8
1.693	93.0	91.5	91.0	93.8	92.0	93.0	69.4	59.3	15.6
1.710	93.0	92.4	91.1	93.8	93.4	92.1	69.4	63.0	18.2
2.000	92.1	90.0	89.7	92.6	90.5	90.2	86.0	69.9	23.3
2.200	46.5	43.9	41.7	46.5	43.9	42.9	43.0	32.8	14.0
2.300	80.0	72.7	67.4	80.0	73.2	69.3	64.0	58.6	23.1
2.500	88.9	52.2	47.9	88.9	53.1	50.8	88.9	37.4	19.2
2.600	80.7	35.9	32.4	80.7	35.9	36.6	80.7	22.6	15.5
2.800	2.9	0	0	3.9	0	0	0	0	0
3.000	55.5	27.5	15.0	55.5	27.5	15.9	21.4	20.0	8.4
3.200	65.9	43.3	28.5	66.0	42.8	29.0	35.5	34.8	18.0
3.400	64.3	39.1	28.0	64.3	39.1	29.1	53.5	33.4	23.7
3.600	20.5	8.7	2.3	20.5	9.7	8.2	19.5	9.2	15.2
3.800	4.5	0.8	0	5.0	4.1	3.1	3.9	5.7	0*
4.00	2.0	0	0	2.0	0	0	2.0	0	0

$\delta T(26^{\circ}C) = + .5 \pm .6\%$

$\delta T(526^{\circ}C, 826^{\circ}C) = + .5 \pm .9\%$ ($T_R = 0$), $\lambda < 2$ microns

$+ .5 \pm 1.5\%$ ($T_R = .9$), $\lambda < 2$ microns

$+ .5 \pm 1.1\%$ ($T_R = 0$), $\lambda > 2$ microns

$+ .5 \pm 1.9\%$ ($T_R = .9$), $\lambda > 2$ microns

TABLE XV. Fused Silica-Corning Code 7940, Ultraviolet Grade-Transmittance vs. Temperature, After 30 Day Space Equivalent Irradiation

λ	Uncoated T	Uncoated T	Uncoated T	MgF_2 Coating T	MgF_2 Coating T	MgF_2 Coating T	WBHM Coating T	WBHM Coating T	WBHM Coating T
Microns	26°C	526°C	826°C	26°C	526°C	826°C	26°C	526°C	826°C
0.2303	58.9	61.3	55.3	61.6	62.0	41.0	0	0	0
0.2379	61.5	62.2	58.8	64.5	62.8	44.2	0	0	0
0.2407	62.0	64.7	57.8	64.8	64.0	46.0	0	0	0
0.2447	63.1	66.9	59.9	66.3	66.2	47.1	0	0	0
0.2465	63.7	67.5	59.7	66.5	68.2	47.3	0	0	0
0.2480	64.0	68.9	59.4	66.9	68.9	47.9	0	0	0
0.2653	65.1	69.9	64.1	68.0	69.9	54.6	0	0	0
0.2700	66.0	71.4	64.7	68.4	70.7	56.2	0	0	0
0.2753	66.3	70.9	64.7	68.6	70.3	56.4	0	0	0
0.2805	66.9	70.2	66.7	69.1	70.2	59.6	0	0	0
0.2968	70.2	72.7	69.6	71.9	72.0	60.6	0	0	0
0.3023	71.3	74.1	69.6	73.5	72.8	60.6	0	0	0
0.3127	73.1	76.7	71.2	74.7	74.7	61.9	0	0	0
0.3133	73.4	76.4	71.5	74.9	75.1	61.6	0	0	0
0.3342	75.4	77.2	74.4	76.7	76.6	63.2	0	0	0
0.3651	77.9	80.8	77.5	79.2	80.8	61.0	0	0	0
0.4048	82.0	84.1	81.9	84.0	84.6	61.4	9.5	3.8	0
0.4358	83.3	85.9	80.6	85.2	86.5	61.2	78.1	55.1	10.9
0.5461	86.0	89.7	83.4	88.7	90.4	70.6	80.3	77.3	33.6
0.5771	86.5	89.9	84.2	89.3	90.6	72.3	87.8	83.4	35.2
0.5792	86.6	89.5	84.8	89.4	90.8	72.0	88.0	81.2	31.7
1.014	90.5	86.9	91.4	91.4	87.5	92.5	2.4	1.6	1.1
1.129	90.5	88.0	91.9	91.8	88.5	93.0	1.3	1.0	0
1.368	87.4	85.8	89.3	87.4	85.8	90.4	15.0	9.7	0
1.530	91.6	89.6	93.2	92.5	89.6	95.9	54.0	48.0	0
1.693	91.7	90.2	93.8	92.5	90.7	95.4	72.7	63.6	0
1.710	91.7	89.5	93.6	92.6	90.0	94.2	73.0	67.8	0
2.000	91.0	89.5	93.0	91.7	89.0	94.1	86.3	74.7	34.8
2.200	41.8	38.8	36.8	41.8	38.8	37.6	41.8	31.6	16.4
2.300	80.3	73.0	70.8	80.3	72.5	70.8	72.3	62.9	34.4
2.500	55.2	14.4	29.1	55.2	13.9	29.7	55.2	6.1	16.2
2.600	24.0	9.8	8.6	24.0	10.2	9.4	22.0	8.1	5.3
2.800	1.0	1.1	1.1	1.0	2.1	0	1.0	0	0
3.000	55.0	27.4	18.0	54.6	27.4	19.1	24.2	22.1	13.8
3.200	68.8	45.5	31.9	69.0	44.5	33.0	40.2	39.9	26.6
3.400	63.0	40.4	24.3	63.0	39.9	25.2	52.5	36.6	23.8
3.600	20.0	8.3	2.9	20.9	9.1	8.7	17.0	8.7	3.0*
3.800	3.5	0	0	5.0	2.8	5.1	2.9	2.8	0 *
4.000	2.0	0	0	2.3	0	0	2.0	0	0

$\delta T(26°C) = + .5 \pm .6\%$

$\delta T(526°, 826°C) = + .5 \pm .9\%$ ($T_R = 0$), $\lambda < 2$ microns

$+ .5 \pm 1.5\%$ ($T_R = .9$), $\lambda < 2$ microns

$+ .5 \pm 1.1\%$ ($T_R = 0$), $\lambda > 2$ microns

$+ .5 \pm 1.9\%$ ($T_R = .9$), $\lambda > 2$ microns

TABLE XVI. Aluminosilicate Glass-Corning Code 1723-Transmittance vs. Temperature, Non-irradiated

λ	Uncoated			HEA Coating		
	T	T	T	T	T	T
Microns	26°C	526°C	826°C	26°C	526°C	826°C
0.3023	0	0	0	0	0	0
0.3127	0	0	0	0	0	0
0.3133	0.6	0	0	0.4	0	0
0.3342	17.3	0.5	0	14.2	0.5	0
0.3651	70.6	27.6	7.0	63.4	23.2	2.9
0.4048	88.7	74.4	46.4	88.7	72.2	22.6
0.4358	89.8	86.8	71.0	93.4	86.3	46.0
0.5461	91.1	90.4	89.1	95.3	91.5	70.8
0.5771	91.4	91.7	92.4	95.3	93.4	74.0
0.5792	91.3	93.2	91.5	95.3	94.9	73.0
1.014	87.3	86.0	87.4	85.5	84.4	89.0
1.129	87.6	86.8	86.5	83.5	83.9	87.5
1.368	88.9	89.3	87.8	80.5	83.2	87.3
1.530	89.2	88.3	88.2	81.3	81.9	86.2
1.693	89.2	87.3	88.7	81.4	81.9	85.2
1.710	89.2	88.4	87.7	81.4	83.0	84.7
2.000	89.0	89.0	87.4	81.3	83.5	83.3
2.200	82.3	80.8	73.5	75.3	77.4	69.7
2.300	84.0	83.1	78.7	76.9	78.7	74.7
2.500	76.2	56.7	47.6	68.5	54.4	45.7
2.600	70.0	50.6	40.7	61.0	49.8	39.6
2.800	2.0	0	0	1.1	0	0
3.00	3.0	0	0	2.0	0*	0*
3.200	6.9	7.5	6.5	6.6	7.2*	6.8*
3.400	5.0	5.5	4.6	3.3	5.7	3.2
3.600	0.6	0	0	0.6	0	0
3.800	1.5	0	0	1.5	0	0
4.00	1.5	0	0	1.5	0	0

$\delta T(26^{\circ}C) = + .5 \pm .6\%$

$\delta T(526^{\circ}C, 826^{\circ}C) = + .5 \pm .9\%$ ($T_R = 0$), $\lambda < 2$ microns

$+ .5 \pm 1.5\%$ ($T_R = .9$), $\lambda < 2$ microns

$+ .5 \pm 1.1\%$ ($T_R = 0$), $\lambda > 2$ microns

$+ .5 \pm 1.9\%$ ($T_R = .9$), $\lambda > 2$ microns

TABLE XVII. Aluminosilicate Glass-Corning Code 1723-Transmittance vs. Temperature, After 30 Day Space Equivalent Irradiation

	Uncoated			HEA Coating		
λ	T	T	T	T	T	T
Microns	26°C	526°C	826°C	26°C	526°C	826°C
0.3023	0	0	0	0	0	0
0.3127	0.3	0	0	0.2	0	0
0.3133	0.4	0	0	0.3	0	0
0.3342	10.5	0	0	8.4	0	0
0.3651	56.9	23.4	6.1	47.0	20.1	3.1
0.4048	78.3	68.4	43.4	79.5	68.4	31.1
0.4358	83.6	80.8	66.0	86.4	80.8	57.4
0.5461	88.0	87.9	86.3	91.6	89.6	85.7
0.5771	88.7	88.0	89.6	92.5	90.2	88.4
0.5792	88.7	88.2	88.3	92.5	90.5	87.1
1.014	86.7	86.6	86.0	85.3	84.5	86.0
1.129	87.0	87.0	87.0	83.7	83.3	83.9
1.368	87.0	86.7	86.4	82.0	81.2	82.2
1.530	88.5	88.0	89.2	81.4	82.2	83.4
1.693	88.7	88.8	89.5	81.3	82.5	83.3
1.710	88.7	89.1	89.4	81.3	81.7	84.3
2.00	88.6	88.5	88.7	80.5	83.2	82.4
2.200	80.5	78.9	76.7	74.9	74.5	73.3
2.300	82.6	80.2	78.1	76.1	76.2	73.1
2.500	74.5	69.6	64.8	69.5	66.0	61.8
2.600	67.4	59.1	53.7	62.6	57.0	51.8
2.800	1.0	0	0	0.5	0*	0*
3.000	2.6	0	0	2.6	0*	0*
3.200	5.9	4.0	4.0	5.9	7.7	7.1*
3.400	5.0	5.7	5.1	5.0	5.0	4.4
3.600	0.5	1.5	0	0.5	1.5	1.5
3.800	1.5	0	0	0.6	0	0
4.000	1.0	0	0	0	0	0

$\delta T(26^{\circ}C) = + .5 \pm .6\%$

$\delta T(526^{\circ}C, 826^{\circ}C) = + .5 \pm .9\%$ ($T_R = 0$), $\lambda < 2$ microns

$+ .5 \pm 1.5\%$ ($T_R = .9$), $\lambda < 2$ microns

$+ .5 \pm 1.1\%$ ($T_R = 0$), $\lambda > 2$ microns

$+ .5 \pm 1.9\%$ ($T_R = .9$), $\lambda > 2$ microns

TABLE XVIII. Vycor-Corning Code 7913, Optical Grade-Transmittance vs. Temperature, Non-irradiated

λ	Uncoated T	Uncoated T	Uncoated T	HEA Coating T	HEA Coating T	HEA Coating T	WBHM Coating T	WBHM Coating T	WBHM Coating T
Microns	26°C	526°C	826°C	26°C	526°C	826°C	26°C	526°C	826°C
0.2303	1.4	0	0	0	0	0	0	0	0
0.2379	6.1	0	0	0	0	0	0	0	0
0.2407	7.4	0.6	0	0	0	0	0	0	0
0.2447	9.5	2.1	0	0	0	0	0	0	0
0.2465	10.0	2.1	0	0	0	0	0	0	0
0.2480	10.7	3.7	0.5	0.2	0	0.5	0	0	0
0.2653	14.5	12.9	9.0	1.0	0	0.6	0	0	0
0.2700	16.5	14.6	10.6	1.6	0	0	0	0	0
0.2753	19.1	17.3	14.4	2.7	0	0	0	0	0
0.2805	22.6	19.5	16.9	4.5	4.4	2.5	0	0	0
0.2968	39.6	32.2	28.1	22.2	11.3	5.9	0	0	0
0.3023	44.0	35.2	30.5	27.0	14.5	7.6	0	0	0
0.3127	60.3	47.1	41.4	41.3	23.6	16.6	0	0	0
0.3133	60.8	49.0	42.1	41.8	25.1	16.8	0	0	0
0.3342	78.0	66.3	57.6	56.4	42.9	28.2	0	0	0
0.3651	90.0	83.7	75.6	79.8	73.0	30.2	0	0	0
0.4048	92.7	90.5	85.9	92.7	90.5	45.9	82.5	44.4	2.4
0.4358	88.1	87.9	83.3	89.0	88.5	62.5	86.0	68.1	13.0
0.5461	93.0	94.2	90.5	96.7	95.8	71.5	90.1	86.7	31.1
0.5771	93.0	96.2	89.5	96.5	96.8	69.3	88.5	88.3	20.8
0.5792	93.0	94.1	90.5	96.5	95.7	70.3	88.5	86.1	20.7
1.014	92.5	93.8	90.3	88.6	90.4	90.9	7.0	1.7	0
1.129	92.5	91.5	89.8	85.4	85.3	89.8	4.8	0.5	0
1.368	91.5	90.7	87.9	79.6	91.9	84.4	15.7	38.5	9.7
1.530	92.7	91.2	88.6	81.2	82.0	83.4	83.0	76.3	17.5
1.693	93.0	92.5	89.4	81.9	82.8	83.2	90.0	75.1	24.7
1.710	93.0	92.1	90.0	81.9	82.5	83.8	90.0	72.9	24.5
2.000	92.0	91.1	88.0	81.5	82.5	81.4	86.0	74.9	32.0
2.200	82.6	79.9	74.1	74.5	73.0	68.9	74.5	69.8	31.6
2.300	86.5	83.3	77.1	76.3	75.2	72.0	80.8	67.6	33.0
2.500	77.0	65.7	57.3	71.7	60.8	54.6	65.1	55.9	29.8
2.600	59.0	42.7	36.1	57.6	39.3	35.6	57.6	38.9	19.9
2.800	2.0	3.7	4.1	2.0	3.7	0*	1.0	2.2	0.2
3.000	49.5	42.2	36.7	43.5	38.8	35.7	20.5	36.4	26.1
3.200	58.3	51.4	43.6	53.2	47.4	42.1	34.5	47.9	34.0
3.400	43.0	36.3	29.1	43.0	34.4	29.6	35.5	30.9	26.6
3.600	0.9	0	0	2.0	0	0	0.9	0	0
3.800	7.0	4.8	0	7.0	6.0*	4.0*	7.0	6.0*	5.2*
4.000	2.5	0	0	3.3	0	0	2.5	0	0

$\delta T(26^{\circ}C) = + .5 \pm .6\%$

$\delta T(526^{\circ}C, 826^{\circ}C) = + .5 \pm .9\%$ ($T_R = 0$), $\lambda < 2$ microns

$+ .5 \pm 1.5\%$ ($T_R = .9$), $\lambda < 2$ microns

$+ .5 \pm 1.1\%$ ($T_R = 0$), $\lambda > 2$ microns

$+ .5 \pm 1.9\%$ ($T_R = .9$), $\lambda > 2$ microns

TABLE XIX. Vycor-Corning Code 7913, Optical Grade-Transmittance vs. Temperature, After 30 Day Space Equivalent Irradiation

λ	Uncoated T	Uncoated T	Uncoated T	HEA Coating T	HEA Coating T	HEA Coating T	WBHM Coating T	WBHM Coating T	WBHM Coating T
Microns	26°C	526°C	826°C	26°C	526°C	826°C	26°C	526°C	826°C
0.2303	1.0	0	0	0	0	0	0	0	0
0.2379	3.8	0	0	0	0	0	0	0	0
0.2407	5.0	0	0	0	0	0	0	0	0
0.2447	6.4	0.6	0	0	0	0	0	0	0
0.2465	7.0	1.9	0	0.1	0	0	0	0	0
0.2480	7.4	2.2	0	0.1	0	0	0	0	0
0.2653	11.1	10.8	6.1	0.8	0	0	0	0	0
0.2700	12.7	12.7	8.0	1.4	0	0	0	0	0
0.2753	14.8	15.4	10.5	2.3	1.1	0	0	0	0
0.2805	17.5	17.1	13.1	4.0	4.3	1.3	0	0	0
0.2968	30.0	27.7	21.7	17.0	10.1	3.2	0	0	0
0.3023	31.7	28.1	22.6	24.3	12.4	4.9	0	0	0
0.3127	48.1	41.2	33.7	34.4	21.7	10.6	0	0	0
0.3133	48.3	40.1	33.6	34.5	21.6	11.1	0	0	0
0.3342	66.5	57.5	49.8	47.6	38.7	18.7	0	0	0
0.3651	80.5	74.2	70.8	69.0	66.3	28.2	0	0	0
0.4048	86.0	83.1	83.9	84.2	83.1	52.8	61.6	38.6	2.1
0.4358	87.0	86.2	87.0	88.3	86.8	69.6	63.9	63.3	15.9
0.5461	90.5	90.3	91.0	94.0	93.0	76.2	69.1	80.3	35.8
0.5771	90.7	89.9	91.2	94.0	92.1	77.3	72.0	80.3	17.0
0.5792	90.8	90.5	91.8	94.0	92.1	77.9	72.1	80.9	14.4
1.014	90.7	89.8	90.3	90.0	86.7	89.8	7.0	1.5	0
1.129	92.0	90.0	91.4	86.6	84.5	88.4	3.7	1.5	0
1.368	87.4	86.2	86.9	82.9	87.7	81.1	17.0	29.6	11.6
1.530	92.4	91.3	91.4	81.6	82.1	83.8	86.5	76.4	23.7
1.693	93.0	92.4	92.4	82.4	83.1	84.2	87.8	77.0	28.2
1.710	93.1	92.6	91.7	82.5	82.4	83.6	87.9	73.7	29.1
2.000	92.0	91.0	91.4	82.3	81.8	83.2	85.1	75.6	39.0
2.200	80.5	77.0	79.1	65.5	69.9	73.1	63.5	67.4	38.5
2.300	85.0	83.0	80.9	79.1	75.6	73.9	83.0	66.8	38.2
2.500	79.5	69.6	62.0	71.4	65.7	58.1	61.0	59.0	35.1
2.600	61.0	45.3	47.2	52.5	43.4	40.1	51.0	40.1	24.8
2.800	1.0	1.5	1.7	2.2	1.6	2.2	2.0	0.9	0.3
3.000	47.0	40.0	36.6	45.0	37.7	36.2	20.5	34.1	27.8
3.200	56.5	49.7	44.1	52.5	46.9	41.7	33.0	46.5	37.0
3.400	44.0	37.3	31.3	36.0	36.9	30.3	26.5	31.4	29.8
3.600	1.2	0.5	0	1.0	0.9	0*	0.6	0.9	0*
3.800	6.5	2.7	5.3	5.2	8.2	5.3	4.1	9.1	0*
4.000	2.0	0	0	3.2	0	0	2.0	0	0

$\delta T(26^{\circ}C) = + .5 \pm .6\%$

$\delta T(526^{\circ}C, 826^{\circ}C) = + .5 \pm .9\%$ ($T_R = 0$), $\lambda < 2$ microns

$+ .5 \pm 1.5\%$ ($T_R = .9$), $\lambda < 2$ microns

$+ .5 \pm 1.1\%$ ($T_R = 0$), $\lambda > 2$ microns

$+ .5 \pm 1.9\%$ ($T_R = .9$), $\lambda > 2$ microns

TABLE XX. Fused Silica-Corning Code 7940, Ultraviolet Grade-
Extinction Coefficient vs. Temperature, Non-irradiated

λ Microns	$K \times 10^8$ 26°C	$K \times 10^8$ 526°C	$K \times 10^8$ 826°K
0.23021	9.114	10.82	7.722
0.23783	6.708	7.309	6.538
0.2407	6.702	6.067	8.793
0.2465	5.589	6.844	8.098
0.24827	5.785	7.953	7.411
0.26520	6.706	5.108	4.421
0.27528	6.809	5.719	5.703
0.28035	6.853	5.459	6.159
0.29673	3.714	1.849	4.184
0.30215	2.942	4.627	3.271
0.3130	2.992	3.189	2.880
0.33415	0.4464	0.5008	0.8251
0.36502	0.5292	1.300	1.490
0.40466	0.6137	2.277	1.111
0.43584	0.5937	1.334	1.141
0.54607	0.8787	2.873	3.183
0.5780	0.7354	1.187	1.502
1.01398	4.679	6.962	8.064
1.12866	4.833	10.11	11.35
1.254	12.83	20.66	22.02
1.36728	51.26	50.41	55.55
1.470	6.901	45.30	46.22
1.52452	6.557	15.92	16.11
1.660	4.999	16.82	18.68
1.701	5.264	12.41	20.03
1.981	15.49	34.63	36.89
2.262	402.5	448.7	553.9
2.553	888.8	835.4	968.1
3.00	706.1	1644.	2453.
3.245	395.9	1079.	1674.
3.37	563.9	1196.	1768.

TABLE XXI. Fused Silica-Corning Code 7940, Ultraviolet Grade-Extinction Coefficient vs. Temperature, After 30 Day Space Equivalent Irradiation

λ Microns	$KX10^8$ 26°C	$KX10^8$ 526°C	$KX10^8$ 826°C
0.23021	45.41	41.03	51.42
0.23783	42.48	41.01	46.79
0.2407	42.17	37.32	49.24
0.2465	40.33	33.69	47.01
0.24827	40.13	31.69	47.93
0.26520	41.11	32.43	42.50
0.27528	40.57	32.07	43.12
0.28035	40.25	33.96	40.18
0.29673	36.41	31.51	37.10
0.30215	35.04	29.58	37.84
0.3130	32.54	26.11	35.75
0.33415	30.70	26.91	32.23
0.36502	28.46	22.21	28.81
0.40466	22.52	17.86	22.23
0.43584	21.34	15.27	27.21
0.54607	19.64	9.025	26.23
0.5780	19.08	9.648	24.76
1.01398	14.54	32.21	9.050
1.12866	16.36	29.70	7.509
1.254	21.44	31.93	14.00
1.36728	41.43	51.83	26.96
1.470	36.53	55.89	23.33
1.52452	14.66	28.67	1.400
1.660	15.40	27.41	1.848
1.701	15.92	29.89	1.956
1.981	26.09	39.54	5.048
2.262	493.1	415.6	447.7
2.553	1114.	2369.	2011.
3.000	718.2	1649	2209.
3.245	430.7	1012.	1526.
3.37	559.3	1144.	1753.

TABLE XXII. Aluminosilicate Glass-Corning Code 1723-Extinction Coefficient vs. Temperature, Non-irradiated

λ Microns	$K \times 10^8$ 26°C	$K \times 10^8$ 526°C
0.33415	737.9	2317.
0.36502	120.6	577.3
0.40466	12.39	105.4
0.43584	6.829	25.74
0.54607	2.258	4.588
0.5780	2.734	3.523
1.01398	61.75	80.42
1.12866	64.19	76.25
1.36728	52.28	42.13
1.52452	52.51	70.87
1.660	57.94	103.1
1.701	59.83	77.76
1.981	78.07	75.17
2.262	328.3	374.2
2.553	779.2	1783.
2.665	1514.	2863.

TABLE XXIII. Aluminosilicate Glass-Corning Code 1723-
Extinction Coefficient vs. Temperature,
After 30 Day Space Equivalent Irradiation

λ Microns	$K \times 10^8$ 28°C	$K \times 10^8$ 526°C
0.33415	961.1	3035.
0.36502	225.9	657.8
0.40466	79.62	150.8
0.43584	48.36	67.26
0.54607	25.04	24.95
0.5780	20.75	25.90
1.01398	71.07	71.04
1.12866	74.53	72.79
1.36728	91.65	95.87
1.52452	68.51	77.77
1.660	70.38	65.44
1.701	72.57	59.92
1.981	89.96	90.02
2.262	346.7	426.2
2.553	888.5	1170.
2.665	1792.	2324.

TABLE XXIV. Vycor-Corning Code 7913, Optical Grade-Extinction Coefficient vs. Temperature, Non-irradiated

λ Microns	$K \times 10^8$ 26°C	$K \times 10^8$ 526°C	$K \times 10^8$ 826°C
0.26520	1033.	1097.	1297
0.29673	529.6	657.6	741.7
0.30215	472.5	613.2	703.4
0.3130	280.1	430.0	521.5
0.33415	121.2	234.2	332.2
0.36502	24.43	78.80	155.1
0.40466	3.009	22.09	65.39
0.43584	50.51	51.20	99.31
0.54607	3.106	11.35	31.41
0.5780	3.675	15.06	39.90
1.01398	22.45	35.71	68.70
1.12866	25.79	48.40	90.49
1.254	32.49	54.76	116.2
1.36728	64.41	85.82	173.0
1.470	77.00	100.1	190.5
1.52452	31.63	79.65	169.1
1.660	28.20	49.95	161.8
1.701	25.65	47.95	146.4
1.981	78.78	114.2	254.1
2.262	456.2	649.5	1001.
2.553	1592.	2866.	3648.

TABLE XXV. Vycor-Corning Code 7913, Optical Grade-Extinction Coefficient vs. Temperature, After 30 Day Space Equivalent Irradiation

λ Microns	$K \times 10^8$ 26°C	$K \times 10^8$ 526°C	$K \times 10^8$ 826°K
0.26520	1182.	1196.	1514.
0.29673	703.0	751.6	903.2
0.30215	681.0	756.5	894.1
0.3130	429.9	540.1	665.4
0.33415	233.4	334.4	434.6
0.36502	109.2	170.5	205.5
0.40466	66.77	93.66	85.41
0.43584	62.01	69.07	59.52
0.54607	34.36	35.23	25.09
0.5780	34.08	39.05	20.34
1.01398	64.31	82.63	68.70
1.12866	38.64	87.59	48.62
1.254	81.41	127.7	101.5
1.36728	196.1	232.0	205.9
1.470	173.2	211.3	197.6
1.52452	42.01	76.14	69.41
1.660	28.20	56.56	52.62
1.701	25.65	40.21	52.10
1.981	78.78	118.8	96.36
2.262	580.8	725.9	744.7
2.553	1509.	2693.	2909.

REFERENCES

1. REIC - Memorandum 26, "Radiation Effects on Glass, An Annotated Bibliography," Radiation Effects Information Center, Battelle Memorial Institute, Columbus, Ohio, September 15, 1965.
2. Lockheed Report 3-77-61-2 (SB-61-25), "The Effects of High Energy Radiation Infrared Optical Materials, An Annotated Bibliography." Lockheed Missiles and Space Division, Sunnyvale, Calif., May 1966.
3. R. Bechmann, "Radiation Effects in Quartz, A Bibliography. Nucleonics 16, No. 3, p. 122, March 1958.
4. BNL 6513, "Effects of Radiation on Glass, A Bibliography." M. Comstock and P. Ferrigaro, Brookhaven National Labs, Upton, N.Y. 1962.
5. Al-MEMO-9366, Interim Report on the Apollo Window Materials Radiation Testing Program, Atomics International, Canoga Park, Calif., Feb. 1964.
6. NASA Technical Note NASA-TN D2620, G. A. Haynes and W. E. Miller, "Effects of 1.2 and 0.30 MeV Electrons on the Optical Transmission Properties of Several Transparent Materials," NASA/Langley, March 1965.

6a. NASA Report NASA-CR-60407, "A Bibliography on the Effects of Shortwave and Particle Radiation on Glasses," Lorne Avery, July 30, 1964.

6b. J. M. Chinn et al, "Charge Particle Radiation Effects on Selected Transparent Materials for Aerospace Applications." Special Technical Conference on Nuclear Radiation Effects, Seattle, July 1964. Paper: CONF-617-21.

6c. F. J. Campbell, "Effects of Radiation on Transmittance of Glasses and Adhesives." Proceedings of 17th Annual Power Sources Conference, Red Bank, N. J. PSC Publications Committee 1963, p. 19.

7. A. J. Cohen, Phys. Chem. Solids 13, 321 (1960).

8. D. L. Wood, ibid, 326.

9. Studies in Penetration of Charged Particles in Matter, Nuclear Science Series Report No. 9, publication 1133, National Academy of Sciences, Washington (1964), p. 220.

10. J. E. Wertz, et al, J. Phys. Soc. Japan 18, Suppl. II, 305 (1963).

11. M. E. Wyatt, V. A. J. van Lint, and E. G. Wikner, Proton Correlation Studies, Final Report on Contract AF33(615)-1715 (Technical Report AFML-TR-66-77), General Atomic Report GA-6953, April 1966.

12. D. Pooley, Proc. Phys. Soc. (London) 87, 245, 257 (1966).

13. E. A. Boettner and L. J. Miedler, "Transmittance Changes in Glasses Induced by Ultraviolet Radiation," J. Opt. Soc. Am. 51, 1310-1311, (1961).

14. R. L. Hammel, "Low Energy Radiation Damage to Surfaces" in AIAA 5th Annual Structures and Materials Conference, AIAA publication CP-8, New York, Am. Inst. of Aeronautics and Astronautics, 1964.

15. J. Lindhard, V. Nielsen, M. Scharff and P. V. Thomsen, Mat. Phys. Ned Kgl Dansk Kid Selsk 33, No. 10 (1963).

16. J. M. Stevels, "Network Defects in Non-Crystalline Solids," pp. 412-441 in "Non-Crystalline Solids," edited by V. D. Frechette, New York, John Wiley 1960, p. 412. See also J. M. Sterels and A. Kats, Philips Research Reports 11, 103 (1956).

17. G. Knechtel and A. Scharmann, Z. Angew, Phys. 20, 141 (1965).

18. P. W. Levy, J. Am. Ceramic Soc. 43, 389 (1960).

19. A. J. Cohen, J. Chem. Phys. 23, 765 (1955).

20. P. W. Levy, J. Chem. Phys. 23, 764 (1955).

21. A. J. Gale and F. A. Bickford, Nucleonics 11, No. 8, 48 (1953).

22. J. H. E. Griffiths, J. Owens and I. M. Ward, Reports of Bristol Conference on Defects in Crystalline Solids, p. 81, Physical Society, London (1955).

23. M. C. M. O'Brien and M. H. L. Price, Ibid, p. 88.

24. E. W. J. Mitchell and E. G. S. Paige, Phil. Mag. 46, 1353 (1955).

25. E. Lell, J. Am. Ceramic Soc. 43, 422 (1960).

26. G. V. Byurganovskaya and N. F. Orlov, Optika: Specktroskopiya 12, 278 (1962).

27. C. M. Nelson and J. H. Crawford, Jr., J. Phys. Chem. Solids 13, 296 (1960).

28. P. W. Levy, J. Phys. Chem. Solids 13, 287 (1960).

29. W. D. Compton and G. W. Arnold, Jr., Disc. Faraday Soc. 31, 130 (1961).

30. C. M. Nelson and R. A. Weeks, J. Appl. Phys. 32, 883 (1961).

31. A. J. Shuskus, Thesis, University of Connecticut, Storrs, 1962. Dissertation Abstracts 22, 2848-9 (Feb. 1962).

32. N. K. Kriedl and J. R. Hensler, J. Am. Ceramic Soc. 38, 423 (1955).

33. General Atomic Report GA-7140, Final Report on Contract AF19(628)2926, "Optical Radiation Effects," Sept. 1966.

34. W. Primak and R. A. Uphaus, J. Chem. Phys. 29, 972 (1958).

35. AFAL-TR-64-318, Air Force Avionics Laboratory, "Coherent Light Transmitter Technique," General Atomic Report GA-5733, Jan. 11, 1965.

36. G. W. Arnold, J. Phys. Chem. Solids 13, 306 (1960).

37. I. H. Malitson, M. J. Dodge and M. Gonshery, paper presented at 1965 Annual Meeting of Optical Society of America, J. Opt. Soc. Am. 55, 1583 (1965). Abstract FB21.

See also the same authors, paper ThD21 at 1966 Annual Meeting of Optical Society of America, San Francisco, October 1966.

Also private communication from M. Gonshery.

38. G. A. Noble, private communication. See also G. A. Noble and W. P. MacDonald, Bull. APS Series II, 10, 1086 (1965) (Paper AG 12).

39. G. D. Magnuson, et al., "High Efficiency Metal Ion Source," R.S.I. 36, 136-142 (1965).

40. "An Evaluation of the Radiation Hazard Due to Solar Particle Events," W. R. Webber, Boeing Report D2-90469 (Dec. 1963).

41. R. Stair, W. Schneider, and J. Jackson, "A New Standard of Spectral Irradiance," Applied Optics, Vol. 2, November 1963, p. 1151.

42. R. Stair and R. Johnston, "Calibrations of the National Bureau of Standards Thermal Radiation Standards," J. of Res. of the N.B.S., Vol. 53, October 1954, p. 211.

43. I. H. Malitson, J. Opt. Soc. Amer. 55, 1205 (1965).

44. L. Prod'homme, Verres et Refractaires 10, 267 (1956).

45. O. J. Edwards, J. Opt. Soc. Amer. 56, 1314 (1966).